TEMPORAL AND SPATIAL VARIABILITY OF THE RAS AL-HADD JET/FRONT IN THE NORTHWEST ARABIAN SEA

A Dissertation

by

HILAL MOHAMED SAID AL SHAQSI

Submitted to the Office of Graduate and Professional Studies of
Texas A&M University
in partial fulfillment of the requirements for the degree of

DOCTOR OF PHILOSOPHY

Chair of Committee,	Steven F. DiMarco
Committee Members,	Matthew K. Howard
	Ann E. Jochens
	Anthony Filippi
Head of Department,	Shari Yvon-Lewis

May 2017

Major Subject: Oceanography

ABSTRACT

Thirteen years of 1.1 km resolution daily satellites remote sensing sea surface temperature datasets (2002 - 2014), sea surface winds, sea surface height, Argo floats, daily three-hour interval wind datasets, and hourly records of oceanography physical parameters from mooring current meters were processed and analyzed to investigate the dynamics, temporal and spatial variability of the Ras Al-Hadd Jet off the northwest Arabian Sea. Cayula and Cornillon single image edge detection algorithm was used to detect these thermal fronts. The Ras Al-Hadd thermal front was found to have two seasonal peaks. The first peak occurred during the intensified southwest monsoon period (July/August), while the second peak was clearly observed during the transitional period or the Post-Southwest monsoon (September-October). Interannual and intraseasonal variability showed the occurrence of the Ras Al-Hadd thermal fronts in the northwest Arabian Sea. The southwest monsoon winds, the Somalia Current, the East Arabian Current, and the warmer high salinity waters from the Sea of Oman are the main factors influencing the creation of the Ras Al-Hadd Jet. Based on direct observations, current velocity in the Cape Ras Al-Hadd Jet exceeded 120 cms^{-1}, and the wind speed was over 12 ms^{-1} during the southwest monsoon seasons. The mean width and the mean length of the Jet were approximately 40 km and 260 km, respectively. Neither the winter monsoon, nor the Pre-Southwest monsoon seasons showed signs of the Ras Al-Hadd Jet or fronts in the northwest Arabian Sea.

DEDICATION

All the praise is due to our Allah, the Lord of the worlds, the Beneficent and the Merciful for blessing me with the ability to pursue my graduate studies and seek knowledge.

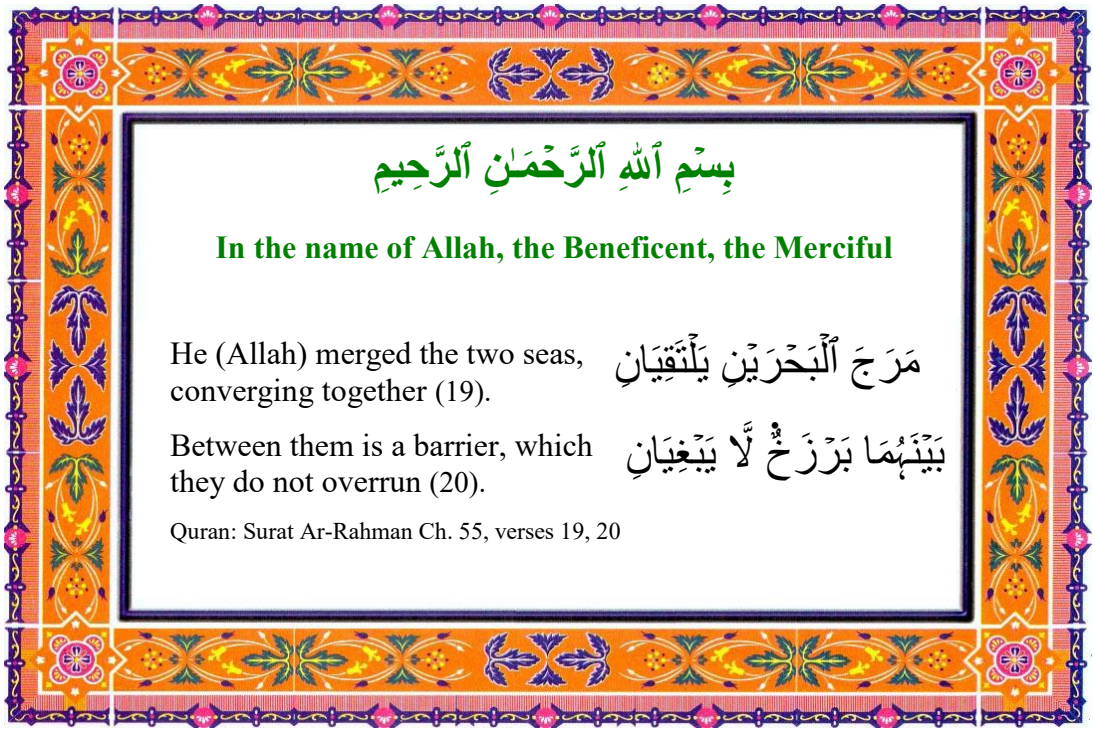

ACKNOWLEDGEMENTS

First of all, I would like to express my deepest thanks to my committee members, starting with my advisor and committee chair, Professor Steven DiMarco, for his excellent assistance, and guidance in my research. He provided me several opportunities to continue my study here at Texas A&M, and I am grateful for his daily involvements and supports during the period I spent here at TAMU. Without his help, I would not have accomplished this research. Dr. Wang (previous committee member) did not hesitate in helping and guiding in necessary Matlab coding that was used in my research. I thank Professor Anthony Filippi from the Department of Geography, for his involvement and guidance in the geospatial analysis, and for providing a Lab spot where all the remote sensing processes and analysis took place. Dr. Matthew Howard and Dr. Ann Jochens did not hesitate for their guidance and supports during my study. Mrs. Marion Stöessel, the data manager, I don't know how to thank her for a great job in providing the mooring dataset used in this study and for her daily involvement in making these datasets usable. Ms. Laura Caldwell, always makes our office 702 a great working environment. My thanks also go to Professor Piers Chapman, the previous Head of the Department who always encourages me, Professor Debbie Thomas, the Interim Dean of College of Geosciences for her help and support, and Professor Shari Yvon-Lewis, the Acting Department Head.

Thanks also go to faculties, staffs, friends and colleagues here at the College of Geosciences for making my time at Texas A&M University a great experience. I am grateful for friends at the Department of Geography, especially, Billy Hales for his help in Python code that was used for the reclassification processes.

I also, would like to express my thanks to the Government of Oman, and Lighthouse R&D Inc. of Houston, Texas to fund my study here at Texas A&M University. Many thanks fly home to Dr. Lubna Al-Kharusi, the Director General of the Department of Fisheries Researches at the Ministry of Agriculture and Fisheries, Oman, for her involvement convincing the Ministry to grant me a time extension in order to finish this study.

Finally, thanks to my family far away home for their encouragements and supports and to my wife and kids who decided to be with me here at College Station for their support, patience and love.

CONTRIBUTORS AND FUNDING SOURCES

Contributors

This work was supervised by a dissertation committee consisting of Professor Steven DiMarco, the Advisor and Chair; Dr. Matthew Howard; Dr. Ann Jochens of the Department of Oceanography; and Professor(s) Anthony Filippi of the Department of Geography.

The Moored time-series datasets described in Chapter II was provided by Professor DiMarco under the project of Lighthouse Research and Development Inc. Remote sensing data sets were downloaded from different US. government websites as described in Chapter II.

All other works conducted for the dissertation were done by myself independently, with some guidance from the advisor and the committee's members. Some Matlab programming was reviewed and modified by Dr. Wang, a former committee member, and by Mrs. Stöessel, the moored data manager in the Department of Oceanography, Texas A&M University. Billy Hales from the Department of Geography, helped to edit and to guide in Python codes used for the reclassification processes in a GIS package.

Funding Sources

This graduate program was supported and funded by many parts starting with a) the Ministry of Agriculture and Fisheries, Government of Oman, and the Lighthouse Research and Development Inc. of Houston, Texas, full support that included tuitions and fees and a monthly stipend, from Spring-2010 to Spring-2014, b) Professor Steven DiMarco supported the tuition and fees for Fall-2014, c) the Government of Oman fully supported again in funding the University tuitions and fees and a monthly stipend for the year 2015, d) College of Geoscience/Department of Oceanography supported 50% of the tuition and fees for Spring-2016, and finally d) self-funded for Fall-2016 and Spring-2017.

NOMENCLATURE

ADCP	Acoustic Doppler Current Profiler
AVHRR	Advance Very High-Resolution Radiometer
EAC	Eastern Arabian Current
EEZ	Exclusive Economy Zone
Cape-RH	The Cape Ras Al-Hadd
GHRSST	Group of High Resolution Sea Surface Temperature
MGET	Marine Geospatial Ecology Tool
MIED	Multi Image Edge Detection
MODIS	Moderate-Resolution Imaging Spectroradiometer
NASA	National Atmospheric and Space Administration
NEM	Northeast monsoon
NOAA	National Oceanographic and Atmospheric Administration
OMZ	Oxygen Minimum Zone
PSU	Practical Salinity Unit
QA/QC	Quality Assurance and Quality Control
RCM	Recording Current Meter
RDCP	Recording Doppler Current Profiler
RH	Ras Al-Hadd
RH-Front	Ras Al-Hadd Front
RH-Jet	Ras Al-Hadd Jet

RHM	The Middle station at Cape Ras Al-Hadd
RHN	The station North of Cape Ras Al-Hadd
RHS	The station South of Cape Ras Al-Hadd
SC	The Somali Current
SeaWiFS	Sea-viewing Wide Field-of-view Sensor
SIED	Single Image Edge Detection
SSC	Sea Surface Current
SSH	Sea Surface Height
SST	Sea Surface Temperature
SSW	Sea Surface Wind
SWM	South West Monsoon
WHOI	Woods Hole Oceanographic Institution

TABLE OF CONTENTS

Page

LIST OF FIGURES

Page

LIST OF TABLES

Page

CHAPTER I

INTRODUCTION

The northwest Arabian Sea is a region located in the northwest Indian Ocean. It is one of the most productive oceans (Smith, 2001) with complex circulation processes and atmospheric effects (Schott *et al.*, 2009). The purpose of this research is to investigate the temporal and spatial variability of the oceanic jet or fronts at Cape Ras Al-Hadd located in the northwest Arabian Sea. This is because, fronts are areas of convergence and region of strong biological productivity. Therefore, many different commercial fish species aggregate in dense groups at this region. The study area for this dissertation is bounded by 21˚N-24˚N and 59.8˚E-64˚E (Figure 1.1). Ras Al-Hadd (RH) is very important fishing region that the fisheries sector of Oman depends on due to the strong biological productivity at this region.

Several studies have investigated the dynamics and the biogeochemistry of the Indian Ocean, but relatively little is known about the oceanic jets in the northwest Arabian Sea. This study combines a variety of remote sensing and observational datasets in order to investigate the temporal and the spatial variability of the Ras Al-Hadd Jet.

1.1 Background

Physical oceanography processes and atmospheric forcing affect the physics and biochemistry of oceans by creating many different features in the ocean such as

cyclones, hurricanes, and oceanic jets or fronts. Jets or fronts have been found to play a great role in transporting ocean properties for hundreds or thousands of kilometers within the ocean. Oceanic jets separate different water masses and are certainly important in biological processes (Barth, 1987, 1989). Therefore, scientists have been putting efforts into studying both the atmospheric and oceanic jets and fronts for their role in affecting both the atmosphere and ocean circulations. Although fronts and jets of the southern Indian Ocean have been extensively studied (e.g., Schott *et al.,* 2001), the northwest part of the Indian Ocean has had very few studies,

Jets and fronts coexist most of the time. The definition and usage of the terms oceanic jet and the oceanic front is rather confused among new oceanographers. Oceanography researchers usually use the term jets and fronts synonymously as two words with the same meaning. Therefore, both jets and fronts are characterized as the area of subduction between two distinctive water masses (Yanagi, 1987). Fronts are known as regions where two water masses meet with horizontal gradients of water properties. These properties can be temperature, salinity, and Chlorophyll differing from the surrounding waters (Yanagi, 1987). In other words, a front is formed where two different water bodies with different property values meet. Also, it can be defined as a region with a sharp horizontal difference in the ocean properties such as temperature, salinity, and Chlorophyll concentration (Belkin, 2003; Wolanski and Hamner, 1998; Barth, 1987; Tong *et al.,* 2010). Similarly, in atmospheric science, a jet stream is formed directly over the center of the strongest area of horizontal temperature difference. Hence, an oceanic

or atmospheric jet is a strong current moving between the two boundaries of a front. These oceanic fronts are classified as coastal, continental shelf, and offshore fronts (Table 1.1).

Table 1.1. The table shows front types as classified by other workers. There are 3 main types and were defined as coastal, continental shelf, and open sea fronts (Source: Yanagi, 1987).

Front	Front type
Coastal	Estuarine front Thermal effluent front Thermohaline front Tidal front
Continental shelf	Shelf/slope front Coastal upwelling front Coastal boundary current front
Open sea	Western boundary current front Warm core front/ Cold core front Subarctic front Subtropical front Doldrum front Polar front

Ocean jets are strong ocean currents created as the results of different water masses that are usually accompanied with a different type of hydrographic properties and increasing in wind stress (Belkin, 2003; Tomczak and Godfrey; 1994; Cushman-Roisin *et al.,* 2011). These jets can sometimes be produced by the hydrographic structures located under the thermocline region (Kessler and Gourdeau, 2006). Jets are long narrow currents and most jets are known to move parallel to the coast then turn and flow nearly perpendicular to the coast (Stewart, 2008). Upwelling jets were found to move parallel to the coast (Barth, 1987). The spatial and temporal scales of ocean jets vary with forcing and location (Ponte and Luyten, 1990), and they can move several hundred kilometers

offshore (Belkin, 2003, Böhm *et al.,*1999). The horizontal scale ranges from several meters to thousands of kilometers and their time scales range from hours to seasons (Yanagi, 1987).

These oceanic jets are widely reported in the literature as the dominant features of the deep circulation in the Pacific, the Atlantic, and the Indian Oceans (Ponte at al., 1990; Luyten and Swallow, 1976). Jets are faster and stronger than other water currents. These oceanic jets or fronts present with different temporal and spatial scales. For instance, the Kuroshio front is formed along oceanic jets, and through coastal upwelling (Kida *et al.,* 2015). The formation mechanisms of these fronts and jets have been investigated and they had gained interest as the area of convergence where the deep-water mixes with the sub surface water (Pollard and Regier, 1992).

Zonal jets in the Equatorial Indian Oceans can reach depths of 200 - 750 m, and they are prevailing features of the deep-water circulation (Luyten and Swallow, 1976), but our understanding about jets in the Indian Ocean is very poor (Ponte *et al.,* 1990; Ponte and Luyten, 1990), due to lack of long-term observations in this region. Strong jets flow near the equator of the Pacific and Indian Oceans have scales between 100 - 300 m and temporal scales that can reach one year (Ponte at al., 1990). But in another study, Ponte and Luyten (1990) concluded that the spatial and temporal scales of fronts vary between the Indian Ocean and of the Pacific Ocean. Zonal jets were also observed in Australian waters (Sokolov and Rintoul, 2000). A comprehensive investigation of fronts and jets in the northwest Arabian Sea is almost absent.

Oceanic jets in the northwest Arabian Sea are also poorly understood. This is due to a lack of observations, limited capability of oceanographic researchers in the surrounding countries, and to the political instability in the region. Consequently, this situation creates a full dependency on developed countries for conducting oceanography studies in the Arabian Sea. As a result, without these advanced countries, the Arabian Sea in general and the northwest Arabian Sea, in particular, will continue to remain the forgotten ocean. Fortunately, eyes in space, satellites, are able to reveal some dynamic variability of the oceans. For instance, oceanic thermal fronts can be detected by satellites and can reveal the spatial and temporal variability of oceanic jets or fronts.

Böhm *et al.,* (1999) were able to show the Ras Al-Hadd Jet (RH-Jet) using the thermal signature derived from Advanced Very High-Resolution Radiometer (AVHRR). The satellite datasets were collected by series of the National Oceanic and Atmospheric Administration (NOAA) polar-orbiting meteorological satellites, at a local High Resolution Picture Transmission (HRPT) Remote Sensing Station located at the Ministry of Agriculture and Fisheries, Muscat, Oman. This team also estimated the RH-Jet's volume transport to be around 2-8 Sv (1 Sv = 10^6 m^3s^{-1}) with a vertical thickness that can reach up to 400 m moving offshore from the Cape Ras Al-Hadd (Cape-RH) into the Arabian Sea. In addition, Flagg and Kim, 1998 were able to detect the RH-Jet with a velocity 80 – 90 cms^{-1} during October 1995 and they did not find any evidence of the Jet during the NEM season. Maximenko *et al.,* (2005) were also able to detect the zonal jet signals of the world ocean in the global satellite altimeter data. This shows that satellite

remote sensing is a very important and reliable tool that can be used to investigate surface oceanic jets.

The RH-Jet creates what is known as the Ras Al-Hadd barrier, which limits to some extent near surface water exchanges between the Sea of Oman (previously Gulf of Oman) and the offshore Arabian Sea. The source of this jet and the water mass interaction between the Sea of Oman and the Arabian Sea are not well known (Wilson-Diaz *et al.,* 2001). Neither is the, general deep-water circulation of the Ras Al-Hadd region. This increases the difficulties in understanding the major physical processes and variability in the region (Johns *et al.,* 2000; Wang *et al.,* 2012).

Understanding the characteristic of the RH-Jet will help to improve knowledge of the main circulation and the distribution of oceanography properties in the Arabian Sea. The RH-Jet can transport a thick layer of a water column hundreds of kilometers offshore (Böhm *et al.,* 1999). This Jet transports cool, upwelled water carrying ocean physicochemical properties from the upwelling area to the offshore of the Arabian Sea (Smith, 2001). It also helps the creation of the two mesoscale eddies, the cyclonic eddy in the Sea of Oman and the anticyclonic eddy in the Arabian Sea (Böhm *et al.,* 1999). These mesoscale eddies can store a significant amount of kinetic energy (Flagg and Kim, 1998). The RH-Jet is considered a strong flow that responds to SWM wind in the northwest Arabian Sea (Smith, 2001; Kim *et al.,* 2001). Recently, worldwide oceanic fronts have been studied significantly due to their importance for fisheries because most

migratory pelagic fish are found in these fronts (Kida *et al.,* 2015).

Furthermore, jets or fronts create a productivity region with a vertical exchange of water and organic matter, with high biological productivity (Kahru *et al.,* 1995), and it is believed that the RH frontal region is the largest unexploited potential fishery in the world (Johns *et al.,* 2000).

1.2 Description of the Study Area

1.2.1 The Northwest Arabian Sea/Indian Ocean

The Indian Ocean is known to play a significant role in affecting the climate both within the region and in other parts of the globe (Schott *et al.,* 2009). This is due to its unique current and wind circulation patterns. The Indian Ocean circulation is known as a seasonal circulation. It experiences a seasonal reversal of atmospheric forcing. Therefore, the wind system, ocean circulations, and physical processes in the Indian Ocean differ completely from the other two oceans, the Pacific and the Atlantic Oceans. The northern Indian Ocean is bounded at around 25^{o} latitude North, where it is surrounded by continents; therefore, the connection to the North Pole (Arctic Ocean) is absent. Consequently, heat exchange, between mid-latitude and the high-latitudes waters is only to the South (Schott *et al.,* 2001). This semi-enclosed nature of the northern Indian Ocean creates the unique wind regime observed in the Arabian Sea. The strong temperature differences between the land and the ocean during summer and winter

seasons generate a reversing wind system (Bauer *et al.,* 1991; Naidu, 1998; Rudnick *et al.,* 1997). The difference in atmospheric pressure over the continents and the ocean (Wilson-Diaz *et al.,* 2001), creates the southwest monsoon (SWM) and the northeast monsoon (NEM) during summer and winter seasons of the northern hemisphere, respectively (Manghnani *et al.,* 1998; Shi *et al.,* 1999, Weller *at al.,* 1998), and greatly affects the ocean circulation of the Arabian Sea (Shi *et al.,* 2000; McCreary and Kundu, 1988).

This project concentrated on the northwest Arabian Sea and focused on the RH-Jet or RH-Front, at Cape-RH, which is located in the RH region. Cape-RH is located where the Sea of Oman meets the Arabian Sea. The Arabian Sea is located in the northern part of the Indian Ocean (Figure 1.1). This important sea is surrounded by six main countries of the region. Oman, Yemen, and Somalia from the western boundaries of the Arabian Sea, while Sri Lanka, India, and Pakistan are located at the eastern boundary of the Arabian Sea. The Arabian Sea connects with the Persian/Arabian Gulf through the Sea of Oman, and the Sea of Oman is connected with the Persian/Arabian Gulf through a narrow passage known as the Strait of Hormuz, located at the northern tip of Oman, through which 40% of the world's oil trade passes. The Bay of Bengal, the second largest Sea in the northern Indian Ocean, connects the eastern part of the Arabian Sea passing south of Sri Lanka. In the southwest, the Gulf of Aden connects the Arabian Sea with the Red Sea through another narrow passage known as the Bab Al-Mandeb Strait (Figure 1.1).

More than 95% of the Europe and North America trades pass through this strait, avoiding the Cape of Good Hope, in South Africa.

The Arabian Sea receives different water masses from the surrounding seas and marginal seas in addition to the Bay of Bengal due to the effects of the SW monsoon and NE monsoon. The Arabian Sea has an estimated area of 3.9×10^6 km^2 (Somasundar *et al.,* 1990). The maximum depth of the Arabian Sea is around 4652 m and the average depth was estimated to be around 2734 m. The Arabian Sea off the Oman coast contains the thickest oxygen minimum zone (OMZ) in the world ocean that can reach a depth of up to 1000 m (Gooday *et al.,* 2000; Levin *et al.,* 2000). On the other hand, during the SWM the southern coast of Oman, experiences an upwelling that extends to over 400 km offshore (Morrison *et al.,* 1998).

There are two main ridges in the Arabian Sea, the Carlsberg Ridge and the Murray Ridge. The Carlsberg Ridge starts from Socotra Island and extends more than 1250 km southeast deep to the eastern Indian Ocean where it is connected with the Central Indian Ridge (Gaedicke *et al.,* 2002). The Murray Ridge is around 269 km East of Cape-RH. It extends over 750 km starting near the Pakistani Exclusive Economy Zone (EEZ) waters and runs southwest between the Oman Basin and the Arabian Basin. The Murray Ridge lies in the depth around 3000 m, but the shallowest points of the ridge are less than 500 m deep (Quraishee, 1984). These ridges play a great role in controlling the deep ocean dynamics of the Arabian Sea (DiMarco *et al*., 2011, unpublished).

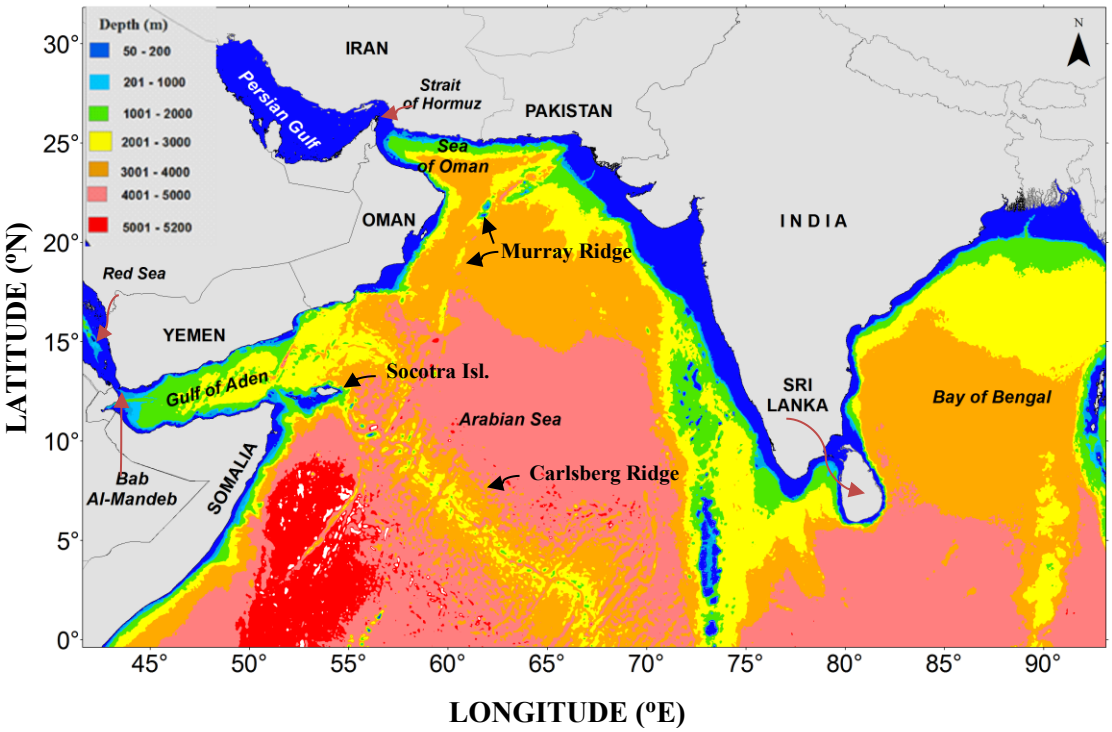

Figure 1.1. Map of the Arabian Sea and the marginal seas in the north Indian Ocean shows countries surrounded by the Arabian Sea, Sea of Oman, and the Persian/Arabian Gulf, and the Gulf of Aden. The bathymetry of the Arabian Sea is shown (bathymetry data is Etopo1. See Amante, and Eakins, 2009).

The continental shelf, which is the coastal water with a depth less than 200 m, is one of the most important habitats of most commercial marine creatures. The western side of the Arabian Sea has a narrow continental shelf that ranges between 50 - 90 km wide, while in the eastern site the shelf is in the range of 40 - 350 km wide. The total estimated area of the Arabian Sea continental shelves is 538 x 10^3 km^2, where 209 x 10^3 km^2 lies on the western Arabian Sea, and 329 x 10^3 km^2 on the eastern side.

Although it is not easy to demarcate the boundary between the Arabian Sea and the Sea of Oman, the differences in water properties during the SW monsoon can show the boundary between the Sea of Oman and the Arabian Sea (Figure 1.2). The southern boundary of the Arabian Sea is not well defined, but the acceptable estimation for the southern boundary is from the coast of East Africa 0°N – 22.53°N, and 40°E to 80°E in a Mercator projection. The Arabian Sea is connected by two marginal seas, the Persian/Arabian Gulf through the Sea of Oman and the Red Sea through the Gulf of Aden (Bower *et al.,* 2000, Banse, 1997, Johns *et al.,* 2000).

The Arabian Sea experiences a complex pattern of dynamical processes and shows strong variability in its physical dynamics and properties (Burkill *et al.,* 1993; Wiggert *et al.,* 2005). This indicates that the region is influenced by many differing forcing mechanisms and processes (DiMarco *et al.,* 2011). The Arabian Sea is also known to be one of the most productive oceans in the world due to its monsoon wind circulation (Banse and English, 1994) and a strong upwelling system, which increases the productivity in the northern Arabian Sea (Smith, 2001).

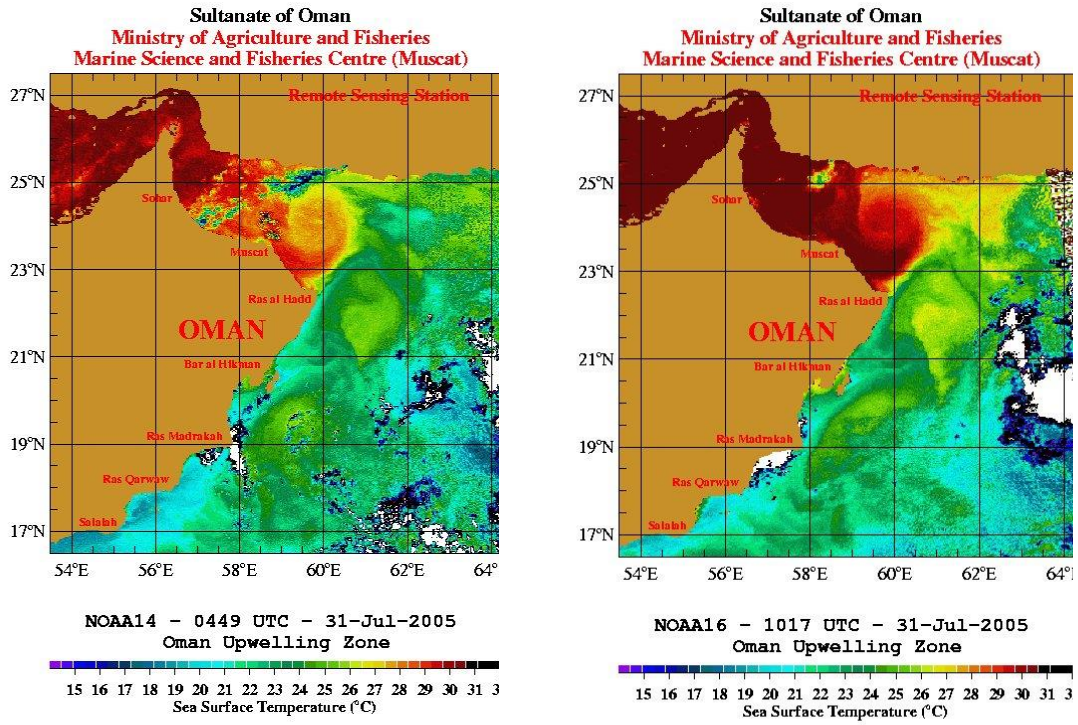

Figure 1.2. Satellite images received from two different satellites NOAA-14 and NOAA-16 at Muscat HRPT Remote Sensing Station on 31 July 2005. The image a) was scanned at 08:49 AM local time, and the image b) was scanned at 02:17 PM local time. Both images show the boundary created by the differences in sea surface temperature between the Sea of Oman and the Arabian Sea. Also, the two cyclonic and anticyclonic gyres can be obviously seen. (Al Shaqsi, unpublished).

At the onset of the summer season in May, the wind strength increases due to the low atmospheric jet (Findlater Jet), which blows strongly and passes over Somalia towards India, crossing Socotra Island (Findlater, 1969). This atmospheric jet has a significant effect in controlling major physical processes of the Arabian Sea (Bauer *et al.,* 1991, Smith *et al.,* 1998; Figure 1.3), and creates a very strong SWM with wind speeds much

stronger than the NEM (Rudnick *et al.,* 1997).

In the Arabian Sea, the NEM winds prevail during northern winter (December - February), while the reversed and stronger SWM winds prevail during northern summer (June - August). The SWM creates significant coastal upwelling along the Omani coast (Morrison *et al.,* 1998; Elliott and Savidge, 1990), causing continuous jets of cold upwelled water that move hundreds of kilometers offshore of the Oman coast (Brink *et al.,* 1998; Böhm *et al.,* 1999; Young and Kindle, 1994). This upwelling is associated with much stronger winds that blow parallel to the Omani coastline (Shi *et al.,* 1999; Burkill *et al.,* 1993; Sastry and DiSouza, 1972). This strong upwelling regime is the result of the Ekman transport of the surface water offshore (Böhm *et al.,* 1999; Shi *et al.,* 1999; Swallow, 1984; Manghnani *et al.,* 1998), and it extends hundreds of kilometers offshore from the Oman coast due to positive wind stress curl (Morrison *et al.,* 1998; Böhm *et al.,* 1999). This SWM causes the maximum current velocity of the RH-Jet to reach 1.0 ms^{-1} (Bohn *et al.,* 1999).

The physical and the biogeochemical properties of the Arabian Sea are also affected by the surrounding marginal seas (Johns *et al.,* 2000). As the results of these effects, some eddies or gyres are created, but the formation mechanism of these eddies is not well known (Wilson-Diaz *et al.,* 2001).

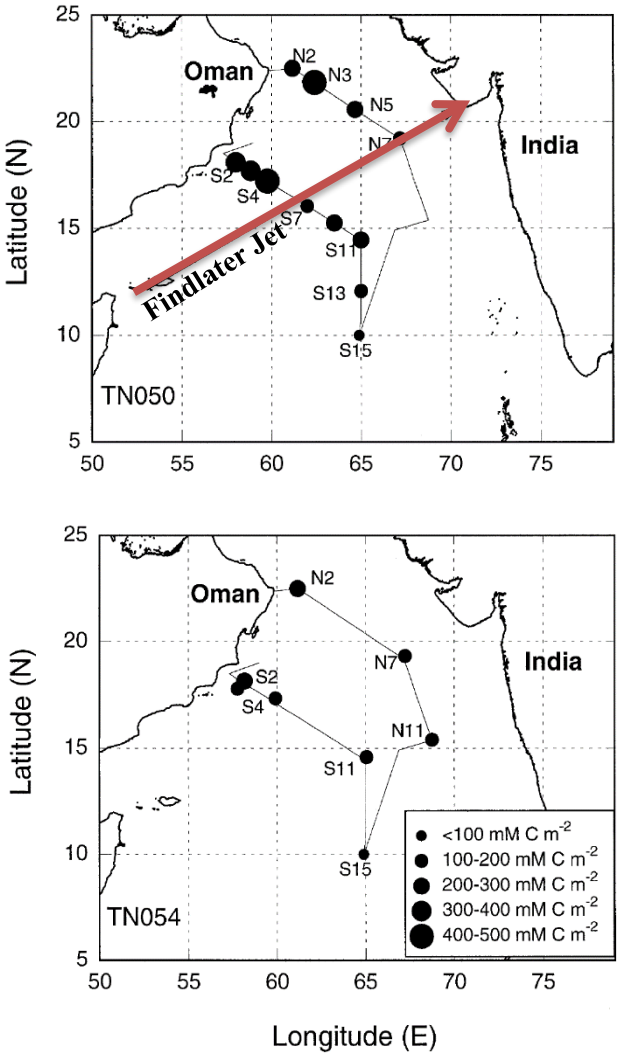

Figure 1.3. The approximate position of the axis of the atmospheric Findlater Jet in the Arabian Sea. The figures show the effects of the Findlater Jet on ocean productivity during the southwest monsoon season (Top panel). The Findlater Jet is absent during the northeast monsoon season (Bottom panel). The diameter of the filled circle indicates the biomass level (Smith *et al.,* 1998. The sampling track is the U.S. JGOFS Arabian Sea study).

Moreover, the Arabian Sea is well known for its high productivity within the Indian

Ocean, which in general possesses higher productivity water masses than other

surrounding oceans (Brock *et al.,* 1991; Naqvi, 1987; Smith, 2001), with the highest productivity being found in the landward side of the Findlater Jet (Figure 1.3).

Studying the northwest Arabian Sea, in particular, the RH-Jet, is important to the understanding of the general circulation and the force's response of the RH region, and how currents or ocean circulation in this region affect or stimulate the distribution and the transportation of plankton and fish larvae in the surrounding areas. Therefore, the main goal of this study is to combine satellite remote sensing long-term datasets with the **first ever long-term time series of moored data** in the RH region and to find out the characterization, and variability, of the RH-Jet and its relationships to physical forcing in the northwest Arabian Sea.

1.3 Scientific Questions and Hypotheses

Since few studies have attempted to understand water circulation and the RH-Jet that flows between the Sea of Oman and the Arabian Sea, there are still many important issues that are not well understood. This study focuses on how the RH-Jet is formed, what the main source of its generation is, and how it varies spatially and temporally. The main objectives/goals of this study are to understand and to characterize the variability of the RH-Jet and its relationships to physical forcing using long-term remote sensing datasets.

The main guiding points are illustrated here in a question form and they are:

- What are the main source and driving mechanisms of the RH-Jet?
- What is the temporal and spatial variability of the RH-Jet?
- What is the role of the SWM in influencing the RH-Jet?
- What is the role of the warmer water masses from the Sea Oman?

This dissertation tests two hypotheses regarding the RH-Jet.

1) The Somali Current is the main source of the RH-Jet, and

2) the SWM is the main driving force for the RH-Jet.

1.4 Organization

This dissertation is organised into five chapters. Chapter I presents an introduction of oceanic jets/fronts in the world oceans, an overview of the study area, the Arabian Sea, including study objectives, and the hypothesis behind this research. Chapter II explains an overview of the data and research methods used in this dissertation. Chapter III presents the results from remote sensing SST datasets that were analysed using the Cayula and Cornillion algorithm (1992) to detect and to determine the temporal and spatial distribution of oceanic thermal fronts. In addition, results of moored datasets, Argo floats, the spatial and temporal variability of SST and geostrophic currents in the study region are presented. Chapter IV presents the discussions of this research. Chapter V summarises the findings in the previous chapters, providing the conclusions of this study, and suggests future studies regarding fronts and jets in the northwest Arabian Sea.

CHAPTER II

DATA AND METHODOLOGIES

2.1 Datasets and Data Sources

This study uses a combination of satellite remote sensing and *in situ* observations datasets. These datasets were obtained from different sources and they comprise remote sensing such as sea surface temperature, sea surface height, geostrophic currents, and sea surface winds. *In situ*, observational datasets are Argo floats, mooring systems, and surface wind measurements (Table 2.1).

2.1.1 Remote Sensing Datasets

The main reason for this project depending mostly on remote sensing datasets was the paucity of observational data for the study area. The mooring system alone was not able to resolve the main goal of the project. This is due to the design of these moorings and to the way in which they were distributed in the northwest Arabian Sea. Remote sensing datasets that were used in this project are the sea surface temperature (SST), sea surface height (SSH), geostrophic current, and sea surface wind (SSW) collected by different type of US. satellites (Table 2.1). Even though satellites have low temporal resolution (daily to monthly) compared to mooring systems, their spatial resolution is high (0.25 km – 10 km). For instance, NOAA weather satellites and NASA Aqua/Terra satellites have wide swath widths. NOAA satellites can

cover a wide range of the Indian Ocean up to 2300 km widths once during the daytime, and once during the night within a very short time of less than 15 minutes. This results in twice daily visits with a high spatial resolution of 1.1 km for AVHRR and MODIS instruments onboard of the NOAA and the AQUA/TERRA satellites, respectively.

Table 2.1. The table shows an example of some US. government websites that provide scientific datasets from satellite remote sensing, observation, and modelling datasets

Product	Website	Resolution	period
SST	http://podaac.jpl.nasa.gov	1.1 km, daily	2002-2014
	http://coastwatch.pfeg.noaa.gov/erddap/griddap/erdG1ssta1day.html/	1.1 km, daily	1995-2012
SSH	http://colorado.edu/realtime/gsfc_global-real-time_ssh/	25 km, 15 days	2005-2013
SSW	http://coastwatch.pfeg.noaa.gov/erddap/griddap/erdQSwindmday.html.	25 km, daily	2002-2012
Argo	http://www.argo.ucsd.edu/		2010-2015
Wind	http://cdo.ncdc.noaa.gov/pls/plclimprod/poemain.accessrouter?datasetabbv=DS3505	3 hrs	1983-2013

2.1.2 Autonomous Mooring System

Moored time-series datasets were obtained from the Oman Ocean Observing System owned and maintained by Lighthouse R&D. Enterprises, Inc. of Houston, Texas, sponsored by the Government of Oman, Marine Science and Fisheries Center. These mooring systems collected data from 2005 – 2014. Ocean current magnitude and

direction, water temperature, dissolved oxygen concentration, conductivity, turbidity, and pressure were collected at each of these four autonomous moorings systems with a sampling frequency of one hour. The first mooring was placed in the Sea of Oman and the other three moorings were located in the Arabian Sea (Figure 2.1). These moorings were first deployed in March 2005 and recording data to the end of 2009, using a single point Aanderaa Recording Current Meter (RCM-11) equipped with Aanderaa Doppler Current Sensor (DCS) technology (DiMarco *et al.,* 2008, Wang *et al.,* 2012).

The first mooring, Ras Al-Hadd North (RHN) was fixed at the Sea of Oman in Quriyat coastal waters, northwest of Cape-RH. The current meters attached to the mooring line were fixed at different depths, and the total water column depth at RHN mooring was approximately 2971 m. The second mooring Ras Al-Hadd Middle (RHM) was in Cape-RH waters where the Arabian Sea meets the Sea of Oman (Johns *et al.,* 2000). This region is the main focal point of this project. The RHM mooring was fixed at the total water-column depth of 2971 m. The third mooring, Ras Al-Hadd South, (RHS) located at Al-Ashkharah in the Arabian Sea waters, South of Cape-RH, and this mooring was fixed at a water column depth of around 3021 m. The fourth mooring was on the Murray Ridge, (RHR) around 263 km East of Cape-RH and this mooring was anchored deep at 2859 m depth (Table 2.2, Figure 2.1).

Table 2.2. The table shows depths of the RCM-11 current meters and the mooring geographic locations at the Ras Al-Hadd region. for RHN, RHM, RHS, and Ras Al-Hadd Murray Ridge (RHR).

Mooring	Instrument	Lat (^{0}N)	Lon (^{0}E)	Current-meter Depth (m)	Total depth (m)
RHN	RCM-11	23.4150	59.4439	255, 1162, 2067, 2971	2976
RHM	RCM-11	22.5414	60.4519	236, 2045, 2954	2971
RHS	RCM-11	21.5661	60.2631	290, 1186, 2099, 3011	3021
RHR	RCM-11	22.8717	62.3417	532, 1030, 1944, 2850	2859

Modified from (DiMarco *et al.*, 2008, Wang *et al.*, 2012).

Datasets from these moorings were manually downloaded from each instrument memory card or a Data Storage Unit (DSU) to a computer connected with a DSU Reader every 12 -18 months using an Aanderaa 5059 data reading program during recovery turnaround cruises (Figure 2.2).

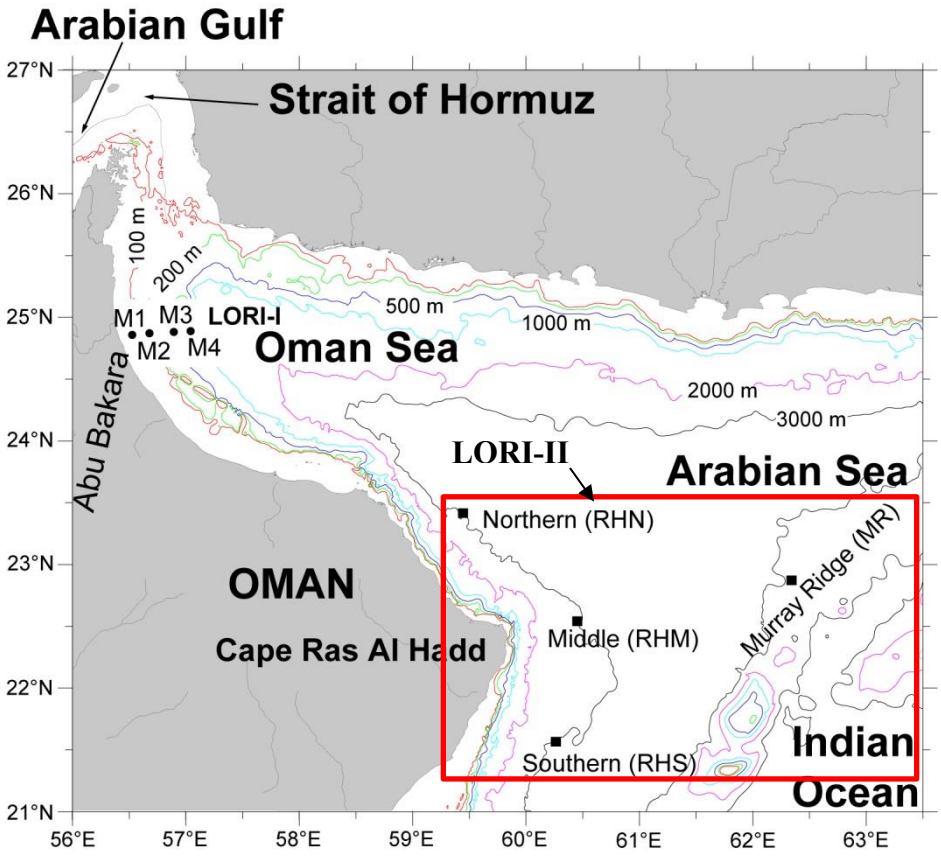

Figure 2.1. The map shows the LORI-I cabled system in the northern part of Oman and the LORI-II mooring sites. The mooring system was deployed at North of Cape Ras Al-Hadd (RHN), at the Cape Ras Al-Hadd (RHM), South of Cape Ras Al-Hadd (RHS), and the Murray Ridge (RHR). The red rectangle represents the study area. (From DiMarco *et al.*, 2011)

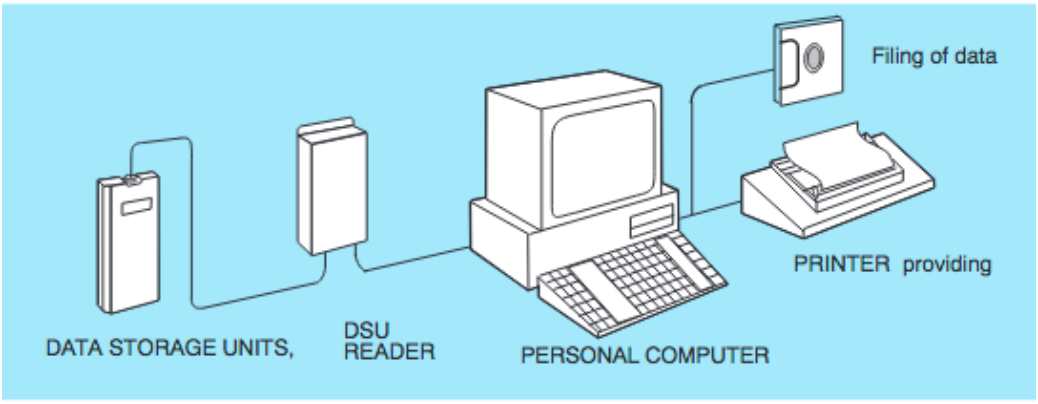

Figure 2.2. The schematic diagram shows how an RCM-11 current-meter raw data is downloaded during the recovery cruise. (Source: Aanderaa RCM-11 Operating Manual, 2002).

Fresh calibrated, and fully serviced RCM-11 current meters were used to replace the recovered moorings. Once the datasets were downloaded, the retrieved RCM-11 current meters were taken back to the shore station to be serviced, batteries replaced, and to be fully calibrated following oceanography standard techniques in accordance with the UNESCO Oceanography Manual (Unesco, 1991). Mooring cables or lines that showed a worn-out sign were removed and replaced with new marine cables.

2.1.3 Ras Al-Hadd Cabled Mooring System

The cable array in Ras Al-Hadd region is the 3-node LORI-II cabled observatory installed in late 2009. This was the first oceanographic deep cabled system to be established in the northwest Arabian Sea. The cabled moorings were fixed at the same locations of the autonomous moorings (Figure 2.3). The first node (RHN), the second node (RHM), and the third node (RHS) were located around 62, 112, and 205 km from the shore station, respectively.

This cabled system was installed using RDCP600s. Since most RCM-11 current meters for the autonomous system were fixed at depth greater than 500 m below the surface, a 75 kHz RDI Acoustic Doppler Current Meter and Profiler (ADCP) was fixed on top of each mooring looking upward the water column in order to catch ocean surface variability or the whole water column in the upper 500 m (Figures 2.3, 2.4 and 2.5). The near real-time raw data was sent from the coastal station located at Dhabaab fishing village to the Lighthouse office in Houston, Texas, via satellite communication for

monitoring and recording purposes before being sent to Texas A&M University, Department of Oceanography, at College Station, Texas, for quality assurance/quality control (QA/QC) and for processing (Stöessel *et al.,* 2010).

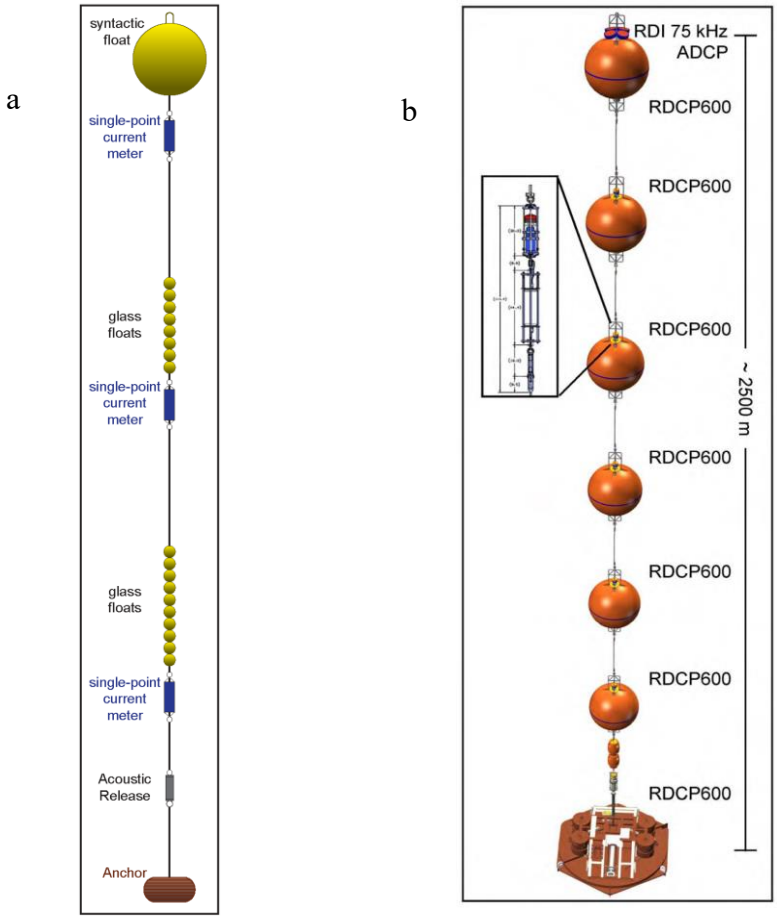

Figure 2.3. Mooring designs by Lighthouse R&D Inc., a) The autonomous single point Aandera current meters that were deployed at Ras Al-Hadd region during 2005 – 2010. The mooring is composed of a single point RCM-11 and glass floats attached at different depths and attached into the seafloor by a couple of heavy train rails, b) The cabled mooring system at Ras Al-Hadd region deployed at the end of 2009 to replace the autonomous mooring system. The mooring is composed of six Aandera RDCP600 attached at different depths and stuck on the seafloor by a base assembly that connects the shore station to the cable system. On the top, there is an RDI 75 kHz ADCP looking upwards the whole 500 m water column to the sea surface. (Adopted from Ingle *at al.,* 2012).

Figure 2.4. Current meters that were used for the autonomous and the cabled mooring systems at Ras Al-Hadd Region. 1) Aanderaa RCM11 single-point recording Doppler current meter with sensors for the autonomous moorings, 2) Aanderaa RDCP600 recording Doppler current profiler for the cabled moorings, and 3) RDI 75 kHz Workhorse Long Ranger ADCP for the cabled moorings (http://www.aanderaa.com/productsdetail.php?Seaguard-RCM-30)

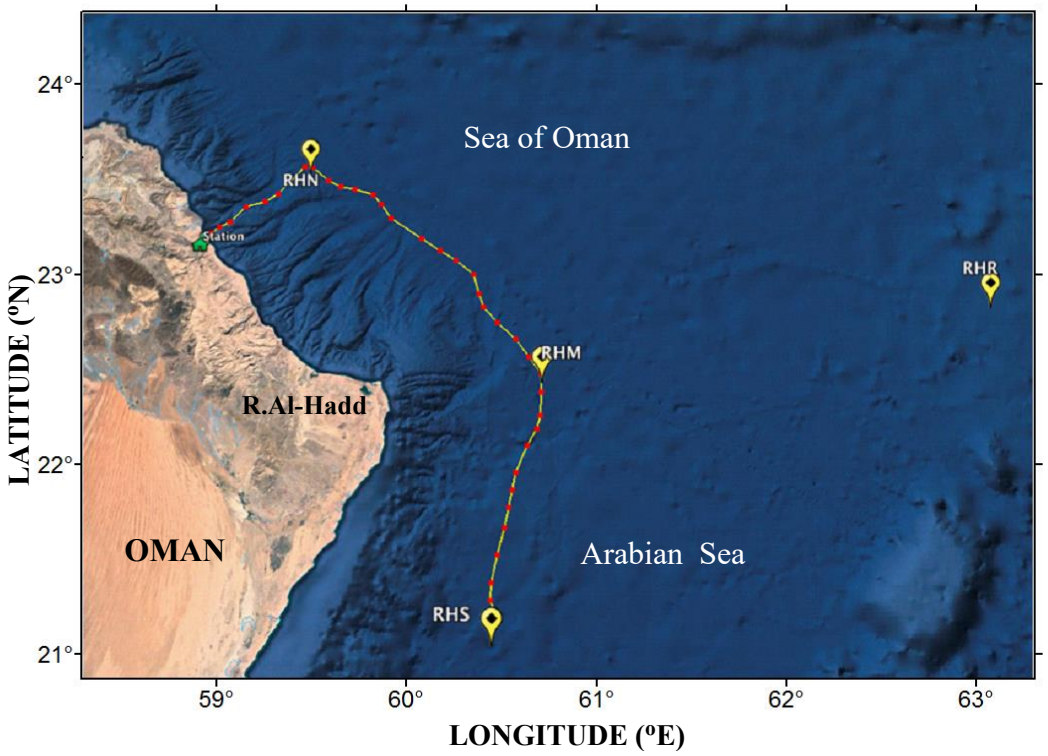

Figure 2.5. A map shows the location of the cabled mooring system and an approximate cable layout. This system was installed in late 2009, covered 3 nodes of the RHN, RHM, RHS connected to a shore station at Dhabaab fishing village. The Murray Ridge mooring (RHR) was not connected to the cabled system due to its distance from the shore station. (Google Earth Map, 2016).

2.1.4 Argo Floats

Argo datasets from 2002 - 2015 were obtained from the USGODAE Argo GDAC data browser (Table 2.1). After processing and performing QA/AC, it was found that these Argo profiles did not cover the entire Arabian Sea, except for the last five years (Figure 2.6). Therefore, only the last five years (2010-2015) of Argo profiles cover almost the

entire Arabian Sea during all seasons, thus providing useful *in situ* observational information in space and time.

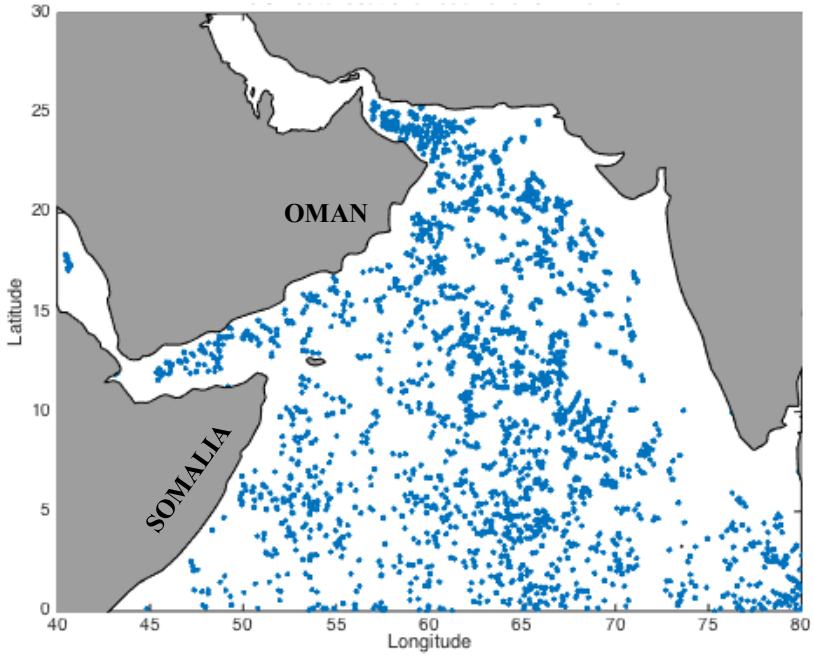

Figure 2.6. This map demonstrates where Argo profiles were available in the Arabian Sea for the year 2002-2015.

Argo floats were used to obtain vertical profiles in the surrounding waters near the Ras Al-Hadd waters. These floats collect physical parameters such as temperature, salinity, and pressure and some floats have an additional oxygen probe. Datasets from these floats were used for comparison with the moored observations. Temperature and salinity maps at different water depths were produced in order to follow water masses in the northwest Arabian Sea.

Argo floats normally profile down to 2,000 m every 10 days. Once a float is deployed it

starts diving at the speed of 10 cm s^{-1} for 6 hours till it reaches a preset depth, where it starts drifting horizontally with ambient currents for about 9 days before ascending to the surface (*NOAA*, 2012). The float then ascends to the surface at the same speed of 10 cm s^{-1}. The float spends about 6-12 hours at the surface waiting to transmit the recorded data to an incoming satellite after completing a full 10-day cycle. These floats record temperature, salinity, and pressure every 5 - 10 m in the upper-water-column and every 100 - 500 m in the deep-water column (Stryker, 2011, Vitale *et al.*, 2017)). A full description of how these floats works can be found at (http://www.argo.ucsd.edu/).
" These data were collected and made freely available by the International Argo Program and the national programs that contribute to it (http://www.argo.ucsd.edu, http://argo.jcommops.org). The Argo Program is part of the Global Ocean Observing System."

2.1.5 Surface Winds Products

Wind datasets were downloaded from the National Climatic Data Center website (Table 2.1, Figure 2.7). Winds have a direct impact on the surface circulation of the ocean and can impact subsurface circulation to some extent. Wind data were used to describe wind frequency and strength during different seasons. Winds recorded at Salalah station were used to represent the Somalia wind system, while winds data recorded at Sur, Ras Al-Hadd, and Masirah Island were used to represent RHN, RHM, and RHS, respectively. Moreover, sea surface winds were obtained from the National Aeronautics and Space Administration (NASA) website (Table 2.1). Sea surface wind datasets were used to

study wind patterns where there is no wind station such as the Somali and the Yemen coastal areas. Some of the data types used in this project are summarized in table 2.3.

Table 2.3. Part of the datasets, and their coverage period used in this project

Type	Measurement	Period
Moored	Current velocities, temperature.	2006 - 2012
Argo floats	Salinity, temperature, depth.	2010 - 2015
Satellites	SST, SSH, SSW, SSC.	2002 - 2014
Winds	e/w and n/s velocity components, direction.	1983 – 2013

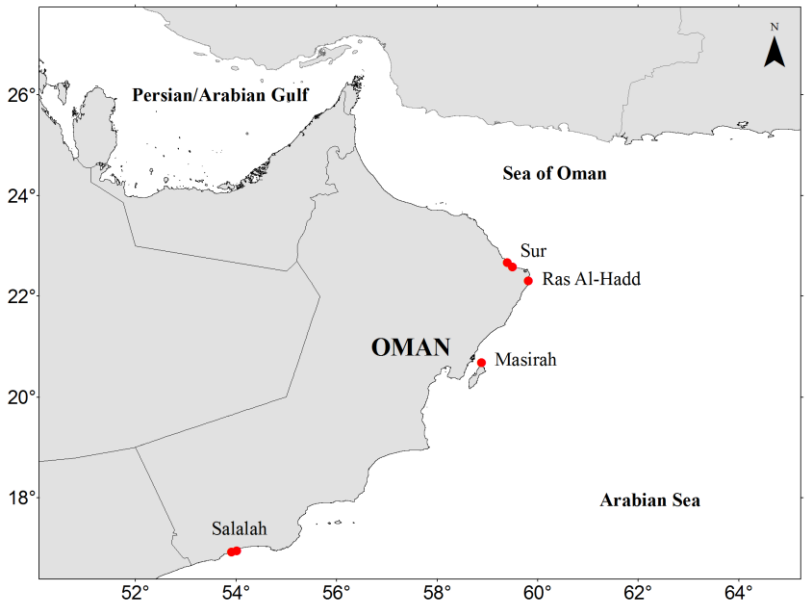

Figure 2.7. The Map shows the location of wind's stations or buoys (Red dots) along the coast of Oman. Some of these buoys are belongs to US. Airforce (USAF) and other are for the Oman Meteorology Department.

2.2 Methodologies

2.2.1 Basic statistics

Current meter raw datasets were converted into ASCII format using the 5059-Aandera software. Data quality assurance and quality control (QA/QC) were performed and the data were processed and analysed using MATLAB 2010, 2015, 2016 packages. Basic statistics were also performed to calculate current velocities (zonal and meridional velocities) for only those instruments located near the surface in order to fulfil the goal of this study.

Since RCM-11 current meters record current magnitude and its direction, east/west and north/south velocity components were calculated. The mean, variance, standard deviation, minimum, and maximum values were calculated for each parameter at each instrument. All data beyond 3 standard deviations ($\pm 3\sigma$) were considered as suspect and were flagged.

2.2.2 Frontal Analysis of Remote Sensing Data

Satellite remote sensing has become an important tool in providing environmental information with high spatial and temporal resolutions (Klemas, 2012). Understanding sea surface temperature (SST), sea surface height (SSH), sea surface winds (SSW) and other oceanographic and atmospheric physical/chemical parameters over a large spatial scales and temporal scales is crucial for the oceanography studies. SST is known to have

a direct impact on life for both the land and the ocean, controlling various processes related to both ocean and atmosphere. Moreover, it is one of the mechanisms that causes a threat to coastal residents, through creating hurricanes, tropical cyclones, typhoons and El-Niño, La-Niña, which cause floods in many cities, property damage, death and injury to residents of coastal areas, and marine life mortalities worldwide.

The availability of satellite data has increased and improved the ability to study the characteristics of oceanic fronts from satellite datasets (*Cayula and Cornillon*, 1995; Roberts *et al., 2010*; *Valavanis et al., 2005*). Thus, several edge detection methods have been developed and applied to oceanographic satellite images. Many approaches have been developed for detecting thermal fronts from remotely sensed datasets, and widely used edge detection algorithms are the Single Image Edge Detection algorithm (SIED), and the Multi-Image Edge Detection algorithm (MIED) developed by *Cayula and Cornillon,* 1992, 1995, respectively.

SIED is an automated method and can discriminate original thermal oceanic fronts from another thermal gradient on an SST image (*Miller*, 2004). The SIED algorithm is a tool in the Marine Geospatial Ecology Tools (MGET) developed by Duke University, Duke Marine Geospatial Ecology Lab, and can be freely downloaded from their website http://mgel.env.duke.edu/tools (*Roberts et al.,* 2010). A front edge detection is a useful approach in detecting oceanic fronts using SST or *Chl-a* high-resolution dataset (*Ullman*

and Cornillon, 2000). In order to detect the RH-Front, the modified SIED algorithm in the MGET GIS-tools was used.

2.2.2.1 Thermal Frontal Analysis

The MGET tool was installed and run in the GIS ArcMap 10.2 student package. Thirteen years (2002-2014) of daily SST fronts datasets covering 0.0° - 30°N and 40°E- 80°E were extracted using the modified Cayula and Cornillon (1992) single image edge detection (SIED) algorithm from the Group for High-Resolution Sea Surface Temperature, level 4 images (GHRSST L4 SST) hosted by NASA jet propulsion lab physical oceanography (JPL PO.DAAC).

The SIED algorithm indicates fronts when it detects differences between the mean temperatures of surounding waters that exceed the threshold (*Miller*, 2009). This Cayula and Cornillion algorithm was found to be successful and has been used to detect oceanic fronts in many regions (Podesta *et al.,* 1993; Kahru *et al.,* 1995; Hickox *et al.,* 2000; Mavor and Bisagni, 2001; Ullman and Cornillon, 2000, 2001).

The Cayula and Cornillon (1992) algorithm was developed originally for SST images. It operates at three levels. These are picture, window, and local/pixel levels. The algorithm examines the temperature histogram of each window in the satellite sea surface temperature image. Then it detects the edge using unsupervised learning methods and statistically deciding on the existence of boundaries.

Cloud cover is considered a major obstacle when detecting thermal fronts (Kahru *et al.*, 1995; Cayula and Cornillon, 1992). Most of GHRSST L4 SST datasets are cloud treated. A composite front map technique is used to treat satellite images with some cloud cover (Miller, 2009). This method combines the regions of frontal signals extracted from all clear areas in a series of SST images, to produce an overall view of dynamic ocean features (Miller, 2009). First, the cloud cover and atmospheric contaminations were filtered out by passing a 3 x 3 median-filter over each image. Then the free cloud image was segmented into many windows by passing a running 32 x 32 pixel window. Each window was processed independently to assess the probability that an edge exists in each window. Due to the cloud cover problem, especially during the SWM season, a compositing technique (Miller, 2009), was used by combining all cloud-free frontal data.

By using a 32 x 32 moving window with a 16-pixel stride or moving 16 pixels per step, the SIED runs a histogram algorithm to identify windows that show a bimodal histogram, suggesting that two distinct water masses are present, and to determine the value of SST that best separates the two water masses. Any unimodal histograms obtained were discarded because no edge was detected.

The mean difference between these two distinct water masses was calculated for those windows that show sufficiently bimodal distributions. When the mean difference exceeds the SST threshold (0.75^{o}C), then the two populations were considered to have fronts. The pixels were categorised into two population according to the best separation

value, and a spatial cohesion algorithm was applied to determine if these two population are sufficiently spatially separated. In windows that have sufficiently separate populations, any pixels in either water masses that are adjacent to pixels in the other water masses were marked. These marked pixels are the pixels that are along the front that separates the water masses. When all along front pixels have been identified, a contour following algorithm was run which extends fronts on either end as long as sufficient gradient (i.e. in SST) continues in the direction the front was pointing.

The oceanic thermal fronts detected on each day were converted into multiple raster GIS grids. The Cayula and Cornillon algorithm produced daily thermal frontal images. Each daily raster image contains seven different frontal classes that represent land, ocean, weak currents, and fronts (Table 2.4). A reclassification method was used in order to exclude land, ocean, weak fronts and noises in each daily image. In the reclassification method, unneeded features were set as zero and strong fronts were set as one. At the end, the reclassification tool extracted the class that met the criteria and discarded the remaining classes within the thermal frontal image. This method breakdown each frontal image into seven images with different classes that represents moderate and strong fronts. Class 7 represents strong thermal fronts and other classes represent moderate fronts. Monthly and seasonal means for class 7 thermal fronts were calculated. Also, the monthly and seasonal climatology of thermal fronts for 2003-2013 were processed using the reclassification outputs.

Using the reclassified images, climatology fronts were calculated and climatology frontal maps were produced. This explains that for a 13-year period all the 13 Januaries, 13 Februaries, 13 Marchs, and so forth, were combined to get the 13-year mean of each month. The same method was applied in different seasons. For instance, the probability of the SWM season was obtained from combining all June, July, and August months for the entire 13-year period.

Table 2.4. This table shows the result class codes of the thermal image after passing a 32 x 32 moving window on an SST AVHRR images collected by NOAA satellites**.**

Class Code	Coverage	Description
1	Land	The moving window occurs in a region where many of the pixels are masked due to land.
2	Weak fronts	The window is not centered on the front, causing it to contain a disproportionate number of pixels from one population.
3	Ocean	The difference between the mean values of the two populations was too small, compared to the threshold.
4	Weak fronts	The criterion function that was calculated was found to be too small. The two populations are not sufficiently bimodal to indicate that a front exists in the window.
5	Weak fronts	The cohesion of one or the other population was insufficient. The pixels of the two populations are spatially mixed, and are not spatially separate, as occurs when a front is present.
7	Strong fronts	The window passed all of the algorithm's tests and was classified as containing a strong front.

2.2.2.2 Cumulative Frequency Technique

Before calculating the thermal front cumulative frequency, a section at the Ras Al-Hadd region was clipped from the Arabian Sea thermal front raster image using the clipping tool in ESRI GIS 10.3. The clipped area represents 21.00ºN - 24.00ºN, 59.80ºE - 64.00ºE, and covered around 120 x 10^3 km^2. The clipped data was automatically saved in a database format (dbf). These dbf files were then converted to ASCII format to be read by a Matlab package and by Microsoft Office package. Pixel cumulative frequency that represents thermal fronts was calculated, and statistical graphs were then created. Cumulative frequency was estimated by taking the sum of all previous frequencies up to the last point of these frequencies using only the clipped class 7 thermal fronts.

2.2.2.3 Sea Surface Winds and Geostrophic Currents

Sea surface wind speed and geostrophic currents datasets that represent the study area were extracted from the global long-term time-series data. Although these data were QA/QC treated, another QA/QC was applied to make sure that the wind speed and the geostrophic current velocities are within the acceptable range. Any outliers found were flagged as bad data. Base maps representing winds and currents were created in the Matlab package.

2.2.3 Argo Datasets

Although the data supplier passed Argo profiles through a QA/QC, during this study an additional QA/QC was performed. Outliers and spikes were removed by checking the

overall data range (T ≥ 35°C and T ≤ 2°C, S ≥ 40 PSU and S ≤ 30 PSU, P ≥ 2001 dB), where T, S, P, are temperature, salinity, and pressure, respectively. All datasets falling beyond ±3 standard deviations (≥ 3σ and ≤ -3σ), were flagged as bad values.

Argo float datasets were analysed by season and processed using an academy Matlab package. Monthly means were calculated and base maps of both salinity and temperature at different depths were produced. A 5-year climatology of each season was run.

2.2.4 Mooring Systems in the Ras Al-Hadd Region

Current velocities recorded by ADCP from the cabled mooring system were processed after removing outliers. Graphs starting at depth 10 m to around 450 m depth were plotted. For the autonomous mooring system, only RCM-11 current meters located at depths less than 300 m in the Ras Al-Hadd region were used here. This is because the remaining current meters were fixed far too deep and they were designed specifically to record deep water currents. Since the RCM-11 does not directly measure zonal and meridional velocities, therefore zonal and meridional components were calculated from the current direction and magnitude using the following equation:

$$u = Mcos\ \theta \text{ and } v = Msin\ \theta$$

where u is the east/west component, v is the north/south component, M is the current magnitude or current speed, and θ is the compass or the speed direction after converting it to the true North.

2.2.5 Wind Datasets

The 3-hourly interval raw wind datasets were filtered with a 40-hour low-pass filter to remove the tidal and inertial variability. A QA/QC was performed. Outliers and spikes were removed. All datasets falling beyond ±3 standard deviations ($\geq 3.0\ \sigma$ and $\leq -3.0\ \sigma$), were flagged as bad values. monthly means and variances were calculated.

CHAPTER III

RESULTS

In this chapter, the analysed daily satellite remote sensing thermal front datasets (2002-2014) are presented. The Ras Al-Hadd thermal fronts were detected using the Cayula and Cornillon (1992), single image edge detection (SIED) algorithm. The MGET-tool produced approximately 5000 daily output thermal frontal raster images for 13 years of the study period. In addition to the results of thermal fronts, sea surface temperature, salinity from Argo floats, geostrophic currents, sea surface height, currents from mooring systems and wind patterns are also presented here. The study area for this project is the region near Cape Ras Al-Hadd, and is confined within 21.00°:24.00°N and 59.80°:64.00°E, but the Arabian Sea (0°:30°N, 40°:80°E) was also covered in order to track the Somali Current (SC) and the East Arabian Current (EAC) to find out if they have an influence in creating the Ras Al-Hadd Jet.

3.1 Spatial and Temporal Variability of Thermal Fronts during the Pre-SWM

3.1.1 Thermal Fronts

During the Pre-SWM (April/May) the wind force starts to rise gradually, creating the onset of the SWM, which starts in June. The western Arabian Sea experiences the beginning of the roughness of the sea surface. No thermal fronts were detected at Cape-RH during this period (Figure 3.1).

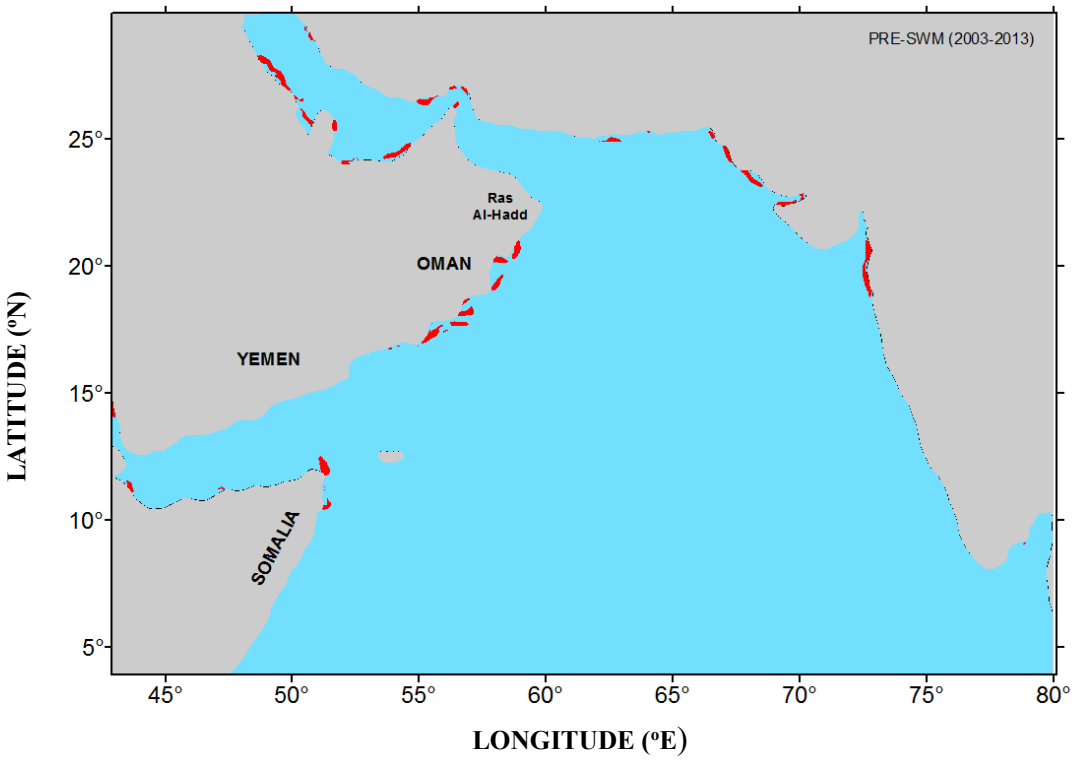

Figure 3.1. This figure demonstrates 11-years climatology thermal fronts (red) during the Pre-SWM (April/May 2003-2013). It also shows currents start forming off the Somalia coast and their movements toward the Gulf of Aden.

3.1.2 Sea Surface Temperature

During this time of the year, the sea surface temperature in the Ras Al-Hadd region ranged between 27 – 29.5°C and the annual mean was about 28°C. The years 2007 and 2010 experienced the highest sea surface temperature during this period of the year (Figure 3.2).

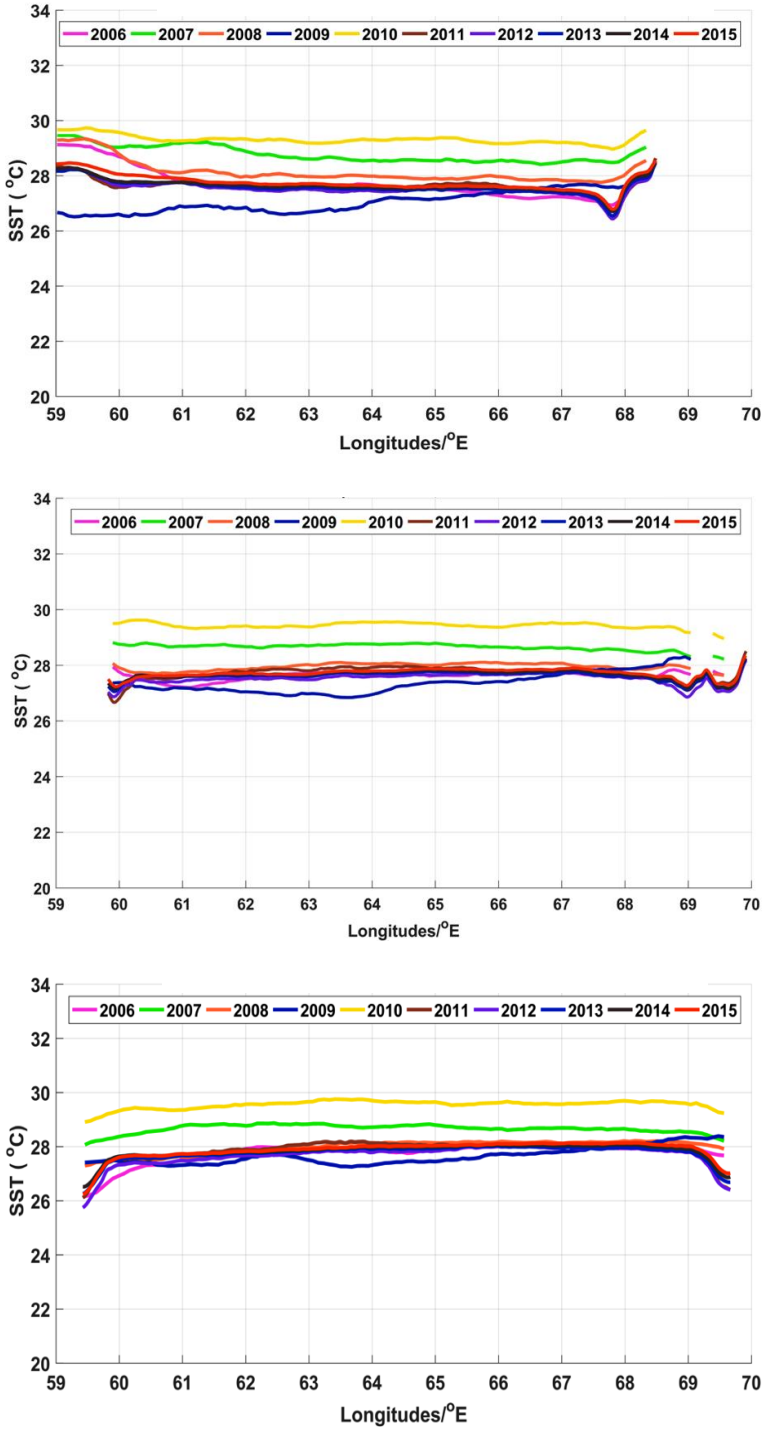

Figure 3.2. This Figures show zonal sea surface temperature during the Pre-SWM season in the Ras Al-Hadd region. The top panel shows the zonal temperature at RHN, the middle panel shows temperature at Cape-RH or RHM, and the bottom panel shows the temperature at RHS.

3.1.3 Argo Floats

Salinity recorded by Argo floats during 2015 showed a high salinity in the Sea of Oman compared to the southern part of the Arabian Sea where low salinity waters are pumped from the Bay of Bengal. Water temperature was low in the Sea of Oman and high in the southern Arabian Sea (Figure 3.3).

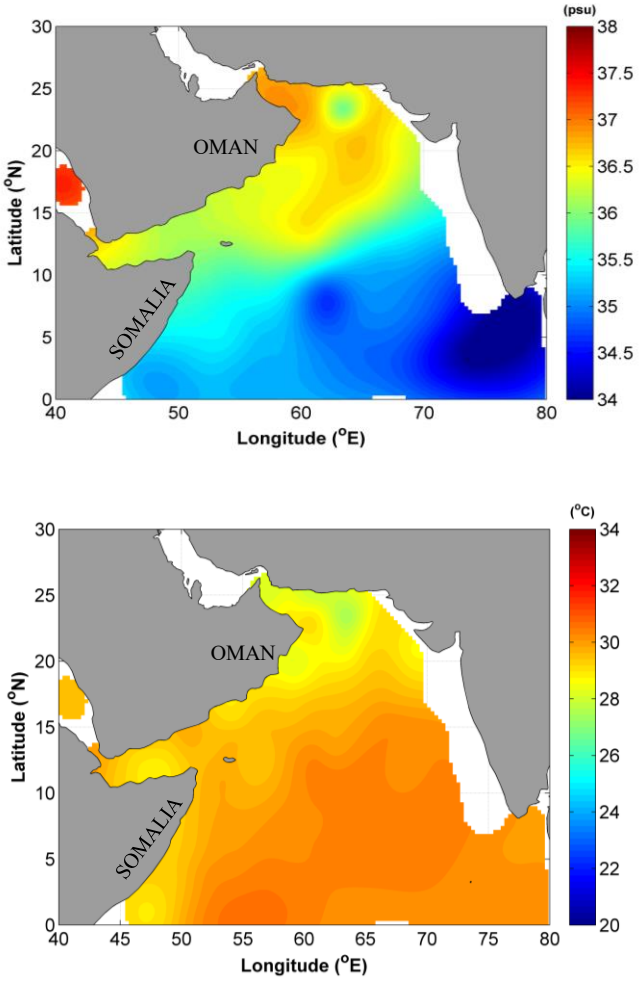

Figure 3.3. The maps show salinity and temperature distribution collected by Argo floats during the Pre-SWM 2015. The top panel shows weak gradients of salinity waters in Cape-RH while the bottom panel shows weak gradients of temperature.

3.1.4 Sea Surface Height and Geostrophic Current

During the Pre-SWM seasons, the wind starts to gain momentum and already reversed to the southwest direction. The Somali Current and the East Arabian Current do not have the force to move northeast to reach Ras Al-Hadd region (Figure 3.4).

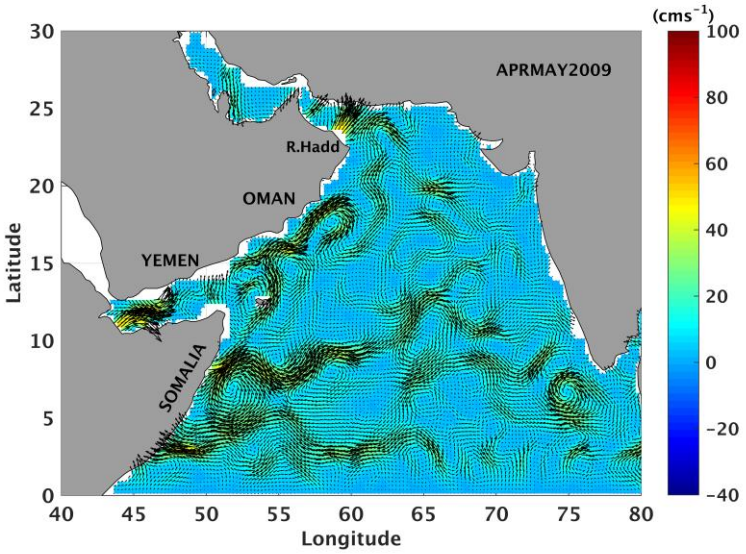

Figure 3.4. The map shows geostrophic current during the Pre-SWM.

3.1.5 Mooring System

The ADCP recorded strong surface currents at Cape-RH but the velocity was under 100 cms^{-1} during April and May 2010 and 2011 (Figure 3.13). During this time, the current direction had changed from NE direction to the SW direction.

3.1.6 Winds System

In April, the wind system in the Arabian Sea completes the reversal of its direction from the northeast to the southwest direction. The wind speed at Ras Al-Hadd region during this time is under 10 ms^{-1} (Figure 3.16; 3.17). The wind station at Masirah Island, which is located approximately 200 km South of Cape-RH show similar wind patterns during the Pre-SWM. The wind station of Salalah, South of Oman, was used to represent the wind patterns of the Somalia coast. The wind system at Salalah exhibited the same Ras Al-Hadd wind's patterns towards the northeast direction.

3.2 Spatial and Temporal Variability of Thermal Fronts during the SWM

3.2.1 Thermal Fronts

During the SWM (June - August) the monsoon intensity rises gradually and peaks during July/August. The surface currents formed a continuous band along the coast of the western Arabian Sea. This current movement is influenced by the Somali Current (SC) and the Gulf of Aden Surface Water (GASW). A part of the Somali Current accelerated northward passing through the Socotra Island and mixed with the Gulf of Aden Surface Water. Both the GASW and the SC moved northeast parallel to the coast of Yemen where they merged with the East Arabian Current (EAC) along the coast of Oman. The EAC, which is the northeast extension of the SC, moves approximately 1100 km northeastward along the coast of Oman until it reaches Cape-RH. When the EAC reaches Cape-RH, it turns right where it meets the warm Sea of Oman water and moves

towards offshore either to the northeast or to the east directions forming the RH-Jet or the RH-Front (Figure 3.5, 3.6). Part of the RH-Jet deviated southward creating the anticyclone eddy south of the RH, and another part creates the cyclonic eddy north of Cape-RH.

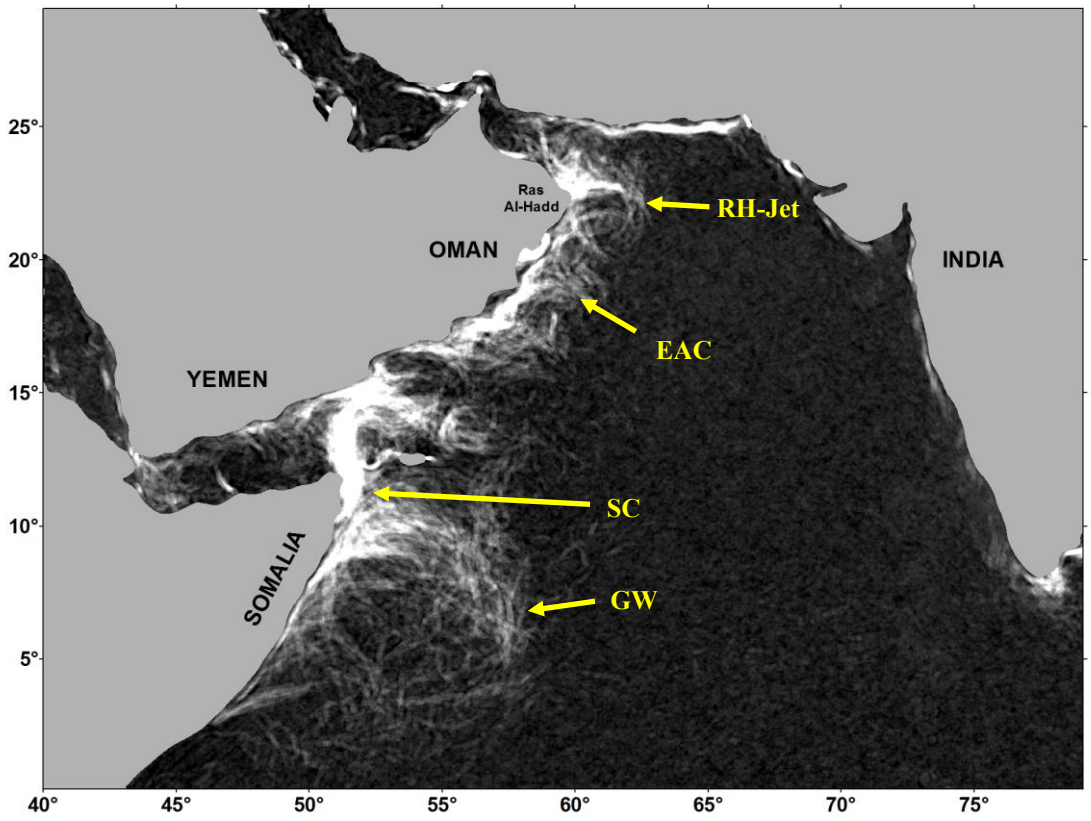

Figure 3.5. The map shows climatology thermal fronts during the SWM season (2012-2013). Currents are already intensified and the SC can be seen moving toward the coast of Yemen, crossing the Gulf of Aden, passing between the Somalia coast and the Socotra Island. The EAC continues moving to the northeast direction until it reaches Cape-RH where it meets with the Sea of Oman warm waters creating the RH-Jet.

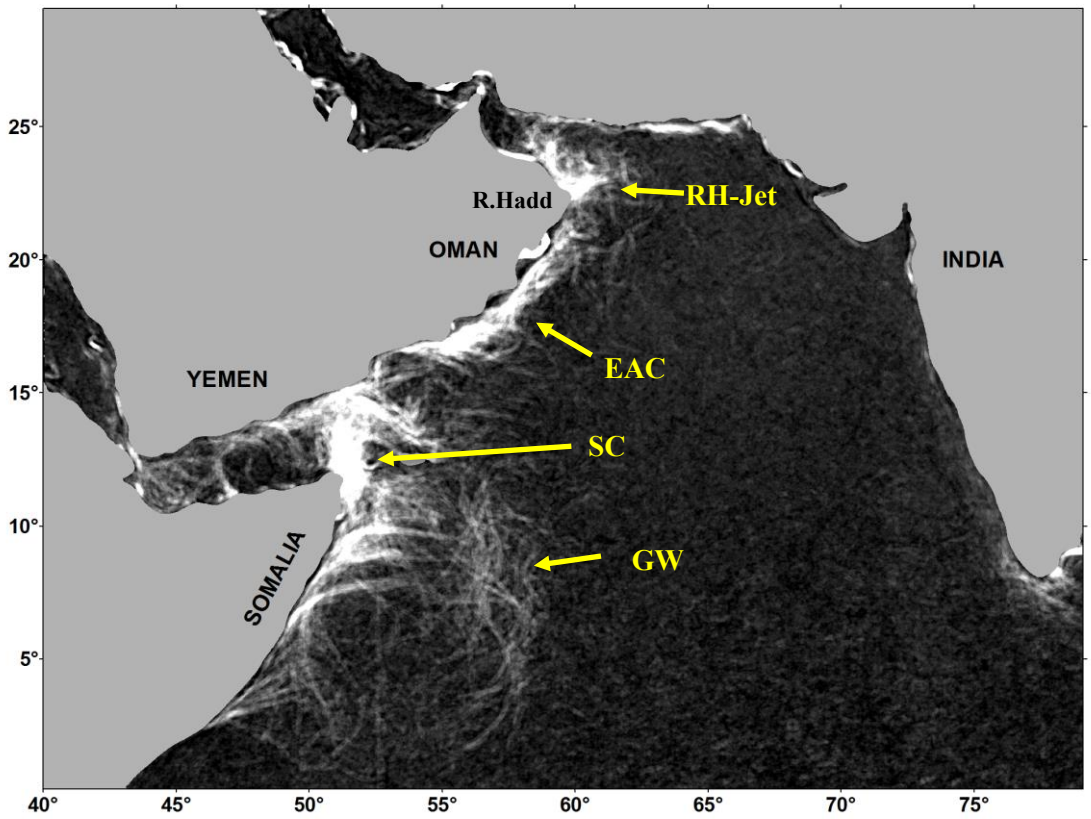

Figure 3.6. The frontal map shows thermal fronts during the SWM 2006-2008. The Great Whirl (GW), the Somali Current (SC), East Arabian Current (EAC), and the RH-Jet, can be seen during this season.

3.2.2 Sea Surface Temperature

During the SWM season, the warm and high salinity Persian Gulf Water mass (PGW) moves southwards and penetrates the Sea of Oman at the depth range 150 – 300 m. The sea surface temperature of the Sea of Oman increases during the summer season, while in the Arabian Sea decreases. The difference in sea surface temperature during this season was observed to be 10 - 15^{o}C less in the Arabian Sea, especially in the upwelling areas of the western Arabian Sea (Figure 3.7).

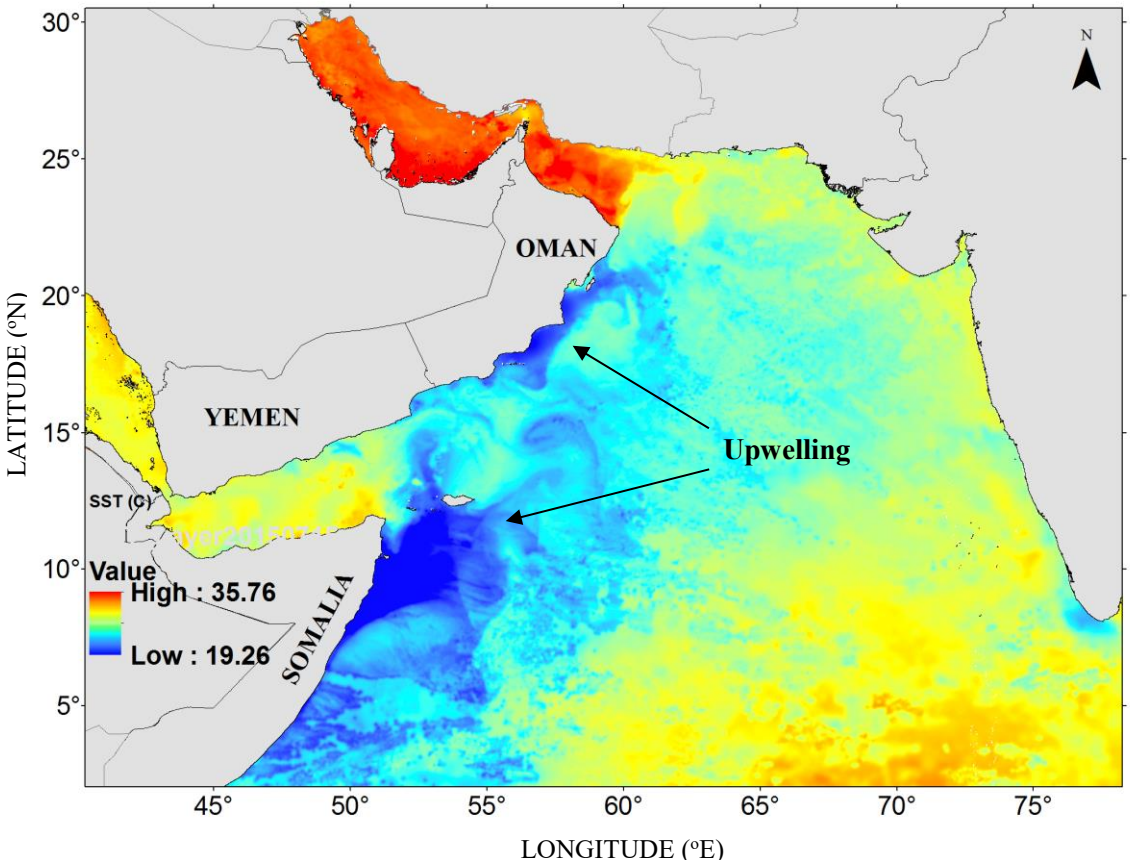

Figure 3.7. This satellite image acquired on July 15, 2015 shows the differences in sea surface temperature between the Sea of Oman and the Arabian Sea during the peak of the southwest monsoon. The minimum detected SST was 19ºC in the western Arabian Sea, while the maximum detected SST was 35.76ºC in the Sea of Oman and the Arabian/Persian Gulf.

During 2009, the mean zonal SST increased to 32°C near the coastal water North of Ras Al-Hadd at latitude 23.00°N and decreased to around 28ºC at longitude 61°E after crossing around 300 km towards offshore of the Arabian Sea (Figure 3.8a). The remaining years (2006 – 2015) the mean water temperature was around 30°C at the coast, then showed a drop of 3°C after crossing around 165 km from the coast of the

same latitudes. Water in the North of Ras Al-Hadd preserved its temperature between 28 and 29^{o}C all the way across the Arabian Sea before declining below 28^{o}C near the west coast of India.

The seasonal mean sea surface temperature (2006-2015) at Cape-RH demonstrated cooler water between 26 and 27^{o}C in the coastal waters of the Omani side, while the temperature keeps increasing across the whole basin at latitude 22.40^{o} N until the Indian coastal waters where the temperature declined again but remained relative warmer by 2^{o}C compared to the cool waters in Cape-RH (Figure 3.8b). The minimum and maximum temperature recorded during the SWM seasons 2006 - 2015 at Cape-RH were 18^{o}C and 28^{o}C, respectively.

The temperature was cooler south of Cape-RH at latitude 21.50^{o}N along the Arabian coast, while these waters become warmer along the Indian coast. The minimum zonal mean SST ranges between 24-26^{o}C of the Oman coast during the SWM of 2006-2015 except 2007 and 2009 when the zonal mean SST increased to 27.8 and 28.8^{o}C, respectively while of the Indian coasts the water mass was warmer between 27-29^{o}C (Figure 3.8c)

a

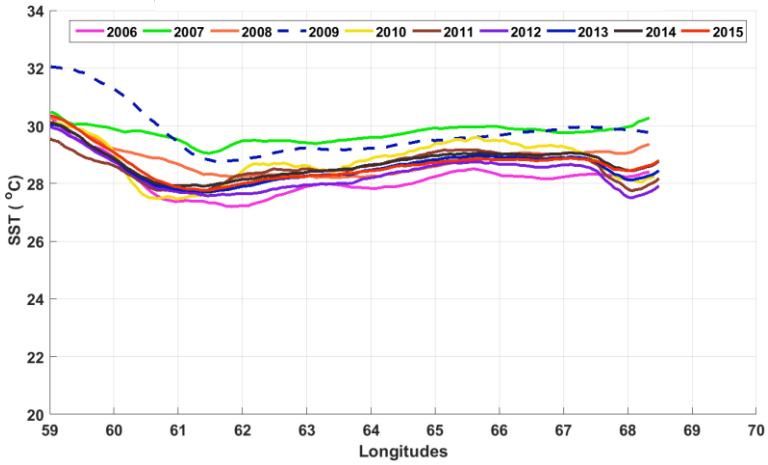

b

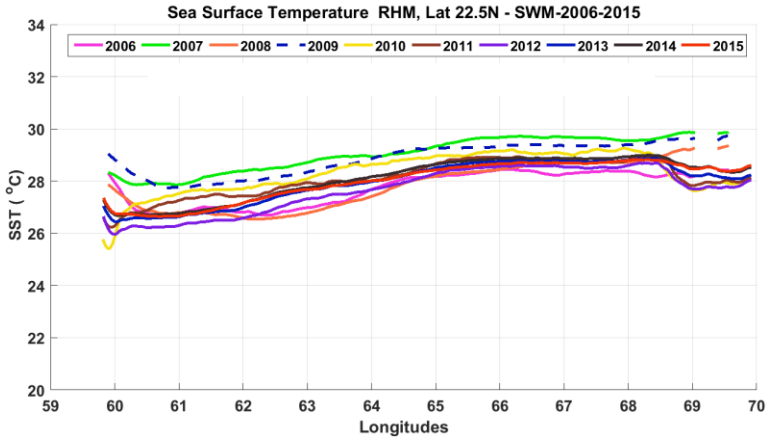

Figure 3.8. Annual zonal SST spatial and temporal variability during the SWM 2006–2015 shows a) Sea surface temperature RHN at the Sea of Oman experienced high temperature near the coast of Oman, The SST decreased gradually to 28ºC at longitude 61ºN and keep rising until the coastal waters of India where the SST plunged to under 28ºC at longitudes 68ºN. b) SST at the Cape-RH shows cooler water in the coastal water of Oman side, while the temperature keeps increasing offshore to the Indian coastal waters where the temperature dropped, but relatively warmer compared to the cool waters in Cape-RH, c) The temperature is cooler at RHS in the Omani side while these waters become warmer in the Indian site.

c

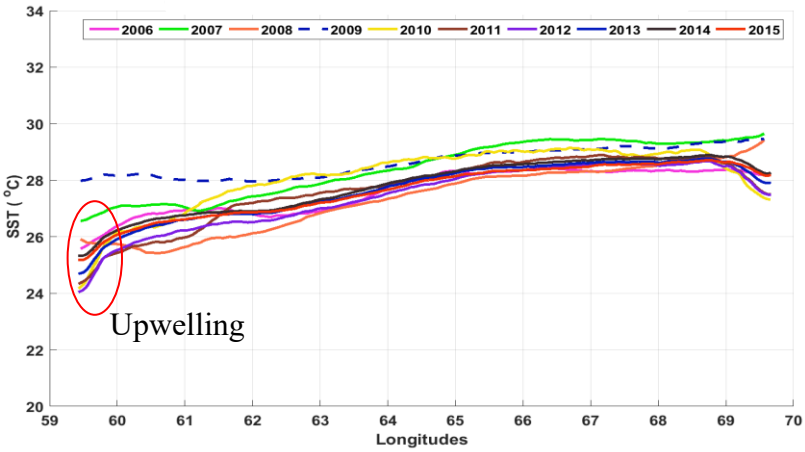

Figure 3.8 Continued

3.2.3 Argo Floats

Although Argo floats covered the Arabian Sea for the year 2002 – 2015, these floats were absent in the coastal waters of the northwest Arabian Sea during the years 2002 - 2012. During this period, most of these floats were concentrated in the central Arabian Sea. Therefore, floats covered the coastal waters of the study area for only the three years 2013-2015.

Argo floats recorded higher salinity in the Sea of Oman during the SWM seasons. The RH-Jet prevented this high salinity water in the sea of Oman from entering to the Arabian Sea. In addition, the southern Arabian Sea was pumped with fresher or less saline waters from the Gulf of Bengal (Figures 3.9 and Figure 3.10).

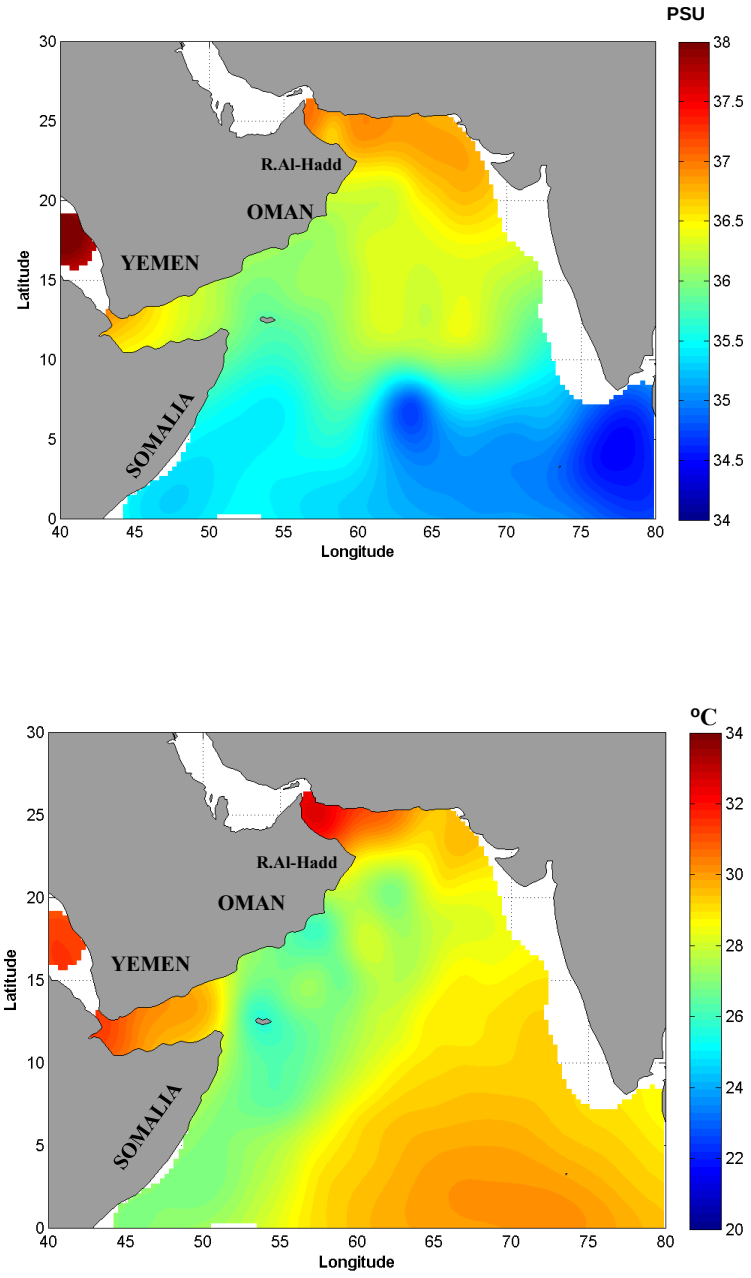

Figure 3.9. Salinity distribution (top panel), and temperature (bottom panel) at 5 m depths from Argo floats during the SWM season June - August 2015. The Ras Al-Hadd front separates warm, high salinity water masses in the Sea of Oman from cooler less salinity water mass in the Arabian Sea. The top panel also shows the effect of the Bay of Bengal on salinity in the southern Arabian Sea. Less saline water from the Bay of Bengal is propagated to the Arabian Sea.

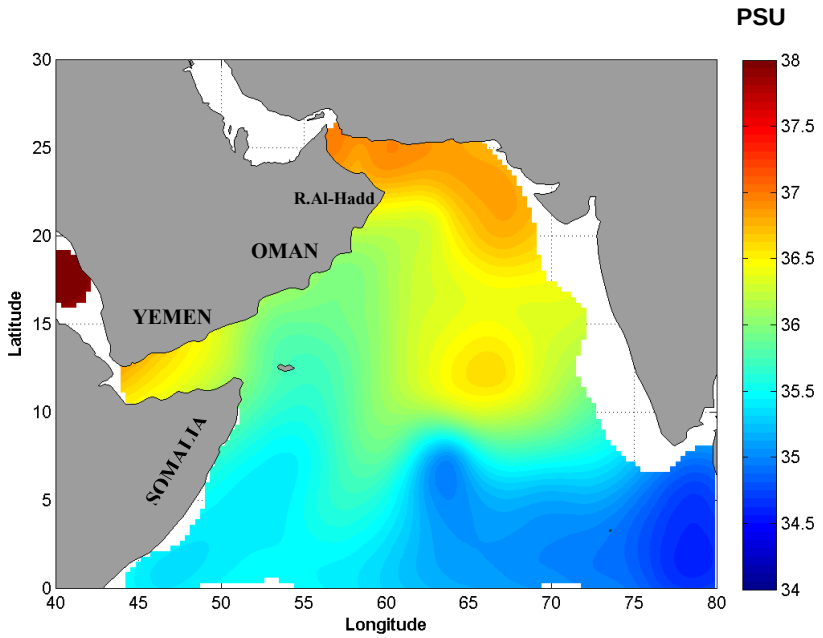

Figure 3.10. Salinity distribution at 5 m depths from Argo floats during the Peak-SWM July/August 2015. The Ras Al-Hadd Front separates water masses of high salinity in the Sea of Oman from water masses of less salty in the Arabian Sea. The image also shows the effect of the Bay of Bengal through the flow of its low salinity waters into the southern Arabian Sea.

3.2.4 Sea Surface Height and Geostrophic Currents

During the SWM seasons, the Somalia Great Whirl was observed near the coast of Somalia and the strong Somali Current was observed moving to the northeast direction where it then joined to the East Arabian Current (EAC). The EAC moves parallel to the coast of Oman toward Cape-RH, creating some eddies of the Oman coasts (Figure 3.11, 3.12). The geostrophic velocities exceeded 100 cms^{-1} for all the years except in 1995 and 1997 when the maximum mean velocity was around 70 cms^{-1}.

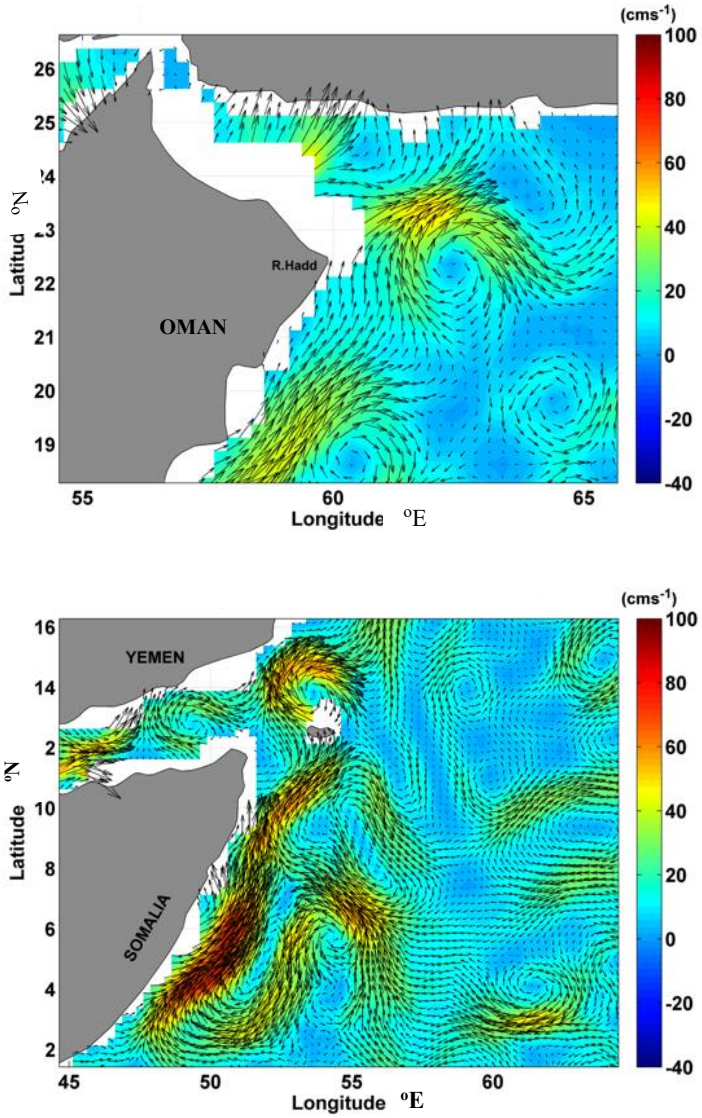

Figure 3.11. These maps show current movements during the SWM 1997. The top panel shows the Ras Al-Hadd region and the bottom panel shows Somali Current waters and the Gulf of Aden. Strong SC is shown moving to the northeast passing near the Socotra Island and mixes with the GOAW, gaining momentum, and moves to the northeast parallel to the coast off Oman and merges with the EAC until reaching Cape-RH where these cool waters meet the warm Sea of Oman water creating the RH-Front due to the differences in both temperature and salinity of these two water masses.

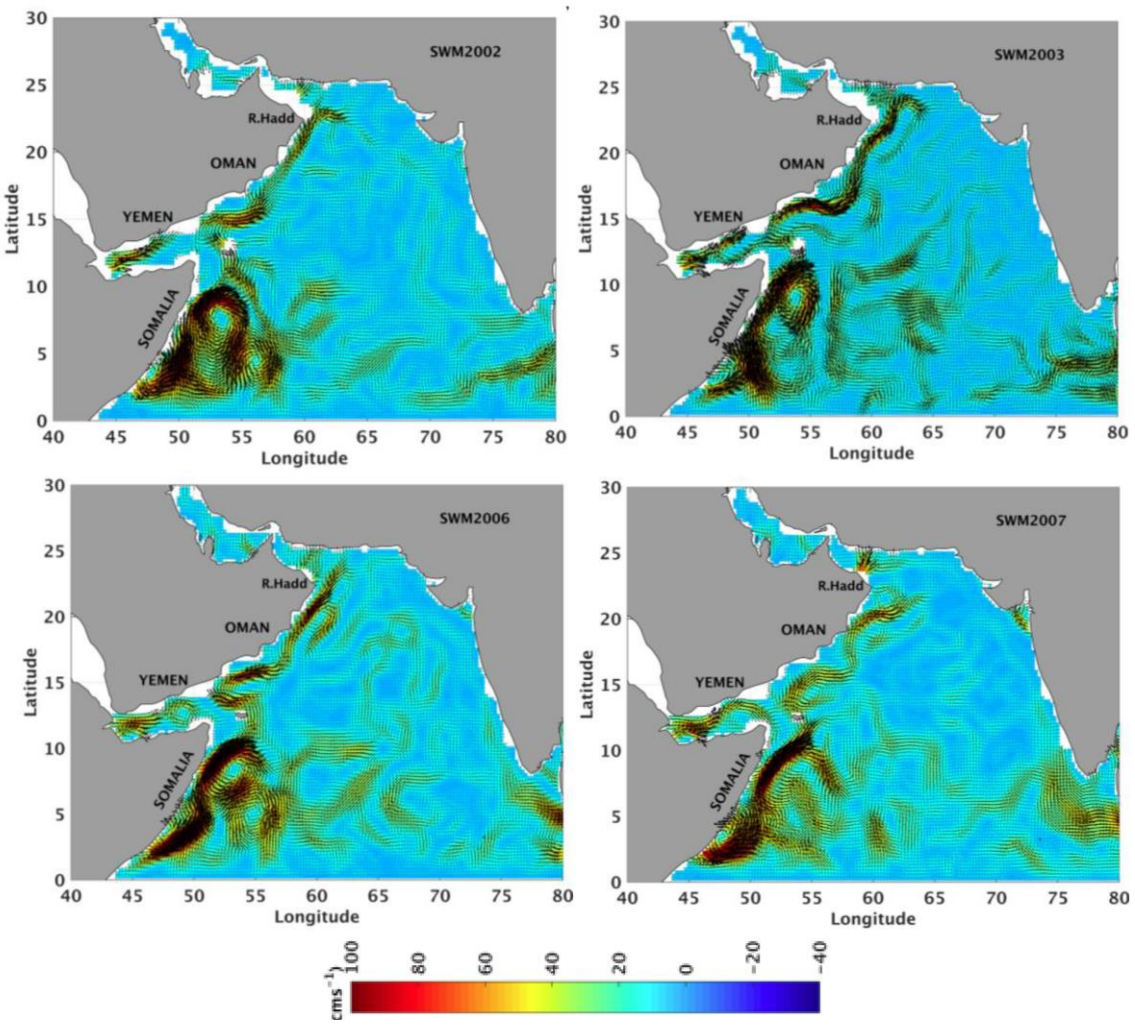

Figure 3.12. These maps show currents during the SWM 2002, 2003, 2006, and 2007. The Somali Current can be seen crossing the Gulf of Aden and merging with the East Arabian Current, which moves towards the northeast.

3.2.5 Mooring System

The stick vectors as a function of depth and time at Cape-RH are shown in Figure 3.13, and 3.14. The currents moved to the northeast direction from April to the end of October during 2010 – 2012. The ADCP recorded strong currents for the upper ocean up to 25 m depth during the SWM. The surface currents at 10 m depth were found to be

approximately 120 cms^{-1} for the year 2010, 2011, and 2012 while these zonal velocities exceeded 100 cms^{-1} during September/October of 2012 (Figures 3.13, 3.14 and 3.15). The ADCP recorded a reversed current direction during the NEM.

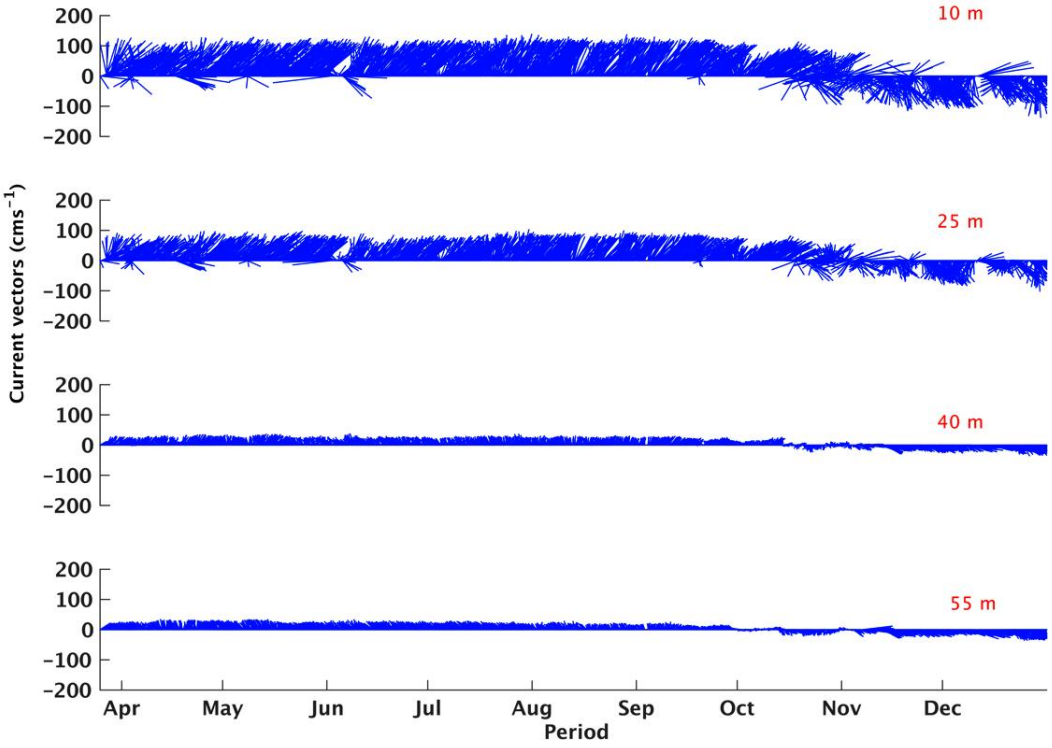

Figure 3.13. Monthly mean current vectors recorded using a 75 kHz ADCP at 10 - 55 m depth at Cape-RH for April to December 2010. The current directions are consistent with what is already known for the SWM and the NEM. Strong currents were observed during the SWM season.

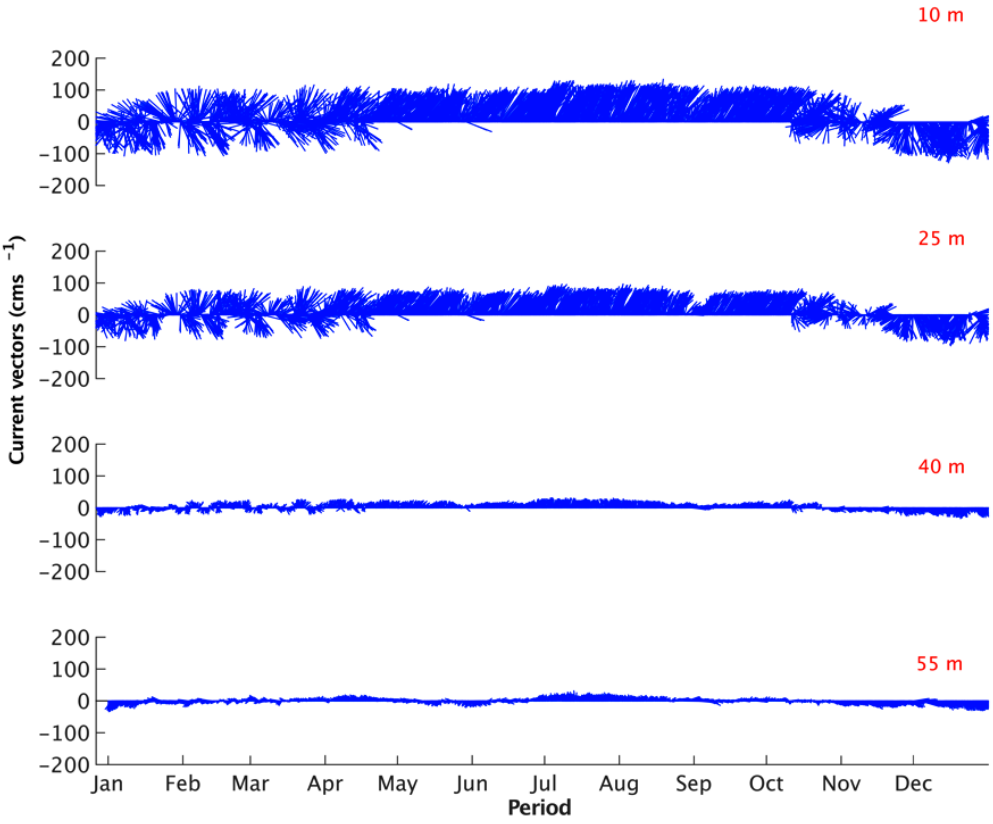

Figure 3.14. Monthly mean current vectors recorded using a 75 kHz ADCP at 10 – 55 m depth in 2011 at Cape-RH, (See the description for Figure 3.13).

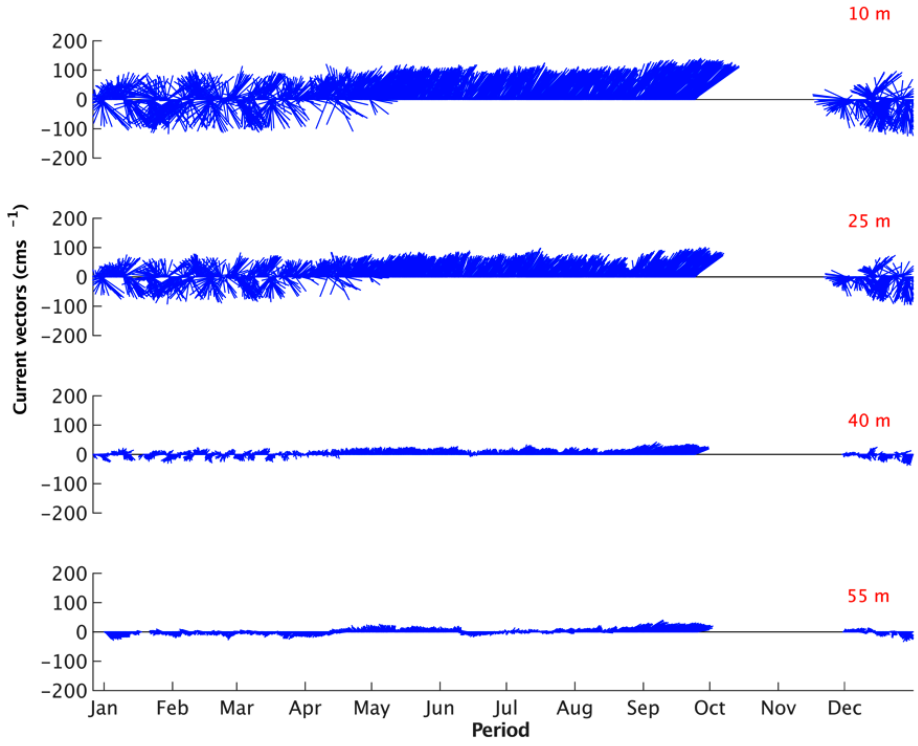

Figure 3.15. Monthly mean current vectors recorded using a 75 kHz ADCP at 10 – 55 m depth in 2012 at Cape-RH. Blank area represents missing data for October and November. (See the description for Figure 3.13).

3.2.6 Winds System

3.2.6.1 Winds System at the Cape Ras Al-Hadd

During the SWM, winds blow from the SW to NE the direction (Figures 3.16, and 3.17). Winds mean speed was high during the SWM, exceeding 18 ms^{-1}, while during the winter monsoon, the winds reverse and wind mean speed was about 10 ms^{-1} and much less consistent. The wind-stress derived from satellite observations showed an increase of wind-stress with longitude and it becomes more zonal (Figure 3.18). The calculated

lowest variances in wind speed were found to occur at the transitions between monsoon seasons (April and October), (Figure 3.19).

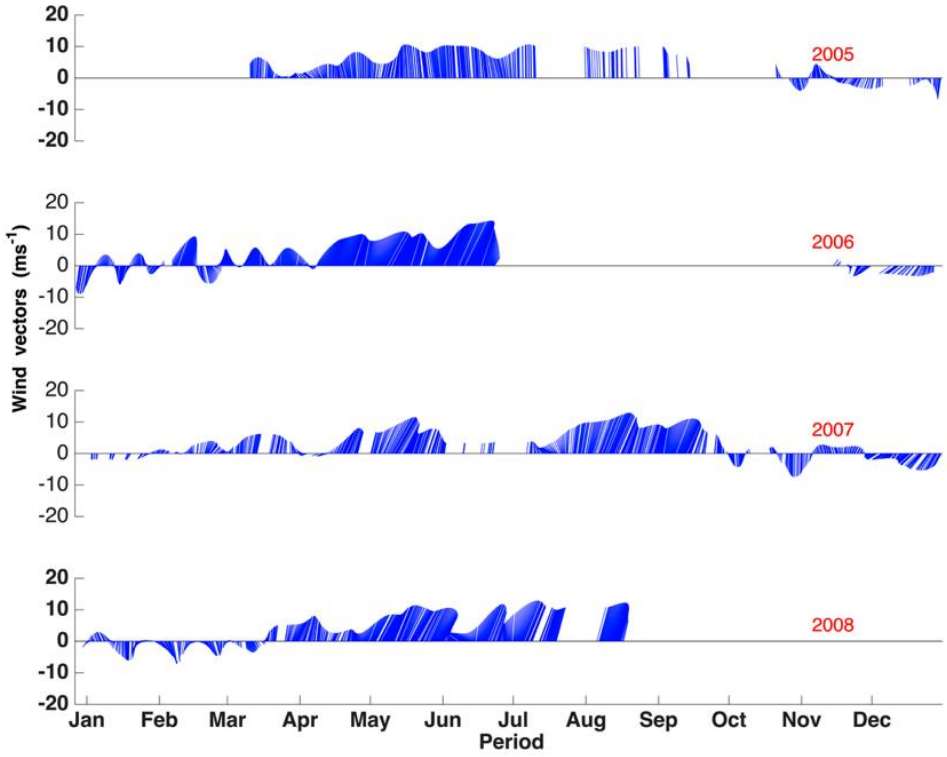

Figure 3.16. The figure shows monthly mean winds system at Cape-RH for 2005 – 2008 after applying a 40-hr low-pass filter. During the SWM (June – August) winds blow from SW to the NE direction and during the NEM (December – February) the system reversed itself and takes the opposite direction. Blank gaps represent missing data.

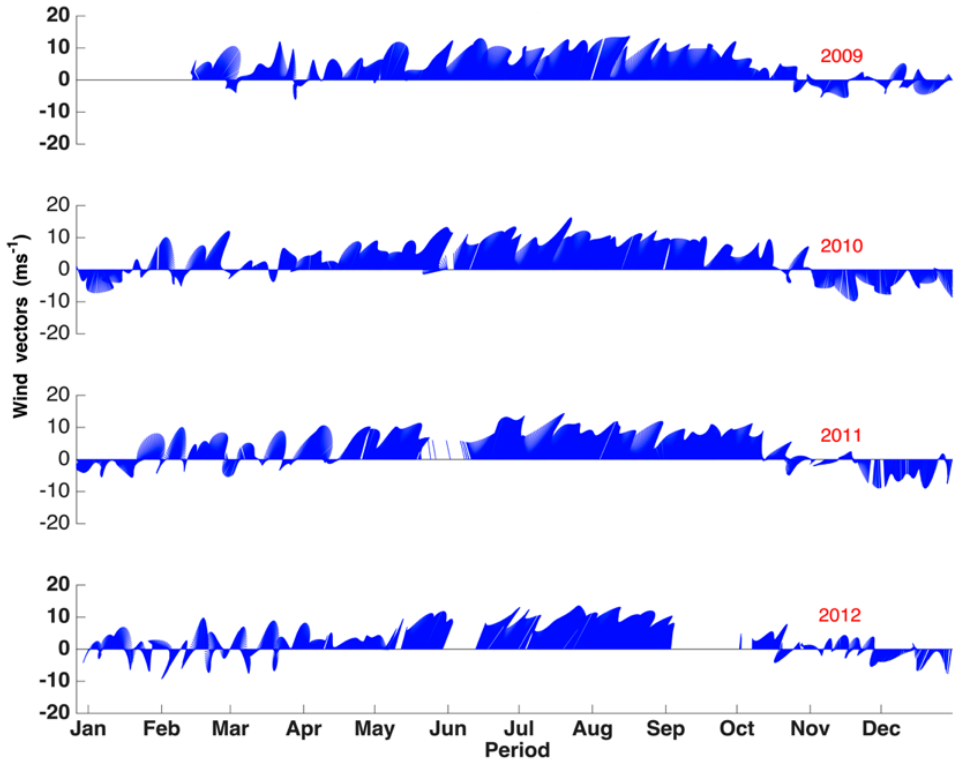

Figure 3.17. The figure shows monthly mean winds system at Cape-RH for 2009 – 2012 after applying a 40-hr low-pass filter. During the SWM (June – August) winds blow from SW to the NE direction and during the NEM (December – February) the system reversed itself and takes the opposite direction. Blank gaps represent missing data.

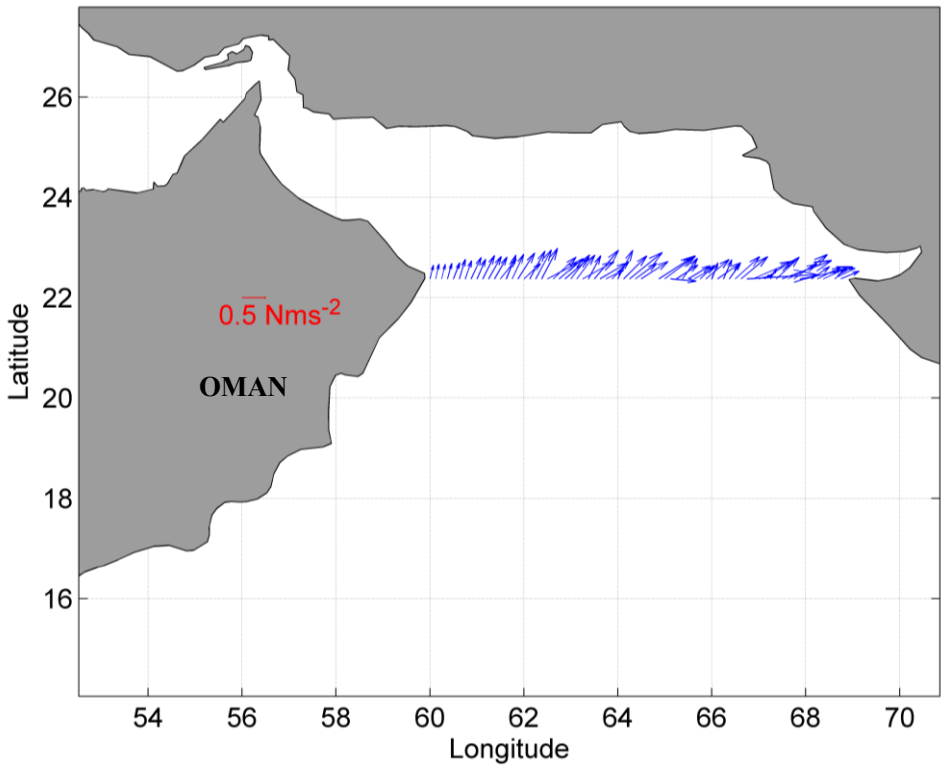

Figure 3.18. This map shows a zonal wind stress at Cape-RH during the Peak-SWM period (July/August 2005). The wind stress increases with longitudes.

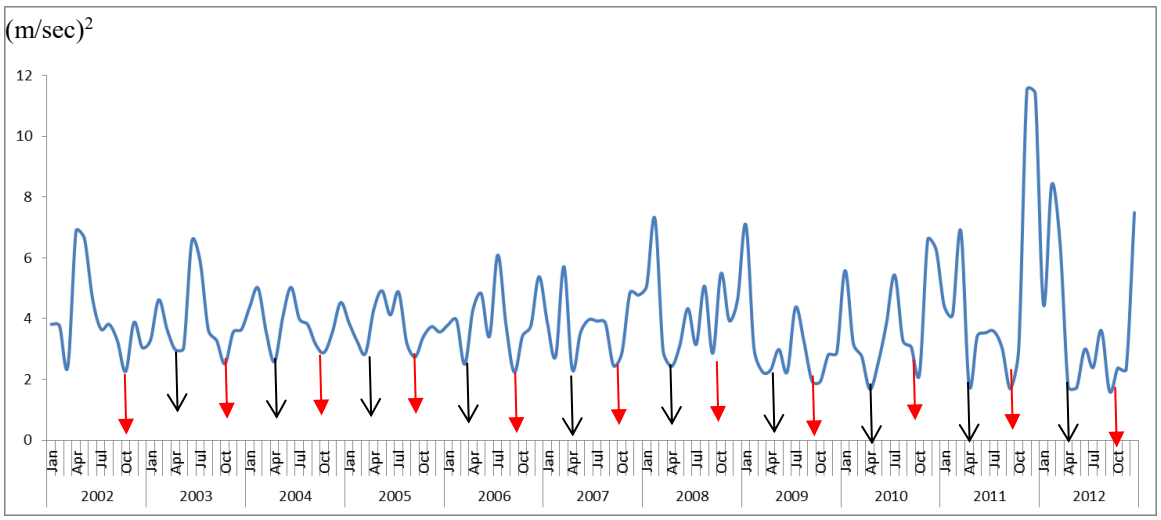

Figure 3.19. The variances of the wind speed show low peaks of wind variances in April and October (2002 – 2012). April is when the winds start to change the direction from NE to SW direction. The end of October is when the wind reverses its direction from the SW to the NE direction.

3.2.6.2 Winds System at Sur

The Sur region is located at the Sea of Oman, approximately 25 km northwest of Cape-RH. Sur is affected by the SWM winds the same way as Cape-RH, but with less strength compared to the wind at Cape-RH. The weather during SWM seasons in Sur coastal waters is warmer compared to the cooler weather in Cape-RH coastal waters. During the SWM the ocean weather in the western Arabian Sea, from southern Oman to Ras Al-Hadd, is cooler, humid, and drier, while it is cooler with high precipitation in the eastern part of the Arabian Sea. Winds recorded in the Sur region showed speeds of less than 15 ms^{-1} during the SWM and the NEM seasons for 2005 to 2008 (Figure 3.20).

3.2.6.3 Winds System at Masirah Island

Masirah Island is in the Arabian Sea, around 270 km southwest of Cape-RH. The Island is also affected by the SWM winds in the same way as Cape-RH. Therefore, winds recorded in Masirah Island demonstrated the same wind patterns as that of Cape-RH. The weather during summer seasons in Masirah coastal waters is also cool. Winds speed in Masirah Island reached up to 20 ms^{-1} during the SWM seasons of 2005 – 2008 and did not exceed 10 ms^{-1} during the NEM season (Figure 3.21).

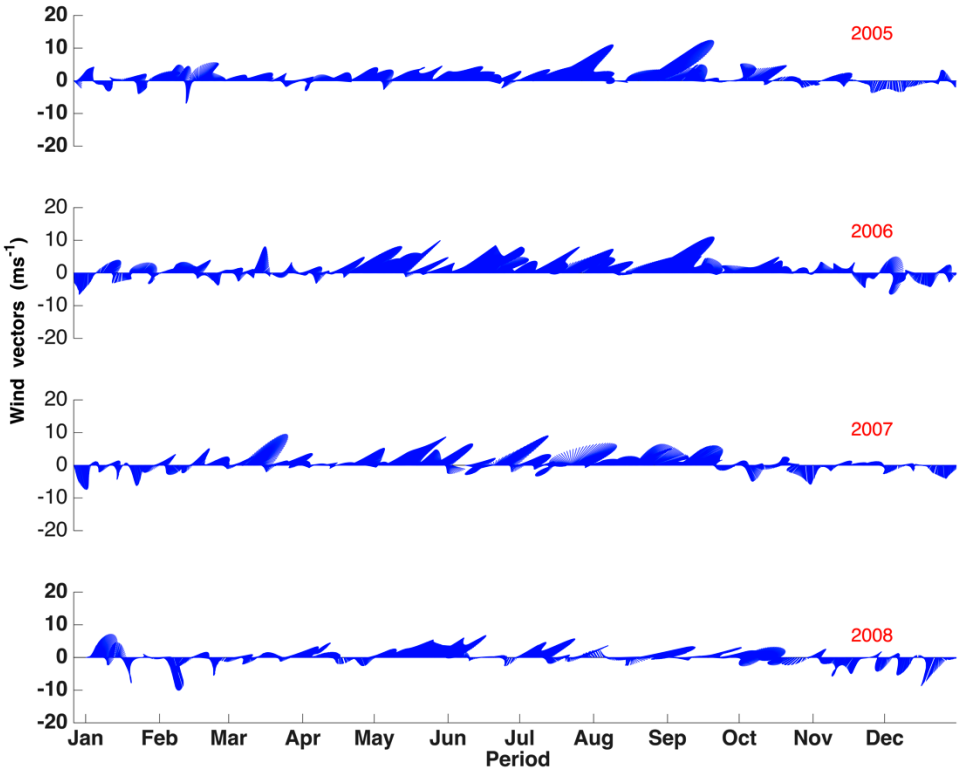

Figure 3.20. The figure shows wind recorded at Sur, northwest of Cape-RH. The wind in this region follows the same patterns of that at Cape-RH. The wind speed is less compared to what was recorded at Cape-RH (See appendix x for more winds plot)

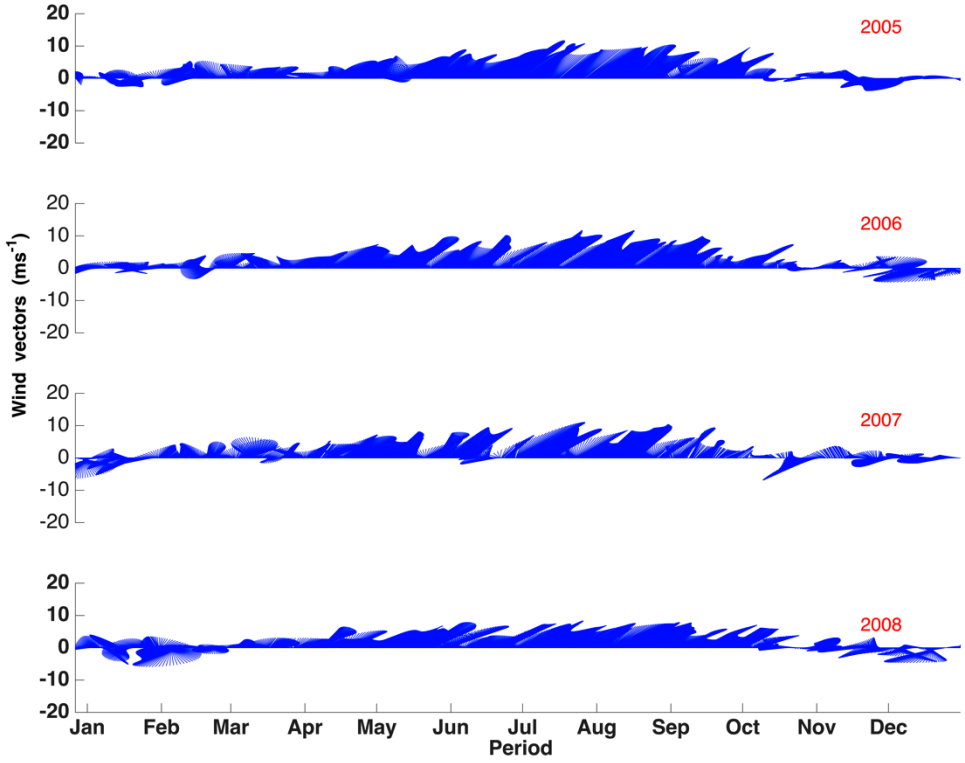

Figure 3.21. The figure shows monthly wind mean velocity at Masirah Island from 2005 – 2008. During the SWM winds blow to the NE direction. During the NEM, the system reversed itself and takes the opposite direction towards the SW direction.

3.2.6.4 Winds System at Salalah

The wind at Salalah, during both the SWM and NEM, was found to be weaker compared to the Ras Al-Hadd region. The wind speed did not exceed 10 ms^{-1} during 2005 – 2008 (Figure 3.22).

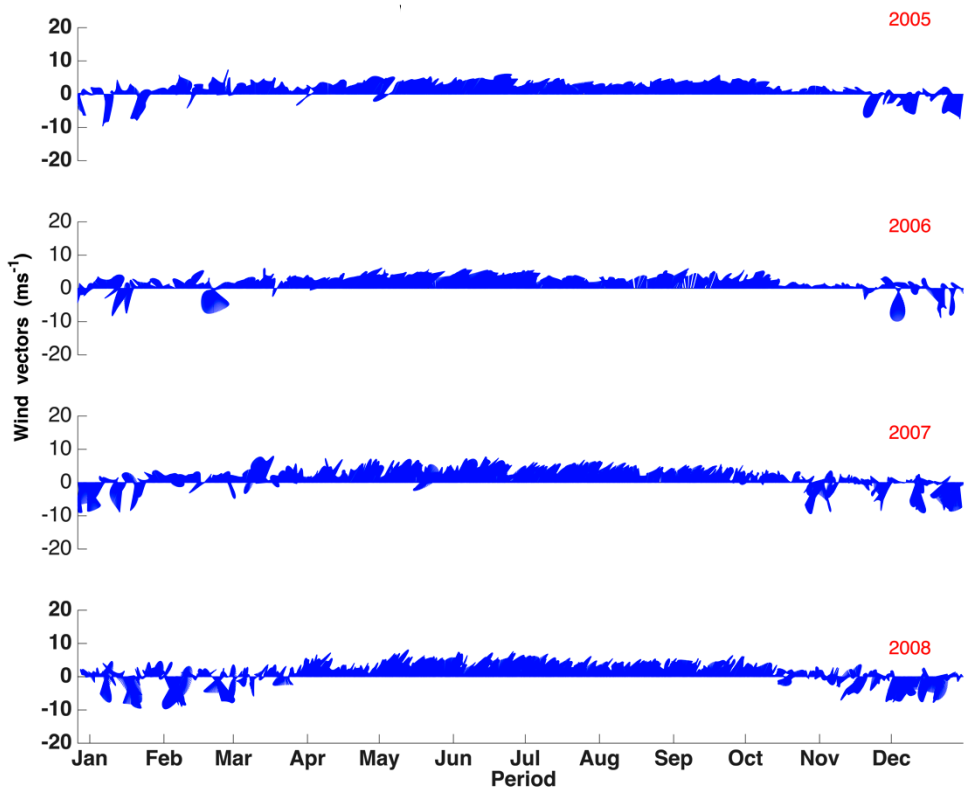

Figure 3.22. Salalah wind system during 2005 – 2008 shows winds for both the SWM and NEM. Winds blow from southwest during the summer seasons and from northeast during the winter seasons.

3.3 Spatial and Temporal Variability of Thermal Fronts during Post-SWM

3.3.1 Thermal Fronts

The transitional period between the summer and the winter monsoons, called here as the Post-SWM (September/October) occurs after the end of the SWM season. Cape-RH thermal fronts were most notable during this time. Statistically, the RH-Jet or Front with high pixel values was observed during the Peak-SWM and the Post-SWM (Figure 3.23).

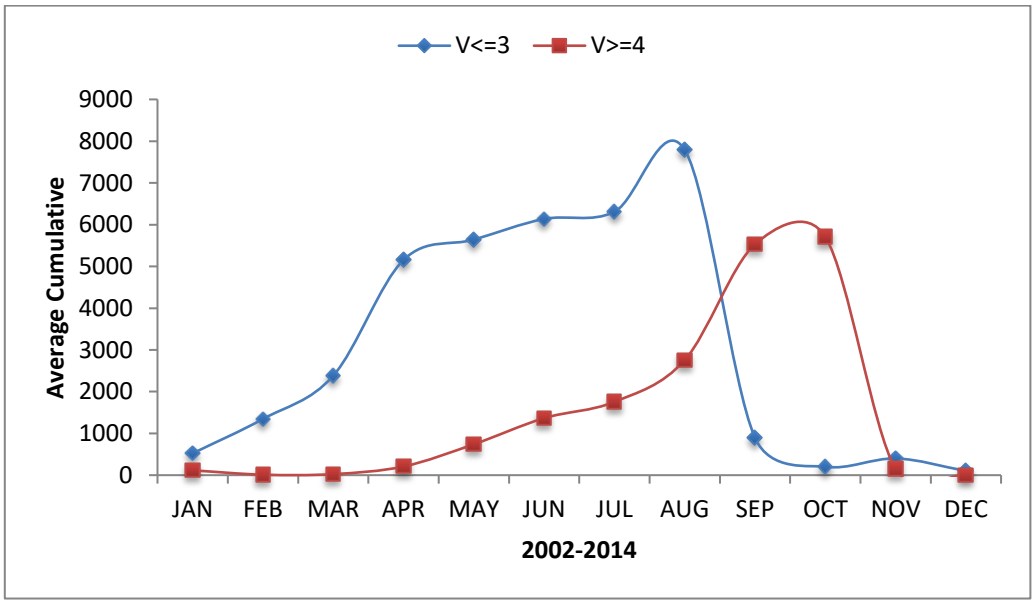

Figure 3.23. This figure represents monthly climatology (2002-2014) of the Ras Al-Hadd front's pixels. Two peaks of the Ras Al-Hadd thermal fronts are shown, where the first peak (Blue line) appears to take place during the intensified southwest monsoon seasons (July/August), and the second peak (Red line) occurred during the transitional period of the southwest monsoon (September/October). The first peak represents moderate thermal fronts with pixel frontal values ≤ 3, while the second peak represents strong thermal front with frontal pixel values ≥ 4.

These thermal fronts at Cape-RH were detected during the study period (2002-2014) except in 2007, where October showed the least frontal coverage. The Ras Al-Hadd thermal frontal distributions (Figures 3.24, 3.25, 3.26, and 3.27) show the existence of the RH-Jet during the Post-SWM. Climatology (2002 – 2014) revealed that the number of pixels that represented thermal fronts are higher during this period (Figure 3.28). In 2010, most of the fronts were concentrated in July to September, dropping in October.

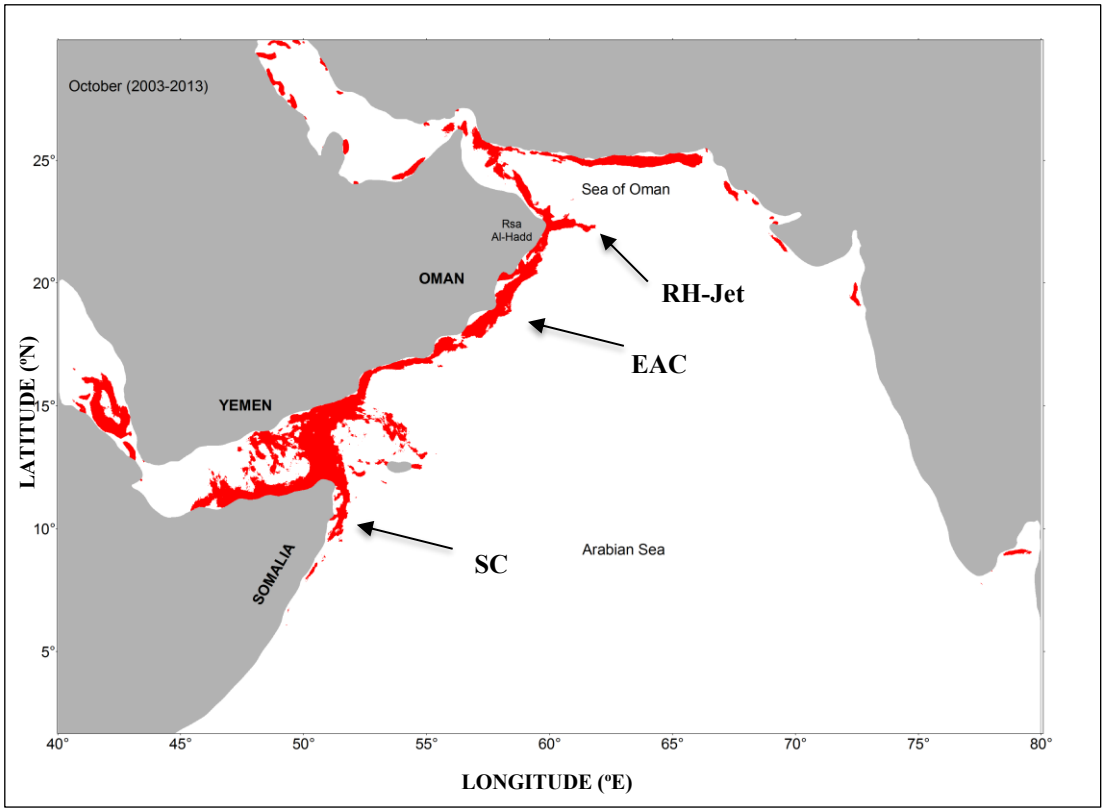

Figure 3.24. Climatology thermal front image shows thermal fronts at Cape-RH during Octobers of 2003-2013. The Somalia Current is merged to the East Arabian Current. The East Arabian Current is shown moving to the northeast direction until the Cape Ras Al-Hadd where the Jest or the front is created.

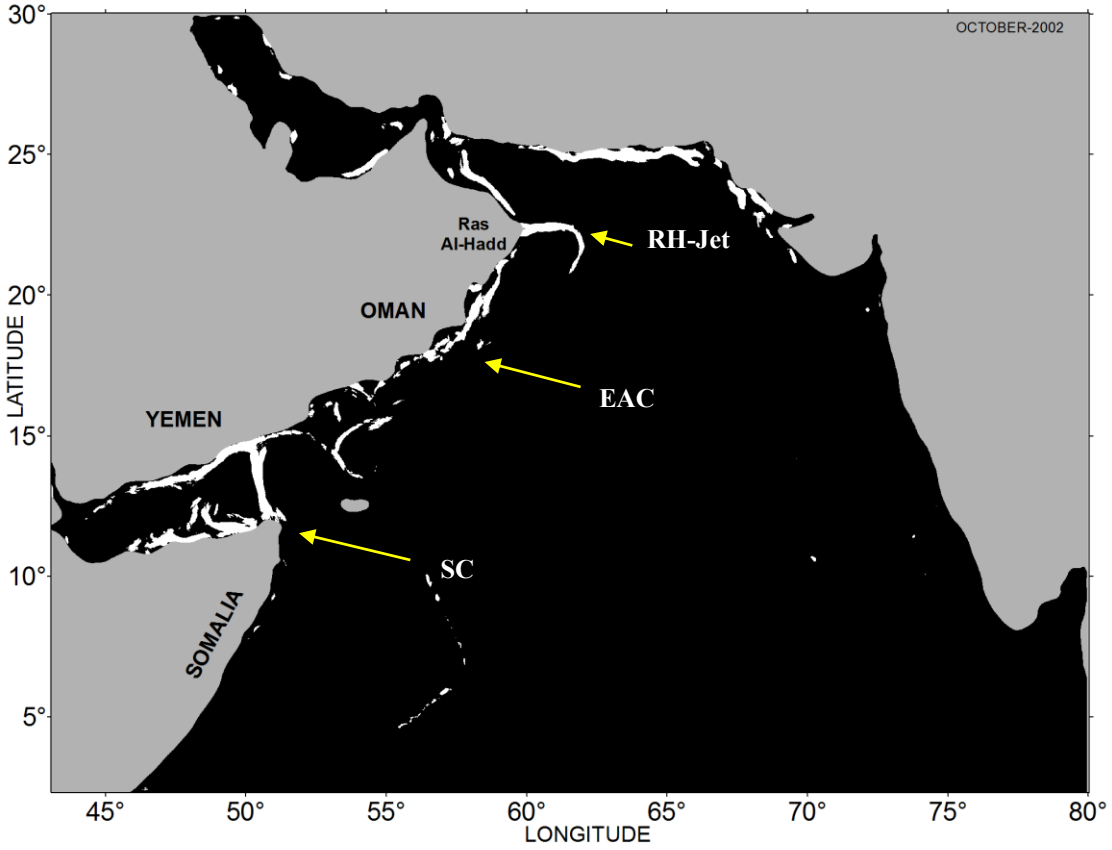

Figure 3.25. This negative-type map demonstrates the Ras Al-Hadd thermal fronts during the Post-SWM October 2002. The Ras Al-Hadd Jet can be seen moving eastward direction for hundreds of kilometers before turning southward, where it creates the anticyclonic eddy south of the Cape Ras Al-Hadd.

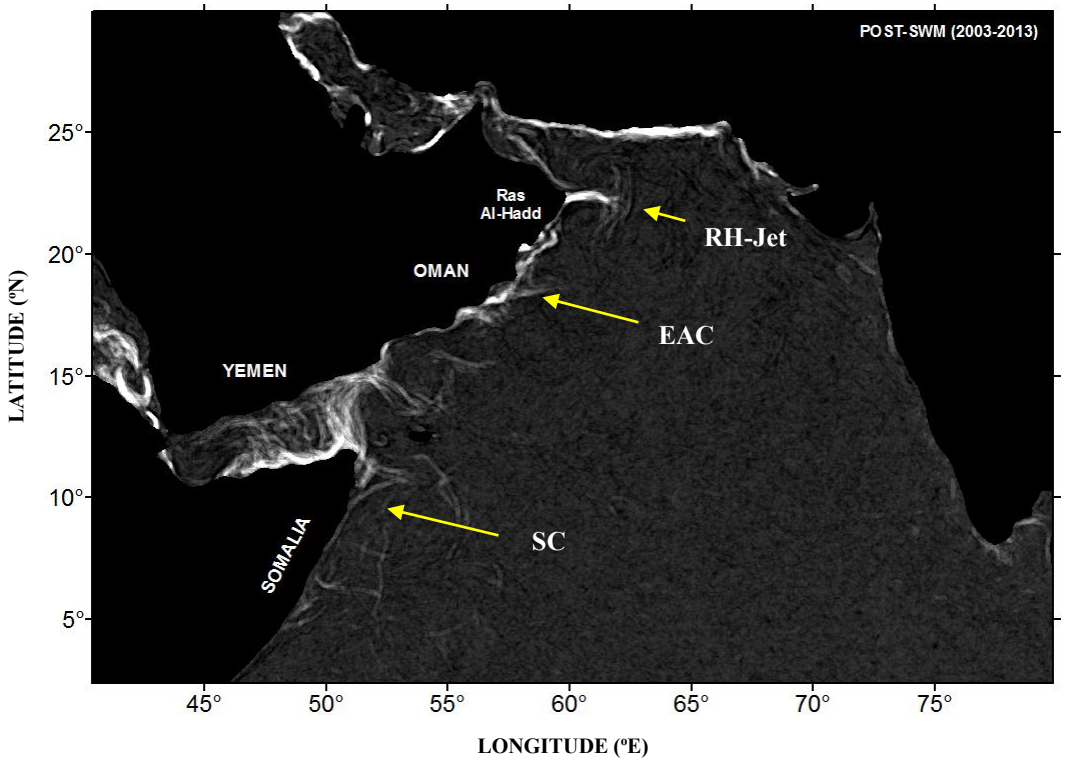

Figure 3.26. This map shows 11-year climatology Post-SWM (2003-2013) during the southwest monsoon transitional period. The map shows currents move from the Somalia coast crossing the Gulf of Aden and merged with the East Arabian Current pushing to the northeast until reaching Cape-RH where the RH-Jet is formed and moved to the eastward direction.

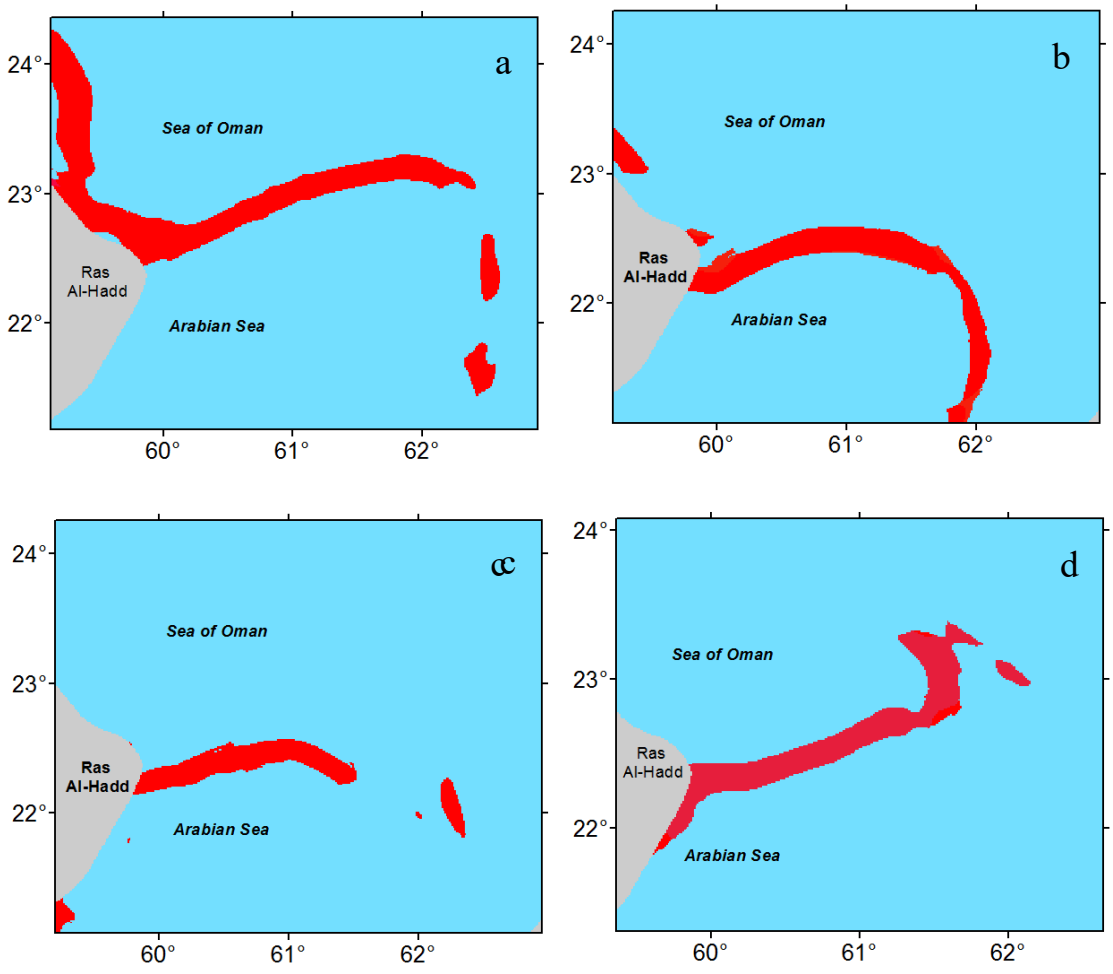

Figure 3.27. Frontal images show the Ras Al-Hadd thermal fronts during the Post-SWM of a) 2006/09/16, b) 2002/10/06 and c) 2002/10/15, and d) 2005/10/15. These fronts have an average length of 250 km and an average width of 40 km.

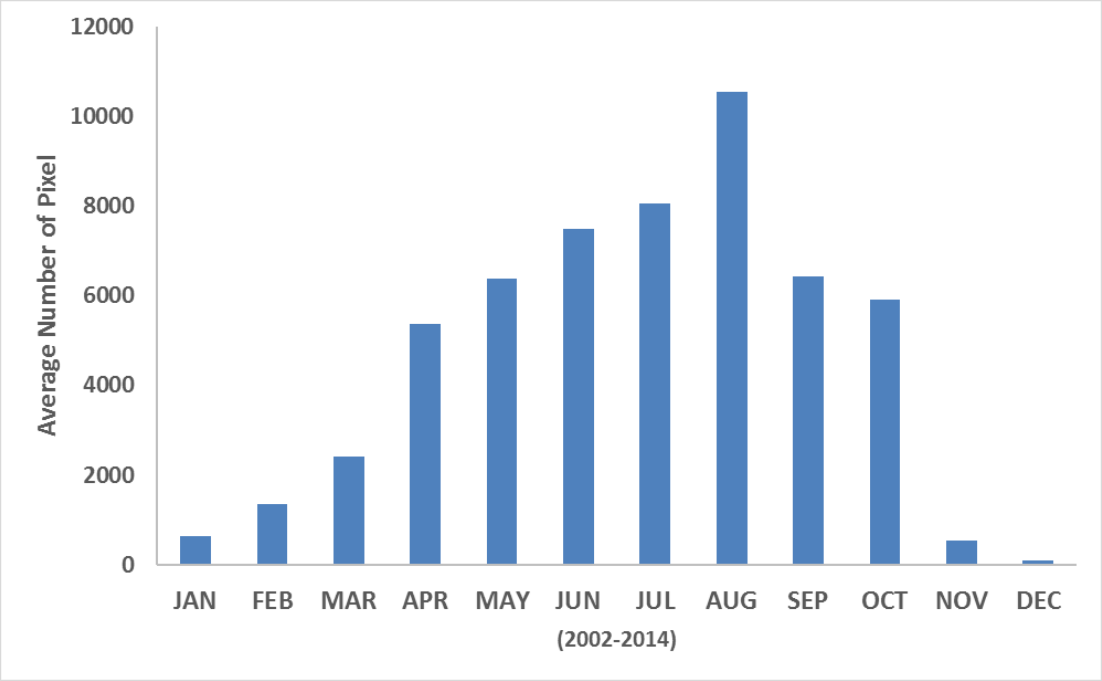

Figure 3.28. The graph shows monthly average pixel counts that represent fronts during 2002-2014 at Cape-RH region. The graph also shows the increasing number of pixels that represent fronts during the SWM and the Post-SWM, while these pixel numbers dramatically decrease during the NEM.

3.3.2 Sea Surface Temperature

Mean sea surface temperature during the Post-SWM (September/October) showed a temperature drop for the year 2009 compared to the mean SST found during the SWM season of the same year at station RHN. The mean SST near the coastal waters of RHN ranged between 29 - 31^{o}C (Figure 3.29a). The remaining years showed cooler surface waters that range between 28 - 29^{o}C for the cross-section towards the Indian coast where the mean SST showed a sudden drop at longitude 68.00^{o}N. The mean SST dropped at Cape-RH, at the station RHM, during this season. The coastal water's sea surface

temperature ranged between 26 - 29ºC, while the offshore waters showed an increase SST that ranged between 27.8 - 29ºC all the way to the Indian coast where the SST again dropped at longitude 69.00ºN (Figure 3.29b).

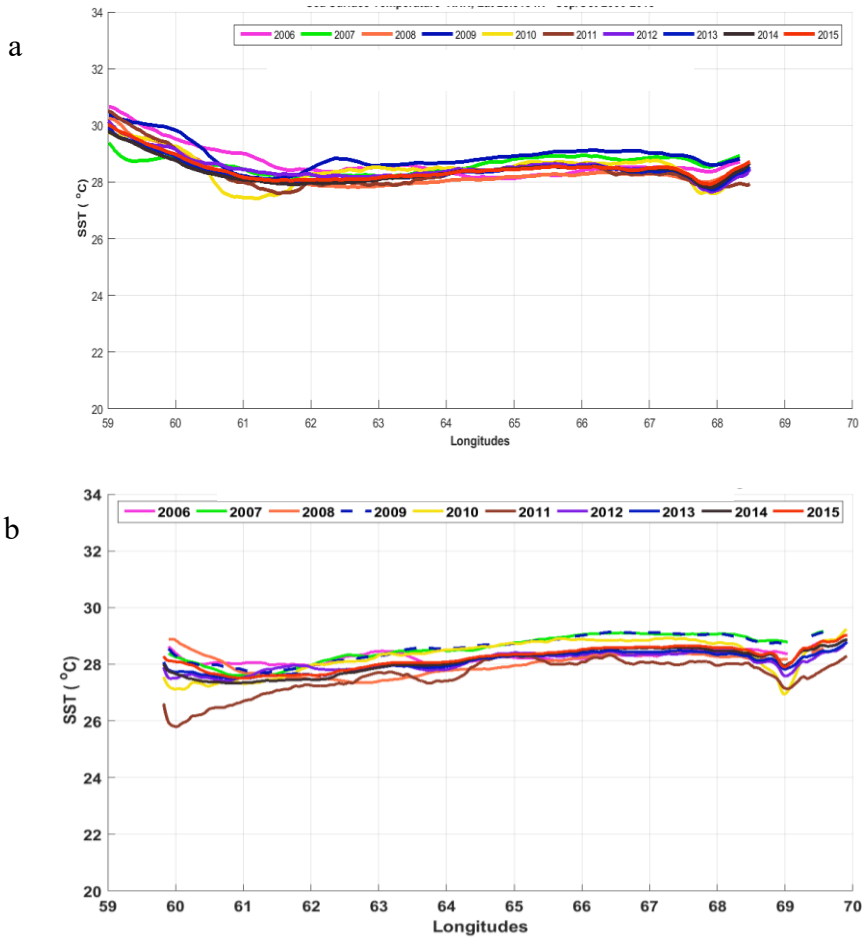

Figure 3.29. The figures show the interannual zonal SST spatial and seasonal variability during the Post-SWM 2006 – 2015. The top panel shows sea surface temperature north of Ras Al-Hadd at the Sea of Oman at the station RHN where it experienced high temperature near the coast of Oman, The SST decreased gradually to 28ºC at longitude 61.00ºN and keeps rising until the coastal waters of India where the SST plunged to under 28ºC at longitudes 68.00ºN. The middle panel shows SST at the Cape Ras Al-Hadd at station RHM. It shows cooler water in the coastal water of Oman, while the temperature keeps increasing offshore to the Indian coastal waters where the temperature dropped, although they remained relatively warmer compared to the cool waters near Cape-RH. The bottom panel shows the temperature was cooler south of Cape-RH at station RHS in the Omani side while these waters became warmer on the Indian side.

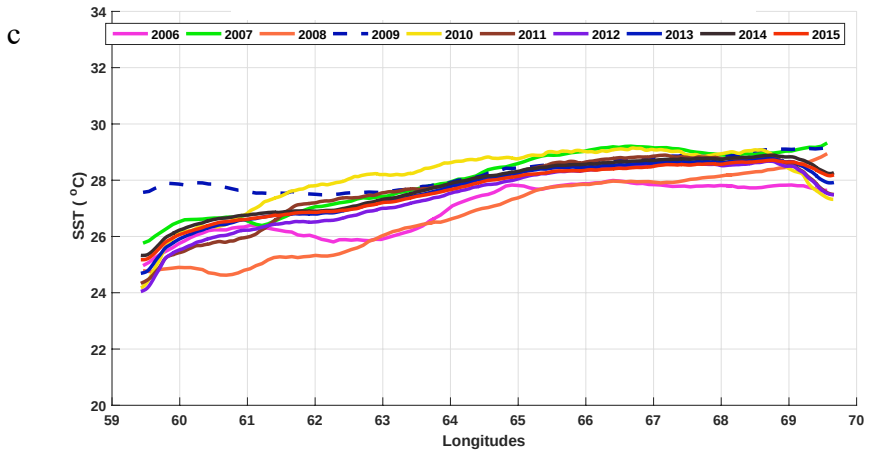

Figure 3.29. Continued

3.3.3 Argo Floats

The Post-SWM period (September/October) is when most of the RH thermal fronts were clearly observed from SST remote sensing analysis. In addition, Argo floats demonstrated the same scenario. The salinity and temperature differences between the Sea of Oman and the Arabian Sea were clearly observed in the Ras Al-Hadd region for the water of 5 m and 20 m depths (Figure 3.30). This explains the consistency with the thermal front results obtained in this study using the Cayula and Cornillon algorithm. The Sea of Oman warmer and high salinity water recorded at 250 m depth was able to cross Cape-RH requiring penetrating into the western Arabian Sea (Figure 3.31).

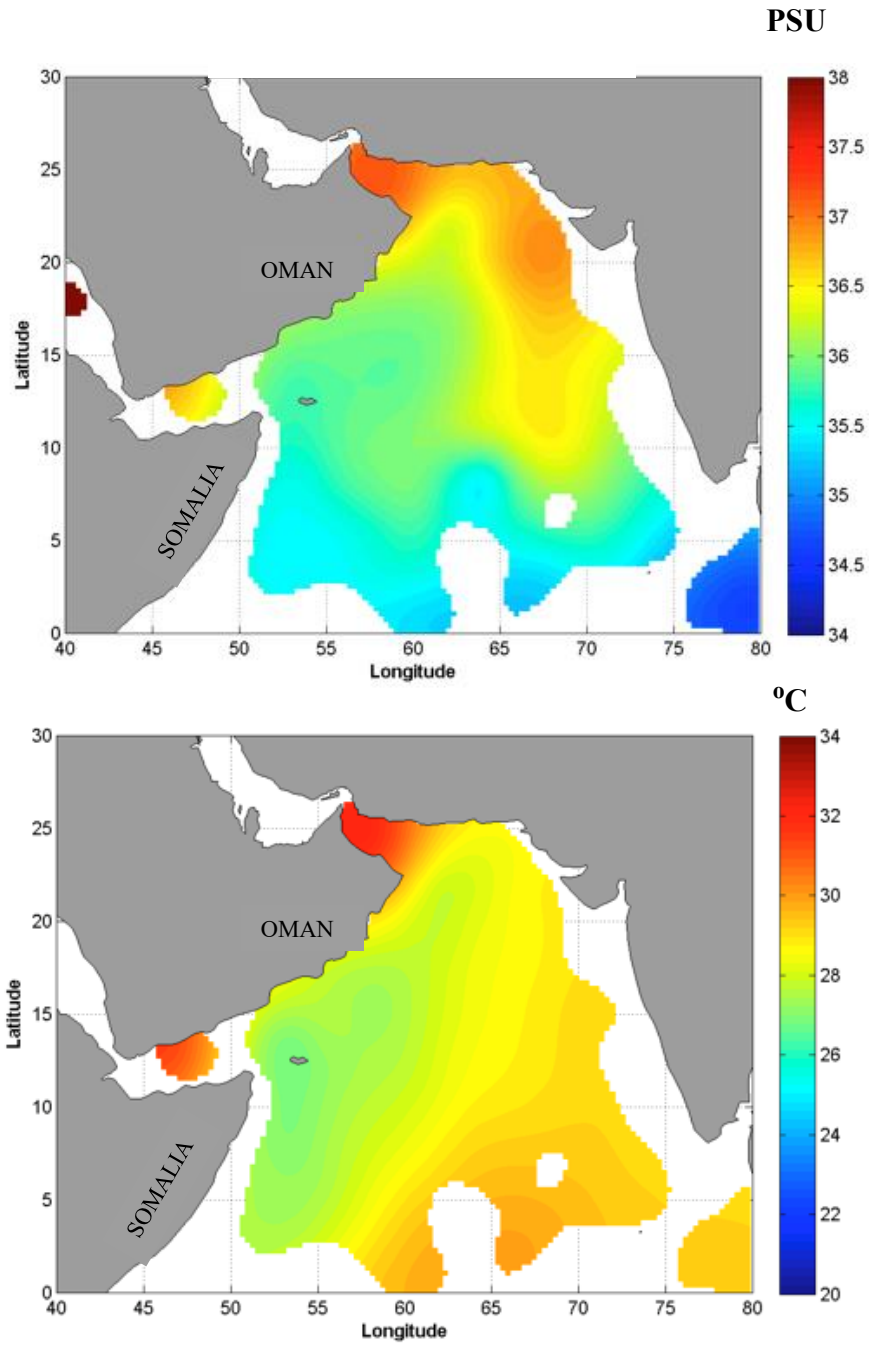

Figure 3.30. Maps show salinity and temperature recorded by Argo floats during the SWM transitional period September/October 2015. Top panel shows near surface salinity distribution at 5 m depths. The salinity front in the RH region can be seen, which is between low salinity south of Cape-RH and high salinity north Cape-RH. Bottom panel shows temperature distribution and warmer water are covered the Sea of Oman while cooler waters are in the Arabian.

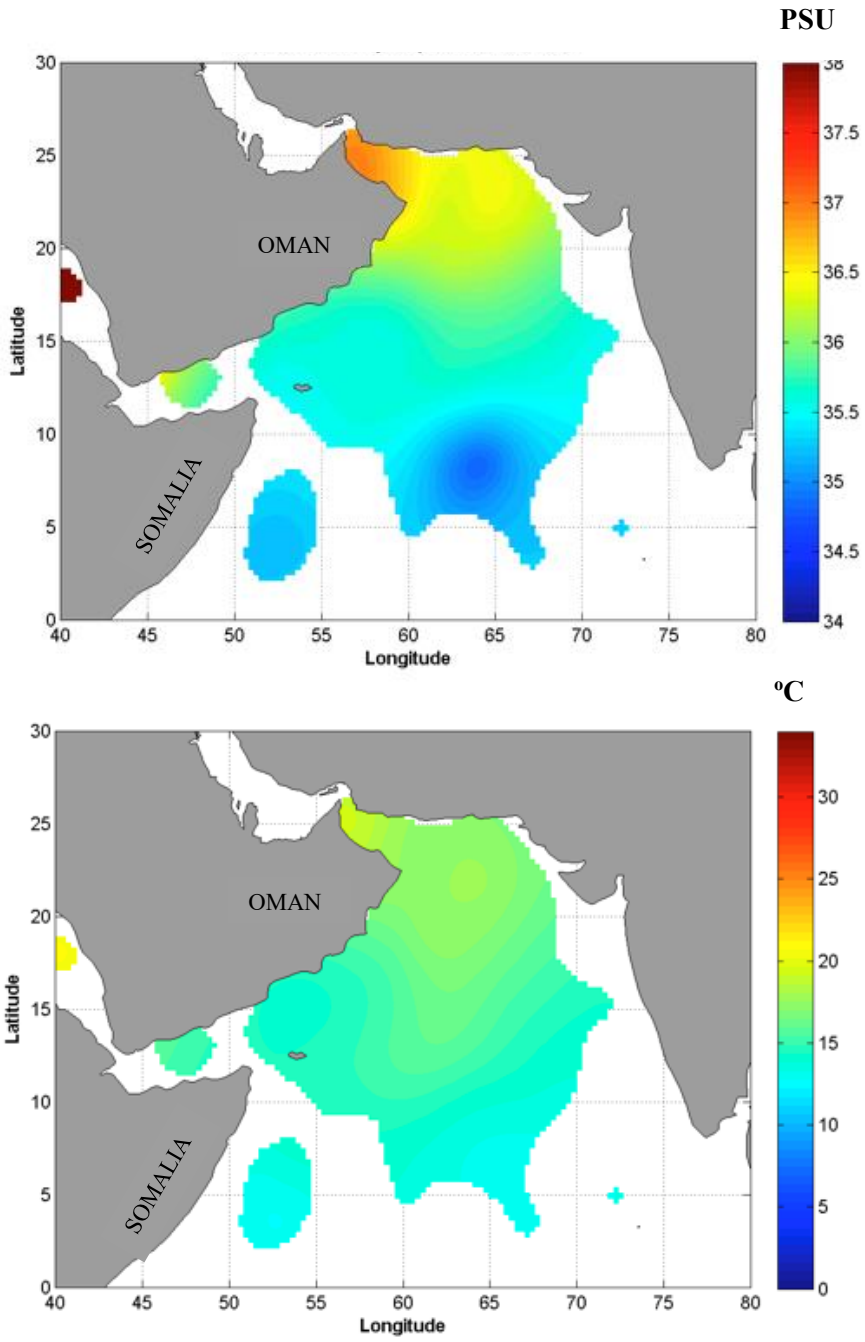

Figure 3.31. Maps show salinity and temperature recorded by Argo floats during the SWM transitional period September/October 2015. Panel shows near surface salinity distribution at 250 m depths. Bottom panel shows temperature distribution at the Sea of the Sea of Oman and the Arabian Sea.

3.3.4 Sea Surface Height and Geostrophic Currents

During the Post-SWM seasons, the Somali Great Whirl, which started during the onset of the SWM, was still active although the eastward flow decreased as it is in its decaying phase. The Somali Great Whirl was observed to spin at high velocity, exceeding 100 cms^{-1}, except in 1995 and 1997 when the maximum mean velocity was approximately 70 cms^{-1} (Figure 3.32), and a positive sea surface height was observed within the Somalia Great Whirl surrounded by a negative sea surface height (Figure 3.33).

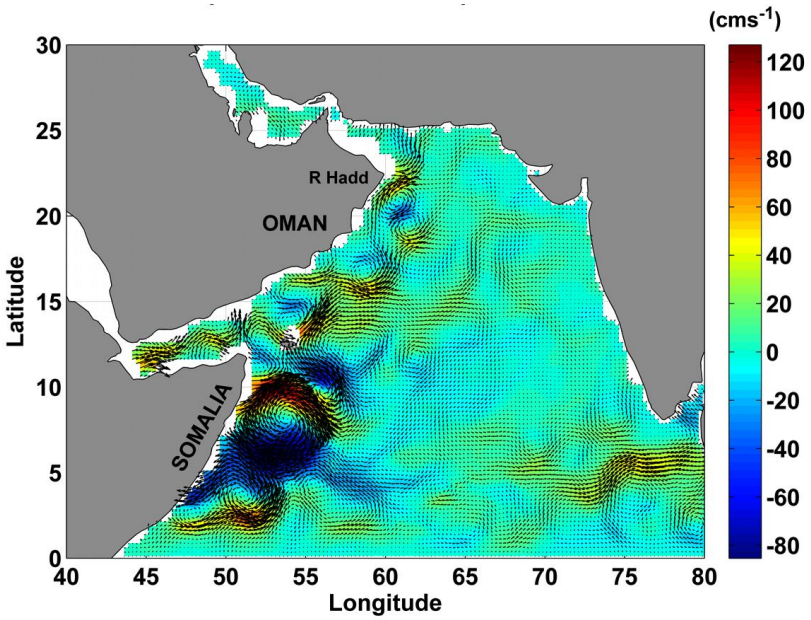

Figure 3.32. This base map shows geostrophic currents in the Arabian Sea during the Post-SWM September 2002. The Somali Great Whirl can be seen near the coast of Somalia. Currents moving towards Cape-RH also are shown in this map.

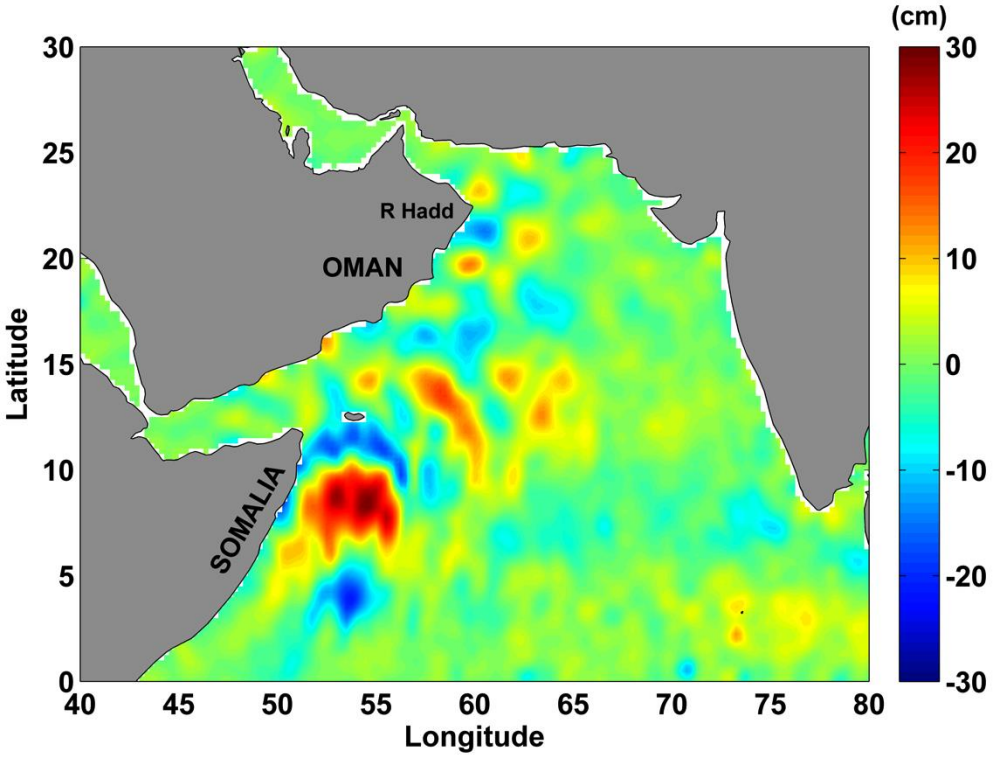

Figure 3.33. Map shows the historical mesoscale altimetry for SSH in the Arabian Sea during August 1999. The map shows positive SSH off the Somali coast where the Somali Great Whirl is located and surrounded by negative SSH.

3.3.5 Mooring System

The near-surface currents during the Post-SWM flowed to the northeast and started reversing the direction in November. The cabled mooring ADCP recorded fast northeast currents in the Ras Al-Hadd region (figure 3.14). During the Post-SWM 2012, the ADCP did not record the current velocity (Figure 3.15). See section 3.2.5 for more information regarding mooring observations.

3.3.6 Winds System

During the Post-SWM, wind forces and direction continued to blow to the northeast direction showing a decrease in the wind speeds (figure 3.16, 3.17). By the end of this season, the wind starts reversing its direction.

3.4 Spatial and Temporal Variability of Thermal Fronts during Winter Monsoon

3.4.1 Thermal Fronts

No thermal front signatures were observed in the western Arabian Sea throughout the winter monsoon for the study period (2002-2014). During this season currents in the eastern Arabian Sea near the coasts of the Indian continent moved from the Arabian Sea towards the Persian/Arabian Gulf, crossing the Sea of Oman (Figure 3.34). By November, the wind system in the Indian Ocean had already reversed its direction from the southwest to the northeast and blew towards the southwest direction. The wind intensity during this period was weaker in the Arabian Sea compared to the SWM wind intensity.

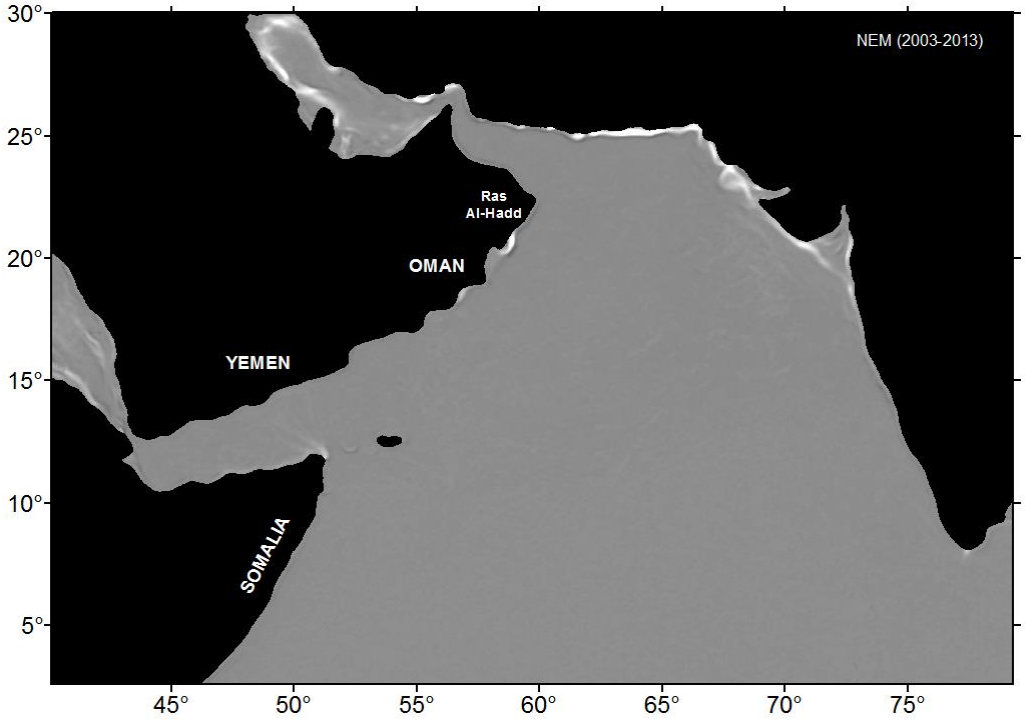

Figure 3.34. In the winter monsoon, no thermal fronts were detected. Few surface currents were observed in the eastern part of the Arabian Sea. Some currents move toward the Persian/Arabian Gulf through the Hormuz Strait. During this time, the NEM is considered strong in the Sea of Oman. This frontal thermal image shows the absence of the Ras Al-Hadd jet during the northeast monsoon (winter monsoon).

3.4.2 Sea Surface Temperature

During the winter monsoon, the temperature is expected to drop. In this study, the NEM window is from December to the end of February. In this season, there was no noticeable change in sea surface temperature between the Sea of Oman and the Arabian Sea, except that the Sea of Oman became a little cooler than the Arabian Sea. All the three stations at the Ras Al-Hadd region, RHN, RHM, and RHS, had almost the same mean SST between 25-25.8ºC in the Oman coast. The SST on the eastern side of the Arabian Sea and the Sea of Oman showed a decrease in temperature and the detected mean temperature was

between 22-24ºC. The minimum mean SST was found to be around 21ºC in RHN for the year 2013 and 2015 (Figure 3.35).

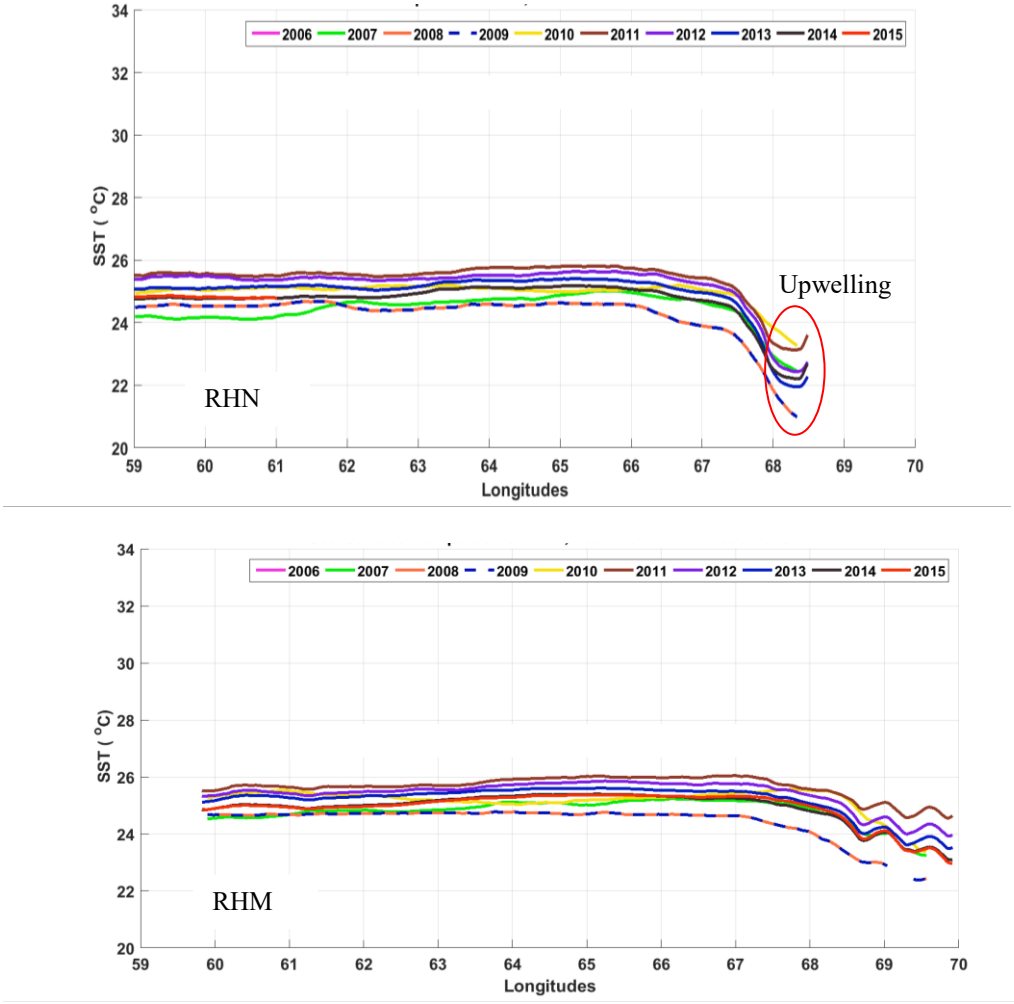

Figure 3.35. Zonal SST during NEM (December - February) shows sea surface temperature that is cooler than the SWM season. The top figure shows zonal temperatures to the north of Ras Al-Hadd (RHN) at the Sea of Oman with low sea surface temperature for the whole basin, and a sharp drop near the Indian coast. The middle figure shows zonal SST at Cape-RH (RHM) with the sea surface temperature dropped and cooler water in the Oman coastal waters, while the temperature keeps increasing with longitudes until the Indian coast where the temperature dropped and becomes cooler than in Cape-RH. The bottom figure shows low temperature South of Cape-RH at RHS in the Omani side while these waters become warmer in the Indian site compared to the previous two locations.

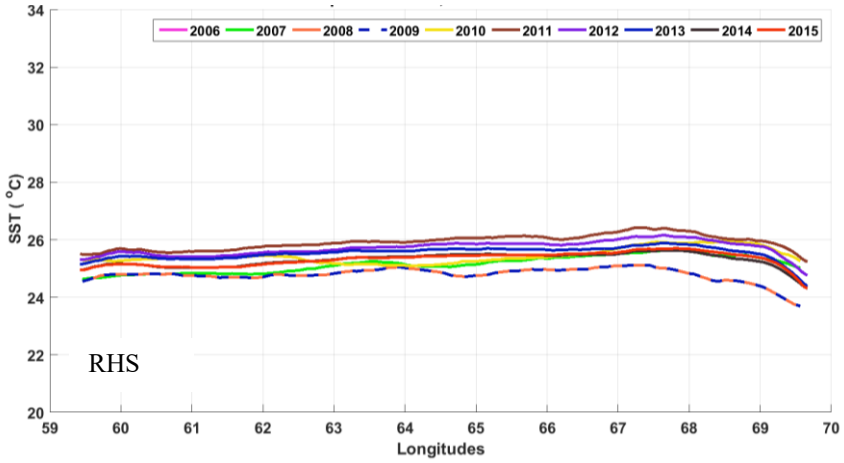

Figure 3.35. Continued

3.4.3 Argo Floats

During the winter monsoon, salinity and temperature variability recorded by Argo floats at the RH region were low. While surface salinity in the Ras Al-Hadd region did not show any fluctuation, it dropped at the eastern parts of the Arabian Sea south of latitude 17.00^{o}N to under 35.5 PSU. In the central Arabian Sea, the salinity was around 36.5 PSU. Highest salinity waters were observed in the Sea of Oman and the northwest Arabian Sea associated with low temperature (~ 25^{o}C). The southern and eastern Arabian Sea experienced a low salinity, with warmer waters (Figure 3.36).

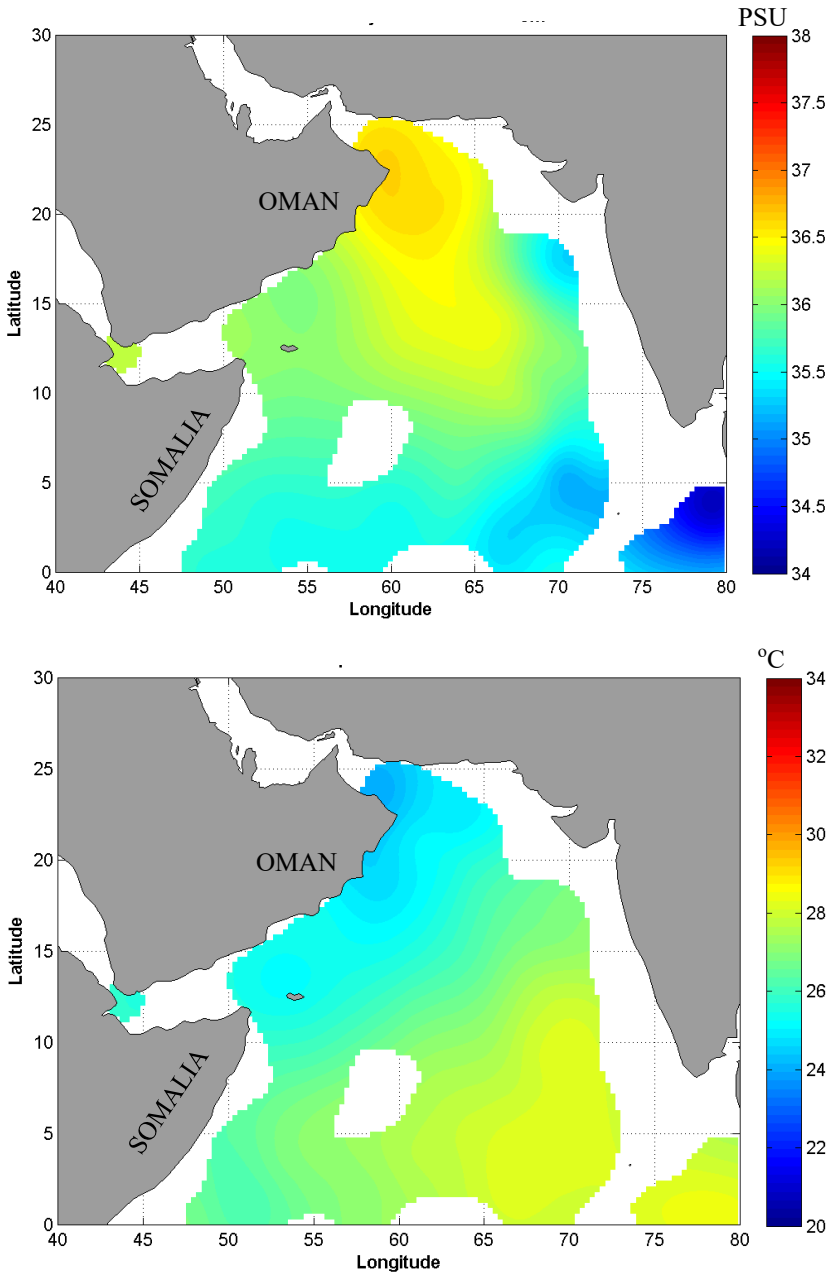

Figure 3.36 Salinity distribution (Top panel), and Temperature (Bottom panel) at 5 m depths from Argo floats during the NEM season, December to February 2010. The absence of the RH-Jet allowed high salinity and cooler waters in the Sea of Oman to cross the RH boundary to the Arabian Sea. The top map also shows the effect of the Bay of Bengal on the salinity of the southern Arabian Sea, as less saline water from the Bay of Bengal is propagated to the Arabian Sea reaching the Somalia coast.

3.4.4 Sea Surface Height and Geostrophic Current

During the winter monsoon, the wind system reversed and currents flow from the northeast to the southwest. The coastal waters of the Arabian Sea are calm while in the Sea of Oman they became rougher.

3.4.5 Mooring System

Currents recorded by an ADCP during the winter monsoon flow in the opposite direction those of the summer monsoon. The current velocity was also less than that recorded in the SWM. For more mooring description, see section 3.2.5 and (Figure 3.13, Figure 3.14, and Figure 3.15).

3.4.6 Winds System

During the northeast monsoon, the wind in the Indian Ocean changed its direction from the southwest to the northeast direction. As the result, the ocean currents in the Arabian Sea move to the southwest direction or to the southeast. No fronts or jet was observed in Ras Al-Hadd region. For more winds description see section 3.10, Figure 3.16, and Figure 3.17.

CHAPTER IV

DISCUSSION

In this chapter, the results and the significant findings of this study are discussed. This study has focused mainly on satellite remote sensing datasets to investigate the formation of the oceanic jet in the Cape Ras Al-Hadd, its source, the mechanism on how is it generated, and the spatial and temporal variation of this Jet. I present new details of the interannual and intraseasonal spatial and temporal evolutions of the Cape Ras Al-Hadd Jet and the thermal fronts in the northwest Arabian Sea.

The primary objectives and goals of this study are to understand and characterize the variability of the RH-Jet using long-term satellite remote sensing datasets and data from a mooring system. In this study, the effort was made to determine the main source of the RH-Jet, the temporal and spatial variability of the Jet, and the role of the SWM in influencing the RH-Jet. Therefore, these two hypotheses were tested 1) the Somali Current is the main source of the RH-Jet, and 2) the SWM monsoon is the main driving force for the Ras Al-Hadd Jet.

4.1 Ras Al-Hadd Jet during the Pre-Southwest Monsoon

No fronts or jets were observed during the Pre-SWM in Cape-RH. Even though by the end of March winds start to reverse their direction from the NE to SW, the surface winds near the Somali coast are still weak during this transition period (Saha, 1974; Schott,

1983). In addition, the atmospheric Findlater Jet, which has a great impact on the dynamics of the Arabian Sea, is not yet developed. Therefore, the momentum or the force for the creation of the SC was missing. Hence, the EAC which is the extension of the SC was not fully developed, or it was in its early developing phase and weak (Figure 3.1 and Figure 4.1). In a study by Lighthill (1969), it was found that the SC is strong and flows northward only after the onset of the SWM starting in June. In addition, McCreary *et al* (1996) found that in the western Arabian Sea the winds start to gain momentum during mid-May.

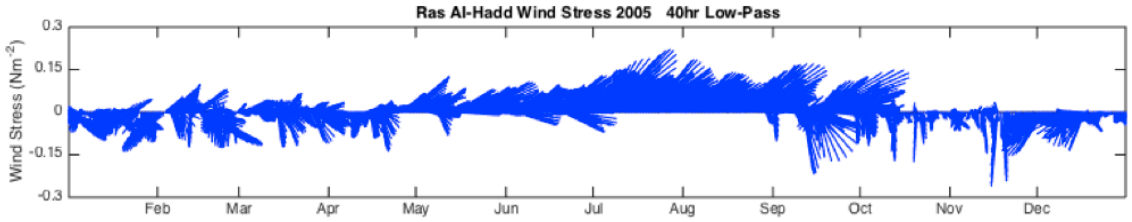

Figure 4.1. Wind stress (40 hr low-pass filter) at the Cape Ras Al-Hadd during 2005. The plot shows a strong positive wind stress during the SWM (June- August), and the Post-SWM (September/October). While weak wind-stress was during the Pre-SWM.

The zonal SST at Cape-RH showed a constant trend of sea surface temperature. However, in the eastern Arabian Sea, a cooling was observed with a fluctuation in SST. There was no signal of upwelling or downwelling in Cape-RH during the Pre-SWM period. (Figure 3.2)

4.2 The Ras Al-Hadd Jet during the Southwest and Post-Southwest Monsoons

The Somali Current, the Great Whirl, the southern Indian Ocean, and the atmospheric and oceanographic dynamics in the Indian Ocean equatorial regions have been extensively studied (Schott and McCreary, 2001). However, the northwest Arabian Sea, particularly the Ras Al-Hadd region, has fewer oceanography studies. In this study, it was found that by the onset of the southwest monsoon (SWM) a portion of the Somali Current (SC) has moved to the north passing through a narrow passage between Socotra Island and the northern tip of Somalia, and then the SC mixes with the Gulf of Aden Current (GOAC), before being merged to the East Arabian Current (EAC). This propagation of the SC is in agreement with many previous studies such as Frantantoni *et al.,* 2006; Udaya, 2010; Schott and McCreary, 2001; and Schott *et al.,* 2009.

Thermal fronts derived from satellite remote sensing high-resolution datasets show the formation and development of the RH-Jet during both the SWM, and Post-SWM. I found the existence of two peaks of the Jet (Figure 3.23). The first peak of the thermal fronts occurred during the Peak-SWM (July/August), and the second peak was observed during the Post-SWM (September/October). The occurrence of the RH-Jet during the Post-SWM was consistent with Böhm *et al.* (1999) in which a thermal Jet in Cape-RH was observed moving northeast using SST datasets. The current's strength and the roughness of the western Arabian Sea gradually decreased during the Post-SWM (September/October).

The RH-Jet is a thermal front, which is a result of mechanisms and factors stated in the hypothesis of this study. One of these factors is the difference in water temperature between the Sea of Oman and the Arabian Sea. The zonal sea surface temperature at Cape-RH shows that the current flows between a cool and a warm water mass (Figure 4.2**)**. The cool upwelled water masses were transported from the Arabian Sea by the EAC to Cape-RH, while warm and high salinity waters from the Sea of Oman were transported to Cape-RH by the coastal current**.** Many studies (See Pous *at al.,* 2004; Pierre *at al.,* 2016; Johns *et al.,* 2000; Wiggert *et al.,* 2005) show that the PGW flows toward Ras Al-Hadd during the winter monsoon; therefore, there is no influence of the PGW for the creation of the RH-Jet during the SWM. The explanation on how the Sea of Oman contributes the creation of the Jet is that warm waters, which are part of the cyclonic mesoscale eddy north of Cape-RH, escape the eddy and flow towards the Cape-RH, where they meet with the EAC. Another speculation is that warm waters coming from Cape Ras Al-Hamra in Muscat, flow a long Muscat coast toward Cape-RH. Therefore, a thermal front is created between these two water masses, which carry different temperatures values. The current that flows between the warm and the cool water is an indication of the existence of the Ras Al-Hadd Jet or the RH-Front during the Post-SWM September/October (Figure 4.2).

The interannual variability during 2006-2015 of the zonal sea surface temperatures at Cape-RH shows that 2007 and 2009 were the two years of highest SST (Figure 3.8). In June 2007 cyclone Gonu passed over the Arabian Sea and the Sea of Oman. Wang *et al*.,

(2012) found a warm trend and a sudden warm event that raised the temperature after tropical cyclone Gonu. During 2007, the dynamics of the coastal waters in the northwest Arabian Sea and the Sea of Oman might have been affected due to the impact of tropical cyclone Gonu. The zonal SST climatology during 2006-2009 showed that the ocean was warmer compared to what was found during 2010-2015 (Figure 4.3). Cyclones can strongly affect the ocean dynamic and the physicochemical processes through vertical mixing and Ekman Pumping (Wang and Zhao, 2008).

The seasonal SST climatology during the Post-SWM period exhibited warmer water from the Sea of Oman and cool water from the Arabian Sea. These two water masses with different thermal properties meet at Cape-RH during this period (Figure 4.3, Figure 4.4).

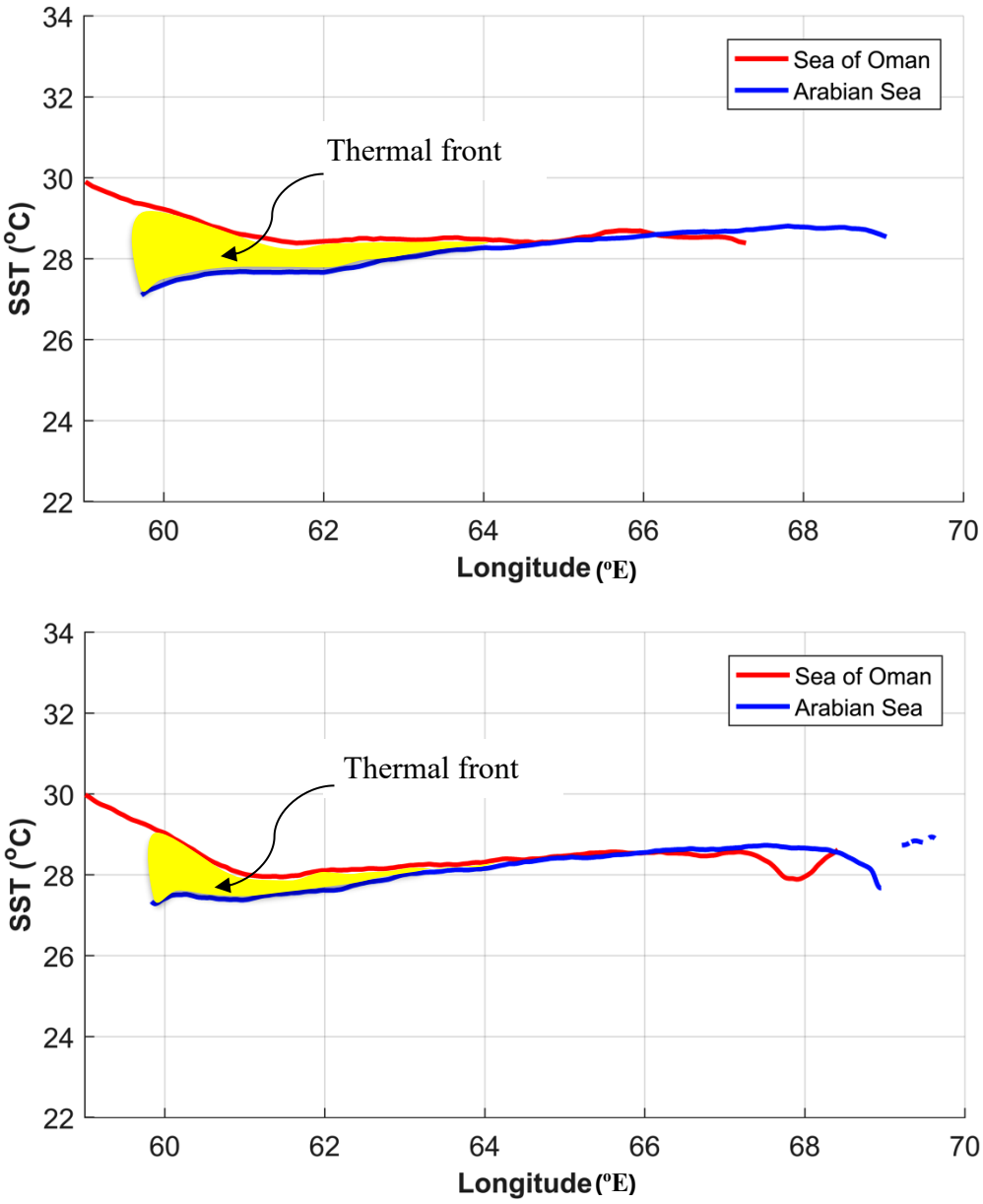

Figure 4.2. This graph shows the zonal SST climatology at Cape-RH during the Post-SWM, September/October. Red line represents warm water from the Sea of Oman while the blue line represents cool water from the Arabian Sea. The top figure represents the climatology September/October 2006-2009 and the bottom figure represents the climatology September/October 2010-2015. These figures show where two water masses with different temperature meet, creating the Ras Al-Hadd Jet (yellow area) moving offshore crossing approximately 270 km from the Ras Al-Hadd coast.

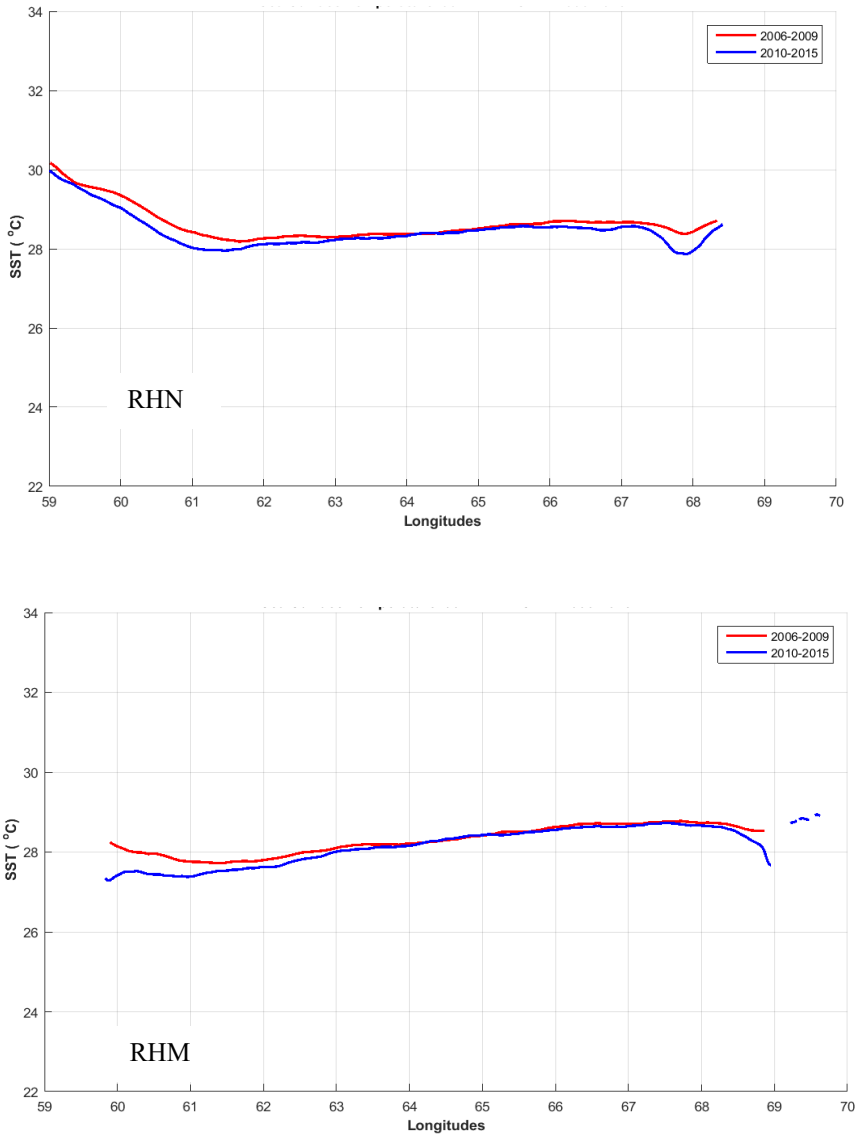

Figure 4.3. The figures show the zonal SST climatology during 2006-2009 (Red) and 2010-2015 (Blue). Coastal waters were warmer in 2006-2009 compared to the period of 2010-2015 in the Sea of Oman (Top panel) and the Arabian Sea (Bottom panel)

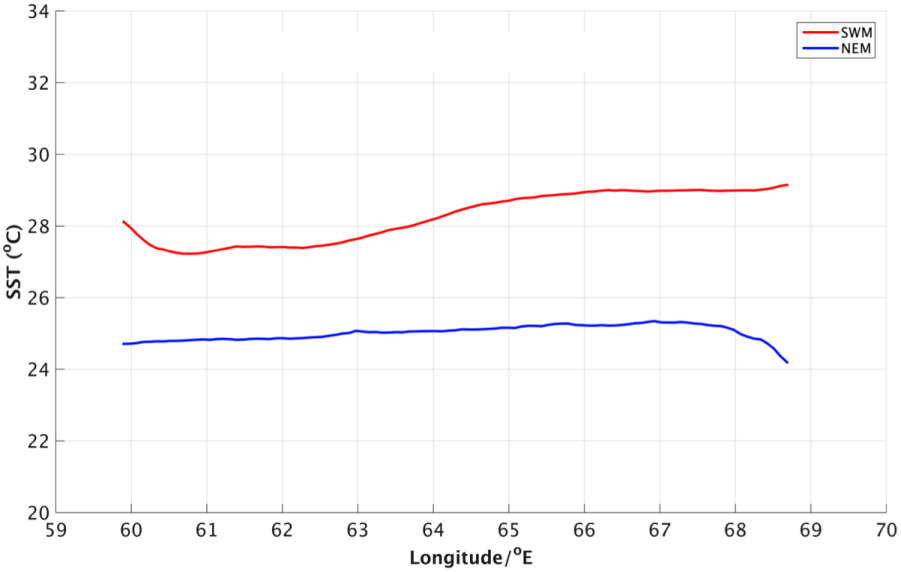

Figure 4.4. This figure represents the seasonal climatology zonal SST (2006-2009). It shows the difference in SST at Cape-RH between the two monsoonal seasons. The SWM (Red line) and the NEM (Blue line).

During the SWM, warmer and high salinity waters move from the Sea of Oman toward the Arabian Sea. These water masses were not able to cross the Ras Al-Hadd barrier because of the existence of the RH-Jet. However, in the eastern Arabian Sea, these warmer and high salinity waters crossed and penetrated into the Arabian Sea due to the absence of the Jet (Figure 3.9).

Current velocity at Cape-RH recorded by a 75 kHz ADCP exceeded 120 cms^{-1} during the SWM. This high-velocity current (Figure 3.13, and Figure 3.15) is the result of the RH-Jet due to the prevailing strong wind stress during the SWM (Figure 3.16, and Figure 3.18).

Strong SWM wind regime creates wind stress curl in the region (Figure 4.6, and Figure 4.7). Positive wind stress curl indicates an existence of an upwelling (Figure 4.5). This wind stress influences the ocean physical characteristic in the region. The study by Kok *et al.*, 2015 showed that wind stress curl influences the formation of the thermal front during the SWM season.

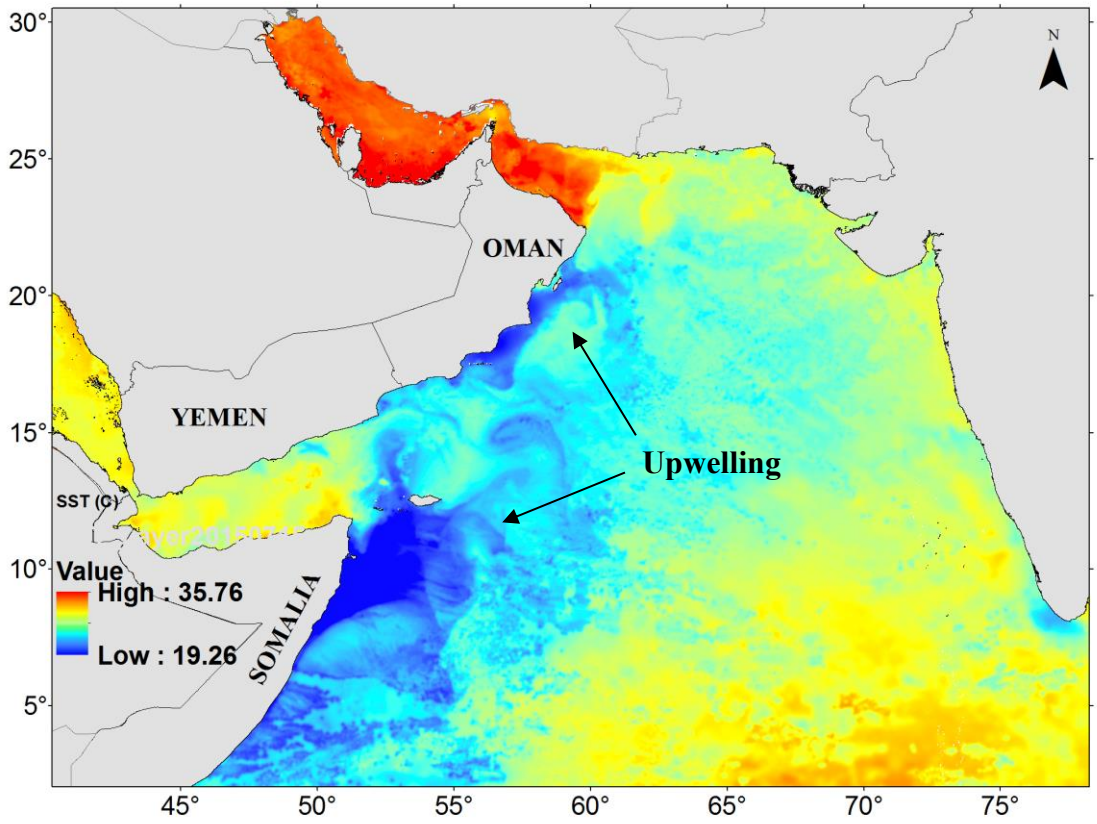

Figure 4.5. This satellite SST image acquired in July 15, 2015, shows the upwelling areas in the western Arabian Sea. The SST in the upwelling areas has decreased to 19ºC, while higher SST can be seen in the Sea of Oman with the maximum temperature of 35.76ºC.

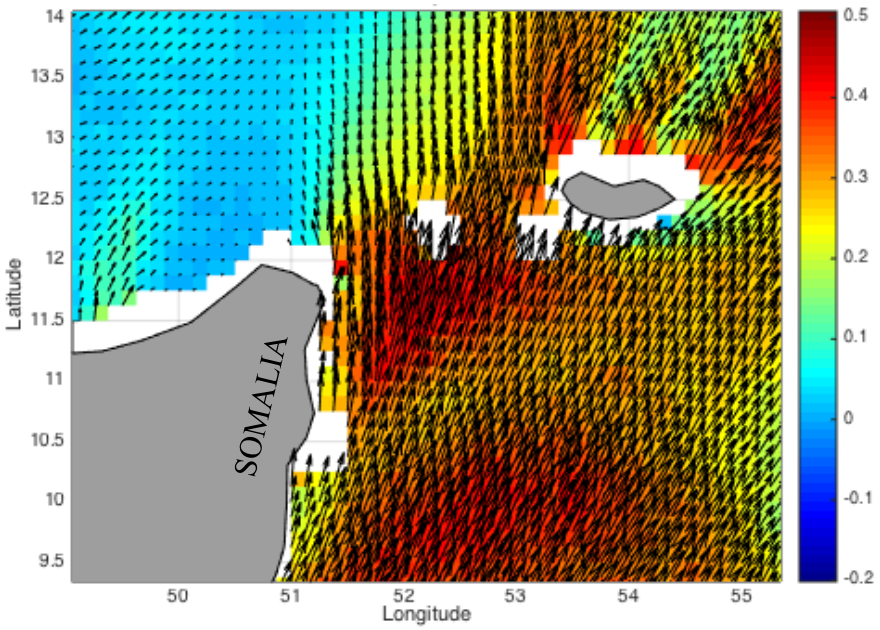

Figure 4.6. The map demonstrates wind-stress at the northern tip of Somalia during July-2005. Strong wind-stress (Nm^{-2}) can be seen moving to the northeast towards the coast of Yemen. This strong wind stress is believed to be the creation of the EAC, which is the extension of the SC.

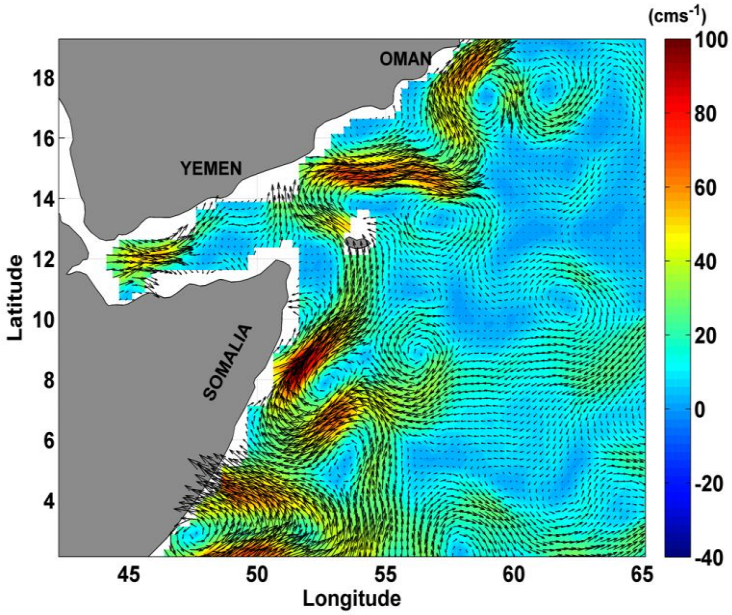

Figure 4.7. The graph demonstrates strong geostrophic currents during the SWM 1995. The currents flow from the Somali coast as the SC towards the Oman coast and are merged to the EAC, which continues flowing until it reaches Cape Ras Al-Hadd.

4.3 The Ras Al-Hadd Jet during the Northeast Monsoon

The northeast monsoon (NEM) season also known as the winter monsoon occurs during December – February and can extend to the end of March. During this season, winds are relatively calm in the Arabian Sea but moderate and strong in the Sea of Oman and the Persian/Arabian Gulf. Previous studies showed that the prevailing NEM winds drive a southward current that brings warmer and saltier water from the north of the Sea of Oman to the Arabian Sea (Almasroury, 1997; Prasad *et al.*, 2001).

This study did not find any evidence of the Ras Al-Hadd Jet formation during the winter monsoon in the northwest Arabian Sea. This is because during this time the wind system in the Arabian Sea had reversed its direction. The winds near Cape-RH are not strong enough during the NEM compared to the summer monsoon (Figure 3.16, 3.17). The other factor contributing to the absence of the RH-Jet in the northwest Arabian Sea during winter monsoon is the absence of water masses that carry different temperature between the Sea of Oman and the Arabian Sea in the RH region (Figure 4.8) Moreover, both the EAC and SC take the opposite direction toward the southwest during the NEM.

In this study, the findings of SST and salinity show no thermal frontal signatures in the northwest Arabian Sea during winter seasons. This study is consistent with that of Puthezhath (2014), who found thermal fronts in the eastern Arabian Sea during the winter monsoon, but did not observe any front during the summer monsoon in Indian coastal waters (Figure 4.9).

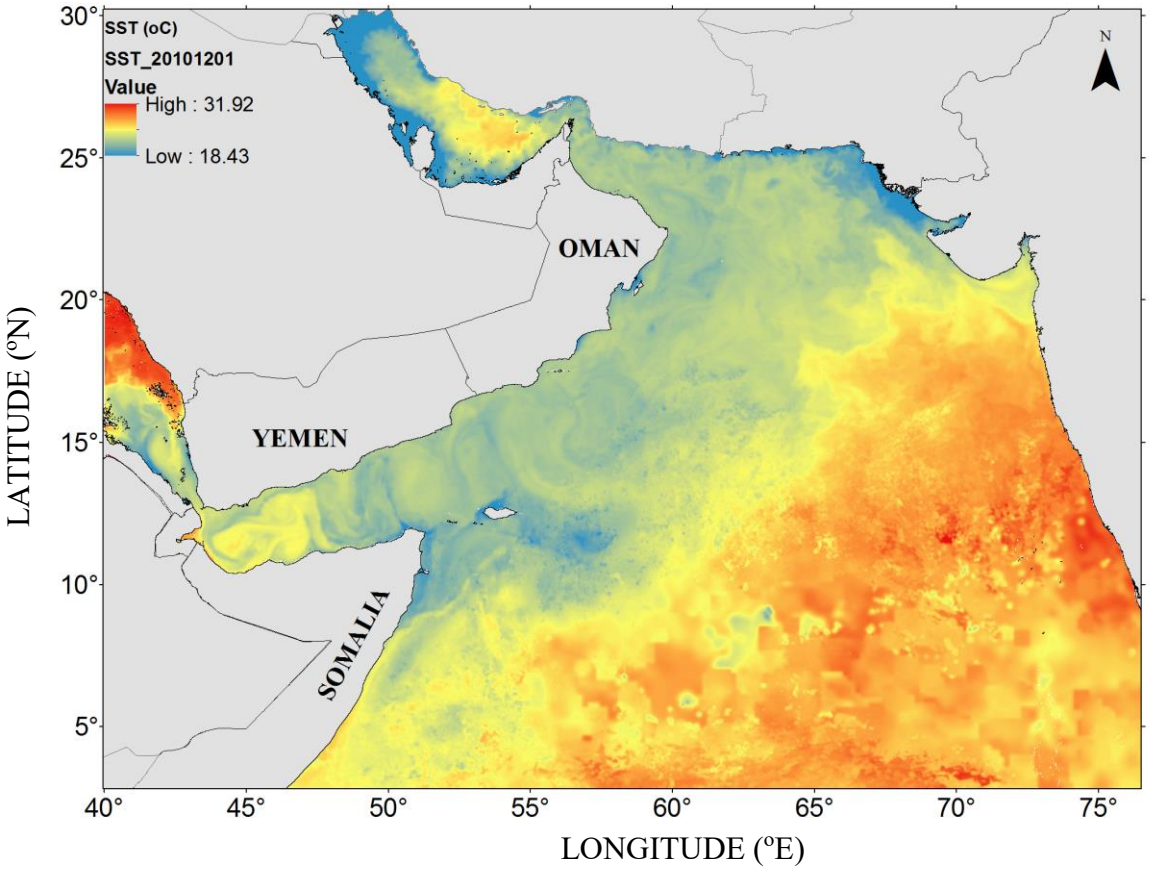

Figure 4.8. Satellite remote sensing SST image acquired in December 01, 2010, shows low water temperature during the winter season in both the Sea of Oman and the western Arabian Sea.

The zonal SST during the NEM reveals that water masses in the northwest Arabian Sea were warmer than the Sea of Oman. The difference in sea surface temperature between the Sea of Oman and the Arabian Sea is too small to create a horizontal temperature gradient that can be captured by the algorithm used in this study (Figure 4.10, and Figure 3.35). In this study, currents were observed in the eastern Arabian Sea moving towards the Persian/Arabian Gulf penetrating through the northern part of the Strait of Hormuz.

Because of the absence of the RH-Jet during the winter monsoon, high salinity waters from the Sea of Oman cross Cape-RH raising the salinity in the Ras Al-Hadd region (Figure 3.36).

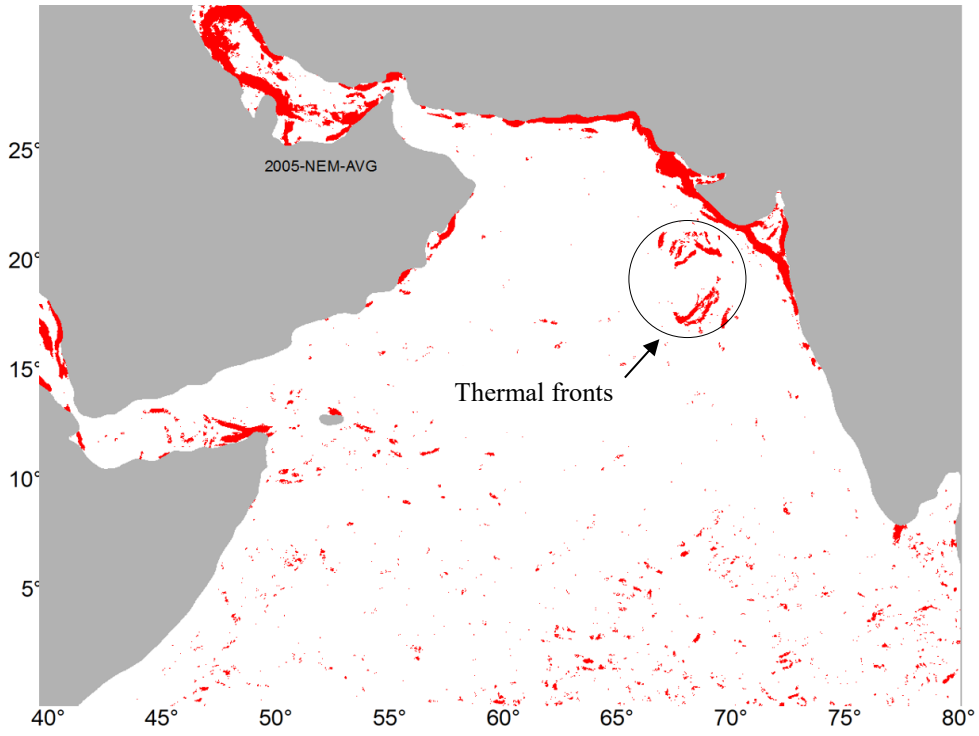

Figure 4.9. The frontal map shows the existence of some thermal fronts in the eastern part of the Arabian Sea during the NEM 2005, while the RH-Jet is absent in northwest Arabian Sea during this season.

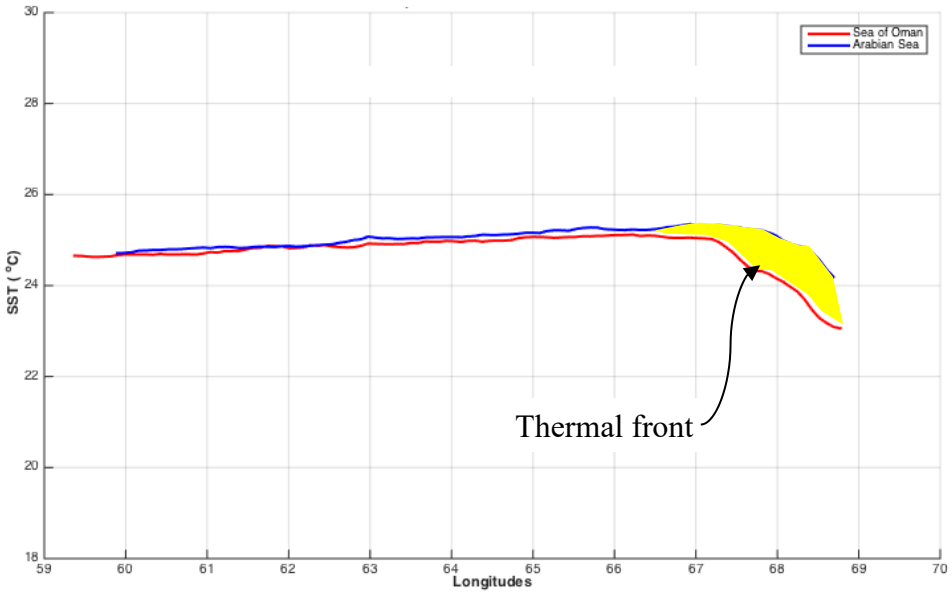

Figure 4.10. Climatology zonal SST 2006-2009 at Cape-RH (blue) and North of the Cape in the Sea of Oman (Red) demonstrates the absence of the RH-Jet during the winter monsoon while a front exists (Yellow) in the eastern Arabian Sea near the coast of India.

CHAPTER V

CONCLUSIONS AND FUTURE DIRECTIONS

Few studies before the mid-90s attempted to understand the ocean dynamics around Cape-RH, the region where the Sea of Oman and the Arabian Sea meet. The northwest Arabian Sea was left intact since the mid-90s and conducting oceanographic studies were stopped for the reasons mentioned in Chapter 1 of this dissertation. The only non-stop mission that visits the Arabian Sea and collects oceanography parameters at least once a day is the satellite remote sensing led by the US. NASA/NOAA government organisations and some European institutes and organisations.

5.1 Conclusions

Many studies have investigated oceanographic processes in the Persian/Arabian Gulf, the Red Sea, the eastern and the southern Arabian Sea, and the southern Indian Ocean, but little is understood about the northwest Arabian Sea, especially the ocean dynamics in the Ras Al-Hadd region. This dissertation has put together observations from satellite remote sensing, Argo floats and a cabled mooring system to study the spatial and temporal variability of the Ras Al-Hadd Jet located at Cape Ras Al-Hadd.

Satellite remote sensing technology has proved its ability to collect different types of scientific oceanographic long-term datasets, such as sea surface temperature, sea surface salinity, ocean color, sea surface wind, sea surface height, and many other

oceanographic properties. Altimetry satellites have been providing useful datasets that help to study the ocean surface topography. Satellites can scan and take a snapshot of a wide ocean area covering millions of square kilometers on a daily basis with a high spatial resolution.

The dramatic advance in personal computer (PC) technology with huge storage capacity, big memories, fast central processing units (CPU), and the continually decreasing prices has helped individuals and college students who possess these powerful PCs. Additionally, increases in the number of open sources scientific software, algorithms, and programming codes, have increased the capability of personal computers on handling and processing satellite datasets.

In this study, satellite remote sensing was used to study the spatial and temporal variability of the Cape Ras Al-Hadd Jet in the northwest Arabian Sea. Atmospheric and oceanographic jets are very important features that affect the dynamics of ocean and atmosphere. In the atmosphere, a jet or a front is the result of the existence of two air masses with different temperatures. In oceanography, a jet or a front is formed when two water masses with different oceanographic properties meet.

In this study, I found that the creation of the RH-Jet is influenced by forcing from the SWM, the Somali Current, the East Arabian Current, and the warm and high salinity water from the Sea of Oman. During the SWM and Post-SWM, thermal frontal images

and the geostrophic datasets show the propagation of the Somali Current towards the Omani coast boosting the EAC that flows to Cape-RH. In the Ras Al-Hadd region, observations from ADCPs showed strong currents flow to the northeast during the SWM and the reversal direction of these currents during the NEM. Argo floats revealed the Sea of Oman high salinity water masses flow and cross in to the eastern Arabian Sea during the SWM season. These high salinity water masses from the Sea of Oman were not able to cross the Ras Al-Hadd barrier on the western side of the Arabian Sea due to the existence of the RH-Jet at Cape-RH. Two peaks of the RH-Jet were detected. The first one was during the Peak-SWM (July/August) and the second one occurred during the Post-SWM (September/October). These new findings add valuable information regarding the oceanic jet at Cape-RH that will help decision makers in the fishery sectors and maritime transportation with planning for the improvement of these sectors.

5.2 Future Directions

In addition to the satellite remote sensing technology, more observational studies of ocean dynamics in the RH region are needed in order to broaden our understanding of the Ras Al-Hadd Jet. Long-term *in situ* datasets are essential to provide a thorough understanding of the temporal and spatial variability of the ocean dynamics in the RH region. Therefore, using gliders will help to achieve this goal, and will reveal more scientific keys regarding the hydrography and the dynamics of the RH region. In addition, the energy and the characteristics of two mesoscale eddies north and south of the RH-Jet will be revealed. This will help to widen our understanding regarding the

RH-Jet and the ocean dynamics in this region. In addition to the glider system, there is a need to be deployed shore mooring systems with 75 kHz ADCPs at the Cape Ras Al-Hadd, North and South of the Cape. Furthermore, datasets collected by the coastal ocean High Frequency (HF) radar network belonging to the Oman Tsunami Early Warning System will be used**.** A numerical model needs to be created and this model can be fed using the outputs from gliders, mooring systems, and the coastal ocean HF radar network. This will produce a clear picture for better understanding of the RH-Jet and the ocean dynamics in the Ras Al-Hadd region and its surroundings, therefore providing decision makers with more information to improve control and enhance the fishery stocks and to improve maritime navigation that passes and crosses through Cape-RH region.

REFERENCES

Aanderaa RCM-11 Operating Manual (2002). Doppler Current Meter RCM-11. A State-of-the-Art Recording Current Meter Designed for deep sea operation down to 6000 meters. pp 6. http://www.aanderaa.com/

Almasroory, A.S. (1997). Investigation of Water Exchange Between the Persian Gulf and the Gulf of Oman. *MS Thesis*, Submitted to the Graduate School of the Florida Institute of Technology in partial fulfillment of the requirements for the degree of Master of Science.

Amante, C. and B.W. Eakins, 2009. ETOPO1 1 Arc-Minute Global Relief Model: Procedures, Data Sources and Analysis. NOAA Technical Memorandum NESDIS NGDC-24. National Geophysical Data Center, NOAA. doi:10.7289/V5C8276M [2009].

Banse, K., and D. C. English (1994). Seasonality of coastal zone colour scanner phytoplankton pigment in the offshore oceans. *Journal of Geophysics Research*., 99, 7323-7345.

Banse, K. (1997). Irregular flow of Persian (Arabian) Gulf water to the Arabian Sea. *Journal of Marine Research*., 55, 1049-1067.

Barth, J.A., (1987). Stability of a coastal upwelling front over topography. *Ph.D. Dissertation.,* MIT and WHOI.

Barth, J.A., (1989). Stability of a coastal upwelling front: 1. Model development and a stability theorem. *Journal of Geophysics Research*., 94(C8),10844–10856. http://dx.doi.org/ 10.1029/JC094iC08p10844.

Bauer, S., G. L. Hitchcock, and D. B. Olson (1991). Influence of monsoonally forced Ekman dynamics upon surface layer depth and plankton biomass distribution in the Arabian Sea. *Deep Sea Research.,* 38, 531-553.

Belkin, I.M. (2003). Front, in: Interdisciplinary Encyclopedia of Marine Sciences, edited by Nybakken J.W., Broenkow W.W., Vallier T.L. *Grolier Academic Reference, Danbury, Conn*., pp. 433–436.

Böhm, E. J. Morrison, V. Manghnani, H. S. Kim, C. Flagg (1999). The Ras al Hadd Jet: Remotely sensed and acoustic Doppler current profiler observations in 1994-1995. *Deep-Sea Research.,* II 46, 1531-1549.

Bower, A S, D. Heather, and J. F. Price (2000). Character and dynamics of the Red Sea and Persian Gulf outflows. *Journal of Geophysical Research*., Vol. 105, NO. C3, 6387-6414.

Brink, K., R. Arnone, P. Coble, C. Flagg, B. Jones, J. Kindle, C. Lee, D. Phinney, M. Wood, C. Yentsch, and D. Young, (1998). Monsoons boost biological productivity in Arabian Sea. *EOS.,* 79 165,168-169.

Brock, J., C. McClain, M. Luther, and W. Hay (1991). The phytoplankton bloom in the north-western Arabian Sea during the Southwest Monsoon of 1979. *Journal of Geophysical Research.,* 96, 20623-20642.

Burkill, P.H., Mantoura, R.F.C., Owens, N.J.P., (1993). Biogeochemical cycling in the northwestern Indian Ocean. *Deep-Sea Research.,* II 40, 643-850.

Cayula, J. F., P. Cornillon (1992). Edge detection algorithm for SST images. *Journal of Atmospheric and Oceanic Technology.,* 9 (1), 67-80.

Cayula, J. F., P. Cornillon (1995). Multi-image edge detection for SST images. *Journal of Atmospheric and Oceanic Technology.,* 12, 821-829.

Cushman-Roisin B, and J. Beckers, (2011). *Introduction to Geophysical Fluid Dynamics.*, (101), ISSN 0074-6142, doi:10.1016/B978-0-12-088759-0.00018-3.

DiMarco, S.F., A.E. Jochens, C.J. Jang, L. Belabbassi, and M.K. Howard. (2008). Final *Report*:Physical Oceanography in the Gulf of Oman: Data Processing, Analysis and Synthesis of Cabled and Moored Data for Data Received Through 6 February 2008. 127 pp.

DiMarco, S.F., A. Jochens, M. Stöessel, L. Belabbassi, Z. Wang, and M. Howard (2011). Physical Oceanography in the Sea of Oman. Data Processing, Analysis and Synthesis of Cabled and Moored Data 3 January 2005 through 31 August 2010. *Final Data Report*, Texas A&M University Department of Oceanography College Station, Texas 77843-3146.

DiMarco, S. F., L. Al-Kharusi, Z. Wang, A. Jochens, M. Stöessel, L. Belabbassi, and M. Howard (*unpublished*), Monsoon-driven seasonal hypoxia along the northern coast of Oman.

Elliott, A., G. Savidge (1990). Some features of the upwelling off Oman. *Journal of*

Marine Research., 48, 319-333.

Findlater, J. (1969). A major low-level air current near the Indian Ocean during the Northern summer. *Q. J. R. Meteorology Society.*, 95, 362.

Flagg, C., and H. S. Kim (1998). Upper ocean currents in the northern Arabian Sea from shipboard ADCP measurements collected during 1994-1996 US JGOFS and ONR programs. *Deep-Sea Research.,* II 45, 1917-1959.

Frantantoni, D. M., A. S. Bower, W. E. Johns, and H. Peters (2006). Somali Current rings in the eastern Gulf of Aden. *Journal of Geophysical Research.*, 111, C09039, doi:10.1029/2005JC003338.

Gaedicke, C, H. Schluter, A. R. Roeser, A. Prexl, B. Schreckenberger, H. Meyer, C. Reichert, P. Clift, and S. Amjad (2002). Origin of the northern Indus Fan and Murray Ridge, northern Arabian Sea: interpretation from seismic and magnetic imaging. *Tectonophysics.*, Vol.1–4, 127–143.

Gooday, A.J., J. M. Bernhard, L.A. Levin, and S. B. Suhr (2000). Foraminifera in the Arabian Sea oxygen minimum zone and other oxygen-deficient settings: taxonomic composition, diversity, and relation to metazoan faunas. *Deep-Sea Research., II* 47, 25-54.

Hickox R, I. Belkin, P. Cornillon, Z. Shan (2000). Climatology and seasonal variability of ocean fronts in the east China, Yellow and Bohai Seas from satellite SST data. *Geophysical Research Letter.,* 27(18): 2945-2948.

Ingle, S., L. Belabbassi, K. du Vall, D. Potter, S. F. DiMarco, and Z. Wang (2012). A 4000-meter-rated deep-water cabled ocean observing system: Lessons learned from two years of operation. DOI:10.1109/*OCEANS*.2012.6404959.

Johns, W. E., G. E. Jacobs, J. C. Kindle, S. P. Murray, and M. Carron (2000). Arabian Marginal Seas and Gulfs, University of Miami Technical Report 2000-01, report of a workshop held at Stennis Space Center, Mississippi, 11–13 May, 1999. *Technical Report.*, 60 pp.

Kahru, M., B. Ha-kansson, and O. Rud, (1995). Distributions of the sea-surface temperature fronts in the Baltic Sea as derived from satellite imagery. *Continental Shelf Research.*, 15, 663–679.

Kessler, W. S., L. Gourdeau (2006). Wind driven zonal jets in the South Pacific Ocean. *Geophysical Research Letters*., 33, L03608, doi:10.1029/2005GL025084.

Kida, S., H. Mitsudera, and S. Aoki (2015). Oceanic fronts and jets around Japan: a review. *Journal of Oceanography.,* 71: 469. doi:10.1007/s10872-015-0283-7.

Kim, H.S., C.N. Flagg, and S.D. Howden (2001). Northern Arabian Sea variability from TOPEX/Poseidon altimetry data: an extension of the US JGOFS/ONR shipboard ADCP study. *Deep-Sea Research., II.* 48, 1069-1096.

Klemas, V. (2012). Remote Sensing of Coastal and Ocean Currents: An Overview. *Journal of Coastal Research*., 576-586.

Kok, P. H., M. F. Akhir, and T. F. Tangang (2015). Thermal frontal zone along the east coast of Peninsular Malaysia. *Continental Shelf Research*., 110(2015)1–15.

Levin, L.A., J. D. Gage, C. Martin, and P. A. Lamont (2000). Macrobenthic community structure within and beneath the oxygen minimum zone, NW Arabian Sea. *Deep-Sea Research., II.* 47, 189-226.

L'Hégaret, P., X. Carton, S. Louazel, and G. Boutin (2016). Mesoscale eddies and submesoscale structures of Persian Gulf Water off the Omani coast in spring 2011. *Ocean Sci*ence., 12, 687–701, 2016. doi:10.5194/os-12-687.

Lighthill, M. J. (1969). Dynamic response of the Indian Ocean to the onset of the southwest monsoon. *Phil. Trans of the Royal Meteorol. Society., A*, *A265*, 45–92.

Luyten J. R. and J. C. Swallow (1976). Equatorial undercurrents. *Deep-Sea Research.*, 23. 1005-1007.

Manghnani, V. J. Morrison, T. Hopkins, and E. Böhm (1998). Advection of upwelled waters in the form of plumes off Oman during the southwest monsoon. *Deep-Sea Research., II* 45, 2027-2052.

Maximenko, N. A., B. Bang, and H. Sasaki (2005). Observational evidence of alternating zonal jets in the world ocean. *Geophysical Research Letters.* 32, L12607, doi:10.1029/2005GL022728.

Mavor, P.T., and J. J. Bisagni (2001). Seasonal variability of sea-surface temperature fronts On Georges Bank. *Deep-Sea Research., II* 48 (1–3), 215–243.

McCreary, J.P. and P.K. Kundu (1988). A numerical investigation of the Somali Current during the Southwest Monsoon. Journal of Marine Research., 46, 25-58.

McCreary, J. P., K. E. Kohler, R. R. Hood, and D. B. Olson (1996). A four-component model of biological activity in the Arabian Sea. *Progress in Oceano*., 37, 193–240.

Miller, P. I. (2004). Multi-spectral frontmaps forautomaticdetectionof oceancolour features from SeaWiFS. *International Journal of Remote Sensing.,* 25 (7–8), 1437–1442.

Miller, P. I. (2009). Composite front maps for improved visibility of dynamic sea-surface features on cloudy SeaWiFS and AVHRR data. *Journal of Marine Systems.,* 78(3), 327–336. doi: 10.1016/j.jmarsys.2008.11.019.

Morrison, J., L. Codispoti, S. Gaurin, B. Jones, V. Manghnani, and Z. Zheng (1998). Seasonal variation of hydrographic and nutrient fields during the US JGOFS Arabian Sea Process Study. *Deep-Sea Research., II.* 45, 2053-2101.

Naidu, P.D. (1998). Driving forces of Indian summer monsoon on Milankovitch and sub-Milankovitch time scales: A review. *Journal of Geological Society of India.*, 52(3); 257-272.

Naqvi, S.W.A. (1987). Some aspects of the oxygen deficient conditions and denitrification in the Arabian Sea. *Journal of Marine Research*., 45:1049-1072

NOAA (2012). http://celebrating200years.noaa.gov/magazine/argo/profile _cycle_650 .html.

Podesta, G. P, J. A. Browder, and J. Hoey (1993). Exploring the association between swordfish at chrates and thermal fronts on United-States longline grounds in the Western North-Atlantic. *Continental Shelf Research.,* 13(2-3): 253-277.

Pollard, R. T, and L. A. Regier (1992). Vorticity and vertical circulation at an ocean front. *Journal of Physical Oceanography*., 22:609-625. doi:10.1175/1520-485

Ponte, R.M., J. Luyten, and P. Richardson (1990). Equatorial deep jets in the Atlantic Ocean. *Deep-Sea Research.,* 37. No. 4., 711-713

Ponte, R. M. and J. Luyten (1990). Deep velocity measurements in the western equatorial Indian ocean. *Journal of Physical Oceanography.,* 20, 44-52.

Pous, S., X. Carton, and P. Lazure (2004). Hydrology and circulation in the Strait of Hormuz and the Gulf of Oman results from the GOGP99 experiment: 2. Gulf of Oman. *Journal of Geophysical Research*., Oceans, 109, doi:10.1029/2003JC002146.

Prasad, T. G., M. Ikeda, and S. P. Kumar (2001). Seasonal spreading of the Persian Gulf Water mass in the Arabian Sea. *Journal of Geophysical Research*., 106, 17059-17071.

Puthezhath, A. S. (2014). Identification of thermal fronts in the Arabian Sea using MODIS-SST data. M.S. Dissertation submitted to Kerala University of Fisheries and Ocean Studies. *In partial fulfillment of the requirement for the degree of Master of Science. pp 76.*

Quraishee, G. S. (1984). Circulation in the north Arabian Sea at Murray Ridge during S.W. Monsoon. *Deep-Sea Research Part A- Oceanographic Research Papers., 31,* 651-664.

Roberts, J. J., Best, B. D., Dunn, D. C., Treml, E. A., and– Halpin, P. N. (2010). Marine Geospatial Ecology Tools: An integrated framework for ecological geoprocessing with ArcGIS, Python, R, MATLAB, and C++. *Environmental Modelling & Software., 25*(10) 1197–1207. doi:10.1016/j.envsoft.2010.03.029.

Rudnick, D. L., R. Weller, C. Eriksen, T. Dickey, and C. Langdon (1997). Moored Instruments weather Arabian Sea monsoons, yield data. *EOS, Trans. Am. Geophysics., Union*, 78, 11, 117-124.

Saha, K. (1974): Some aspects of the Arabian sea summer monsoon. *Tellus.,* XXVI (1974) 4. (464-476).

Sastry, J.S., R. S. DiSouza (1972). Upwelling and upward mixing in the Arabian Sea. Indian. *Journal of Marine Scince*., 1, 17-27.

Schott, F. (1983). Monsoon Response of the Somali Current and Associated Upwelling. *Progress in Oceanography.*, Vol. 12, 357-381.

Schott, F. A., S. Xie, and J. P. McCreary (2009). Indian Ocean circulation and climate Variability. *Reviews of Geophysics., 47,* 1-46, doi:10.1029/2007RG000245.

Schott, F A. Julian and P. McCreary Jr. (2001). The monsoon circulation of the Indian Ocean. *Progress in Oceanography.,* 51 (2001) 1–123.

Shi, W., J. Morrison, E. Böhm, and V. Manghnani (1999). Remotely sensed features in the US JGOFS Arabian Sea Process Study. *Deep-Sea Res.,* II 46, 1551-1575.

Smith, S., M. Roman, I. Prusova, K. Wishner, M. Gowing, and L. A. Codispoti (1998). Seasonal response of zooplankton to monsoonal reversals in the Arabian Sea. *Deep-Sea Res.,* II 45, 2369–2403.

Smith, S. L. (2001). Understanding the Arabian Sea: Reflections on the 1994-1996 Arabian Sea Expedition. *Deep-Sea Res.,* II, 48, 1385-1402.

Sokolov, S., and S. Rintoul (2000). Circulation and water masses of the southwest Pacific: WOCE section P11, Papua New Guinea to Tasmania. *Journal of Marine. Research.,* 58, 223– 268.

Somasundar, K., A. Rajendran, M. Kumar, and. R. Gupta (1990). Carbon and nitrogen budgets of the Arabian Sea. Marine Chem., *30,* 363-377.

Stewart, H.R. (2008). Introduction to physical oceanography. http://oceanworld.tamu.edu/resources/ocng_textbook/PDF_files/book.pdf.

Stöessel, M., L. Belabbassi, A. Jochens, M. Howard, S. F. DiMarco, and K. du Vall (2010). Data management protocols for operational ocean observing system off Oman. *Poster presented at AGU meeting.*

Stryker, S. (2011). Deep And surface circulation in northwest Indian Ocean from Argo, surface drifter, satellite, and in situ profiling current observations. *MS Thesis*, submitted to the Office of Graduate Studies of Texas A&M University in partial fulfillment of the requirements for the degree of Master of Science.

Swallow, J. C., (1984). Some aspects of the physical oceanography of the Indian Ocean. *Deep Sea Res*., 31, 639-650.

Tomczak, M., J. S. Godfrey (1994). Regional Oceanography: An Introduction. *Elsevier., Tarrytown, NY,* pp. 422.

Tong, J., Z. Gan, Y. Qi, and Q. Mao (2010). Predicted positions of tidal fronts in continental shelf of South China Sea. *Journal of Marine Systems*., 82(3145–153. http://dx.doi.org/ 10.1016/j.jmarsys.2010.04.011.

Ullman, D.S., and P.C . Cornillon (2000). Evaluation of Front Detection Methods for Satellite-Derived SST Data Using In Situ Observations. *Journal of Atmospheric and Oceanic Technology.,* 17 (12), 1667–1675.

Ullman, D.S., and P.C . Cornillon (2001). Continental shelf surface thermal fronts in winter off the northeast US coast. *Continental Shelf Research.,* 21 (11–12), 1139–1156.

Unesco (1991). Processing of oceanographic station data. JPOTS editorial panel. United Nations Educational, Scientific and Cultural Organization 7, place de Fontenoy, 75700 Paris. ISBN 92-3-102756-5. pp 141.

Valavanis, V. D., I. Katara, and A. Palialexis (2005). Marine GIS: Identification of mesoscale oceanic thermal fronts. *International Journal of Geographical Information Science*., 19:10, 131-1147, DOI: 10.1080/13658810500391206.

Vitale, S.S., S. F. DiMarco, H. F. Seidel, and Z. Wang (2017). Circulation analysis in the northwest Indian Ocean using ARGO floats and surface drifter observations, and SODA reanalysis output. *Dynamics of Atmospheres and Oceans*., 78, 57-70.

Wang, Z., S. F. DiMarco, M. Stossel, X. Zhang, M. Howard, and K. du Vall (2012). Oscillation responses to tropical Cyclone Gonu in northern Arabian Sea from a moored observing system. *Deep Sea Res*., I 64, 129–145.

Wang, D. and H. Zhao. (2008). Estimation of Phytoplankton Responses to Hurricane Gonu over the Arabian Sea Based on Ocean Color Data. *Sensors.,* 2008, 8, 4878-4893; DOI: 10.3390/s8084878.

Weller, R. A., M. F. Baumgartner, S. A. Josey, A. S. Fischer, and J. C. Kindle (1998). Atmospheric forcing in the Arabian Sea during 1994–1995: observations and comparisons with climatology and models. *Deep-Sea Res.* II, 45, 1961–1999.

Wiggert, J. D., R. Hood, K. Banse, and J. Kindle (2005). Monsoon-driven biogeochemical processes in the Arabian Sea. *Progress in Oceanography.,* 65, 176–213.

Wilson-Diaz, D., A. Mriano, R. Evans, and M. Luther (2001). A principal component analysis of sea surface temperature in the Arabian Sea. *Deep-Sea Res.,* II, 48, 1097–1114.

Wolanski, E. and W. M. Hamner (1988). Topographically controlled fronts in the ocean and their biological influence. *Science.,* 241, 4862.

Yanagi, T. (1987). Classification of "Siome", Streaks and Fronts. *Journal of the Oceanographical Society of Japan.,* Vol. 45, 149-158.

Young, D. K., and J. C. Kindle (1994). Physical processes affecting availability of dissolved silicate for diatom production in the Arabian Sea. *Journal of Geophysics Research.,* 99, 22,619-22,632.